POLITECNICO DI TORINO
Repository ISTITUZIONALE

A model of fiber reorientation in fiber-reinforced biological materials combining statistical and configurational mechanics

Original
A model of fiber reorientation in fiber-reinforced biological materials combining statistical and configurational mechanics / Giammarini, A., Pastore, A., Grillo, A.. - In: MATHEMATICS AND MECHANICS OF SOLIDS. - ISSN 1081-2865. - (2025), pp. 1-38. [10.1177/10812865251327765]

Availability:
This version is available at: 11583/3002653 since: 2025-09-15T15:41:22Z

Publisher:
Sage Publications

Published
DOI:10.1177/10812865251327765

Terms of use:

This article is made available under terms and conditions as specified in the corresponding bibliographic description in the repository

Publisher copyright
Sage postprint/Author's Accepted Manuscript

(Article begins on next page)

03 November 2026

A model of fiber reorientation in fiber-reinforced biological materials combining statistical and configurational mechanics

Alessandro Giammarini[1], Andrea Pastore[1] and Alfio Grillo[1]*

Monday 15th September, 2025

[1]Dip. di Scienze Matematiche "G. L. Lagrange", Politecnico di Torino, Corso Duca degli Abruzzi 24, 10129, Torino, Italia.

Abstract

We present a mathematical model for the reorientation of fibers in a soft, fiber-reinforced, fluid-saturated porous medium describing a hypothetical biological tissue. We consider two types of remodeling that, at different scales, concur in determining the structural reorganization of the solid phase of the medium: one pertains to the development of plastic-like distortions, which are introduced as the macroscopic manifestation of processes occurring at lower scales, but not resolved explicitly; the other one, originating at the mesoscale, concerns the capability of the fibers of reorienting in the extracellular matrix. This latter form of remodeling is studied as a Langevin-like process in which two main agencies are recognized: a drift term, which is given by the effects that the deformation of the extracellular matrix exerts on the fibers; a noise term, which accounts for the interactions among nearby fibers. We employ the framework of the Principle of Virtual Power to present our model, in which we "free" the kinematics of the system from the constraints of isochoricity of remodeling and incompressibility of the mixture by appending the Chetaev forms of these constraints to the Principle of Virtual Power. Then, we specialize our model to articular cartilage. We do this for comparing our results with some experimental curves describing the distribution of collagen fibers in a sample of articular cartilage, and for studying, through the simulation of a uniaxial compression test, the interplay between fluid flow and the two aforementioned forms of remodeling. Our main result is the establishment of a framework that captures effectively the mechanical coupling between the fiber distribution specific to a given medium and the mechanical stimuli exerted on such distribution. Quite differently from other works on this subject, our framework is capable of accounting for the stochastic effects of the fibers on the overall evolution of the considered tissue.

Keywords: Biological tissues, Remodeling, Fiber reorientation, Inelastic distortions, Anisotropic materials.

1 Introduction

As recently reported in the work by Gunda et al. [1], a rather common praxis in the biomechanics of soft tissues [2] is to describe soft and hydrated biological tissues as biphasic media [3], comprising at least a solid and a fluid phase. The fluid phase essentially consists of water, and plays a relevant role in a number of chemical and mechanical processes that are vital for the nourishment of the tissues themselves [4, 3, 2], whereas the solid phase represents the "summa" of extracellular matrix, nuclei and membranes of the cells, protein networks and, in some cases, collagen fibers [2, 5, 6]. In fact, fibrous constituents are present in a variety of tissues (e.g. articular cartilage [7], aorta walls [8], cornea [9, 10], among others), and have an impact on their overall mechanical properties and on their capability of being permeated by

*Corresponding author: Alfio Grillo, Dipartimento di Scienze Matematiche "G. L. Lagrange", Politecnico di Torino, Torino, 10129.
Email: alfio.grillo@polito.it

a fluid. Such impact is so high that the ability of a tissue to correctly perform its biological functionality can be compromised when its fibrous constituents are damaged.

Understanding the role played by the fibers is important also for the design and the manufacturing of bio-compatible materials, since, as put forward by Gentleman et al. in [11], *"The development of novel collagen gel/scaffold constructs requires a clear understanding of the mechanical properties of the constituent biomaterial"*.

In fact, many researchers have undertaken large efforts to provide a mechanical framework able to capture the behavior of fiber-reinforced materials. The first works focused on some phenomenological aspects of this problem (see, e.g., [3] for articular cartilage), and, in doing so, they regarded fiber-reinforced tissues as homogeneous and isotropic in spite of the inhomogeneity and anisotropy introduced by the fibers themselves. Then, the focus shifted onto the study of inhomogeneous and anisotropic media, which are described through one or more families of fibers with structural properties. For instance, the constitutive framework developed in [8] for the mechanical description of arteries has been adapted and generalized to many cases of biological interest [12, 13, 9, 14, 15, 16, 17, 10, 18, 19, 20, 21].

To list a few of the many remarkable results in the literature, a class of orthotropic and transversely isotropic strain energy functions satisfying poly-convexity is proposed in [22], whereas transversely isotropic materials are studied by using a different, but equivalent, set of invariants in [15]. Moreover, in [23], the anisotropic part of the Holzapfel–Gasser–Ogden (HGO) model [8] is modified to take into consideration the constitutive response of a material under hydrostatic stress.

In the case of a medium featuring statistically oriented fibers, such as articular cartilage, the constitutive law describing the tissue is extended to consider a statistical distribution of orientation of the fibers, while taking into account that the preferred direction changes with the depth of the tissue. Hence, the constitutive setting requires the introduction of directional averages [24], which have been employed extensively (see e.g. [25, 26, 10, 27, 28, 29, 30, 31, 32, 33, 34, 35]).

In the literature, a line of research of particular relevance in the study of tissues as solid-liquid biphasic media focuses on how the hydraulic properties of a medium change in the presence of fibers [36, 7, 37, 29, 38]. In fact, depending on the direction of orientation, the fibers can favor or hinder the motion of the interstitial fluid permeating a tissue. Such enhancement or inhibition, in turn, may influence the mobility of chemical substances transported by the fluid, thereby affecting their concentration within the tissue. Some consequences of the amount and alignment of collagen fibers on the permeability of cartilaginous tissues were investigated, e.g., by Maroudas and Bullough [39], and more recent studies done in [25, 26, 28, 29] aimed to model their findings.

The study of the mechanical properties of fiber-reinforced media is a relevant topic also in many other chapters of the biomechanical research and, more generally, in the characterization of the mechanical properties of materials. In the following, without the intent of being exhaustive, but with the sole purpose of exemplifying a few contributions, we list some relevant works from different fields, and we refer to the references contained therein for further reads. For example, a robust mechanical setting for dealing with damage, growth and remodeling is developed in [40, 41, 4, 42, 43, 44], whereas a theoretical setting for elastic, polar fiber-reinforced materials is discussed in [45, 46]. Computational schemes are developed and studied in [47, 48, 49], and statistical methods to resolve the distribution of the fibers are investigated in [34, 30, 33, 50].

In our work, we take off from the line of thought previously put forward in [32]. In [32], the problem of fiber reorientation was studied in conjunction with the isochoric remodeling of the solid phase, described as a porous medium permeated by an interstitial fluid and undergoing large deformations ("isochoric remodeling" was understood as a plastic-like reorganization of the solid phase of the tissue in response to mechanical stress). This setting made it possible to evaluate the influence of fiber reorientation and remodeling on the flow of the medium's interstitial fluid and, conversely, the influence of the fluid on the overall mechanical behavior of the system. However, in this present work, we introduce two differences: one methodological and one conceptual.

From the methodological point of view, we base the formulation of our present work on a revisitation [51, 52] of the Principle of Virtual Power (PVP) at the scale of the tissue. Within this approach, we

append the constraint of isochoric remodeling and the constraint of incompressibility of the fluid and of the solid phase to the PVP. The constraints are then addressed with the Lagrange multiplier technique. As a consequence, we isolate the constitutive contribution of the stress from the one that originates from the constraint. The former one is also referred to as *active part* of the overall stress, while the latter one is the *reactive part* of it. Note that the adjective "active" should not be confused with the one sometimes used to indicate the addend of the additive decomposition of stress that is taken as alternative modeling option to the one based on the concept of "active strain" (e.g., in muscle mechanics [53, 54, 55]).

The conceptual difference with respect to [32] consists in a description of the reorientation of the fibers that is borrowed from Statistical Mechanics. Accordingly, we assume to "observe" the dynamic process of the reorientation at the scale of a single fiber, i.e., at the mesoscale, and we characterize it by a *drift* and a *stochastic* term. By doing so, we aim at recovering the probability density distribution supplied initially in [13] as the solution of a stochastic process occurring at a lower scale than that of the tissue as a whole. Hence, instead of speaking of *"target angle"* [47, 56], our aim is to recover a *target probability distribution*, which resembles the one characterizing the material under study.

2 Theoretical background and evolution of the fiber angle distribution

In this section, we recall the framework for studying the evolution of a fiber-reinforced biphasic material that undergoes an anelastic process of structural reorganization, as put forward in [40, 41, 4, 57, 43, 44, 31, 32, 51, 52].

2.1 Modeling Hypothesis and fundamental notation

We turn our attention to fiber-reinforced, soft, and hydrated biological tissues, which comprise, for example, articular cartilage. We model such tissues as *saturated* porous media permeated by an interstitial fluid and consisting of a solid composite material, made of extracellular matrix and reinforcing collagen fibers. A tissue of this type is modeled as a mixture. The interstitial fluid plays a fundamental role in transport-related phenomena, and contributes significantly to the diffusion of bio-relevant markers. As shown by numerous studies, if fibers are present, the capability of the fluid of flowing through the tissue is substantially influenced by the concentration and orientation of the fibers [39, 36, 7, 28, 58, 29, 38, 59, 30, 50].

We hypothesize that each phase of the tissue is *intrinsically incompressible* (see e.g.[2]), and, thus, that the changes of the tissue's overall volume are due to the variation of the porosity of the solid phase, which, in turn, equals the volumetric fraction of the fluid phase because of the hypothesis of saturation. Hence, if, for instance, the porosity of the solid phase diminishes in response to a compressing loading, the fluid, which occupies entirely the pores of the solid phase, has to flow away from the compressed zones, thereby allowing for a global change of volume.

By denoting by $\varphi_{0\mathrm{s}}$ and $\varphi_{1\mathrm{s}}$ the volumetric fractions of the matrix and of the reinforcing fibers, respectively, and by indicating with φ_{p} the *porosity*, i.e., the volumetric fraction associated with the pore space of the solid phase as a whole, the identity $\varphi_{0\mathrm{s}} + \varphi_{1\mathrm{s}} + \varphi_{\mathrm{p}} = 1$ holds true (see e.g. [29]). However, because of the hypothesis of saturation, φ_{p} must equal the volumetric fraction of the fluid phase, φ_{f}, i.e., $\varphi_{\mathrm{p}} \equiv \varphi_{\mathrm{f}}$, which yields the condition

$$\varphi_{0\mathrm{s}} + \varphi_{1\mathrm{s}} + \varphi_{\mathrm{f}} = \varphi_{\mathrm{s}} + \varphi_{\mathrm{f}} = 1, \tag{1}$$

where $\varphi_{\mathrm{s}} := \varphi_{0\mathrm{s}} + \varphi_{1\mathrm{s}}$ is the volumetric fraction of the solid phase as a whole.

In this work, we do not tackle growth phenomena or inter-phase mass transfer processes, but we consider the remodeling of the tissue due to the reorganization of the extracellular matrix or due to the formation of irreversible strains (as is the case for damaged tissues [60, 61]). Moreover, similarly to what is done in plasticity, we describe remodeling in terms of anelastic distortions through the generally incompatible tensor $\boldsymbol{F}_{\gamma}$, introduced by means of the Bilby–Kröner–Lee (BKL) decomposition (see e.g.

[62])

$$\boldsymbol{F} = \boldsymbol{F}_{\mathrm{e}}\boldsymbol{F}_{\gamma}, \tag{2}$$

where $\boldsymbol{F}_{\mathrm{e}}$ characterizes the elastic distortions that take place in the tissue to accommodate for $\boldsymbol{F}_{\gamma}$. For future use, we denote by $J := \det\boldsymbol{F} > 0$, $J_{\mathrm{e}} := \det\boldsymbol{F}_{\mathrm{e}} > 0$, and $J_{\gamma} := \det\boldsymbol{F}_{\gamma} > 0$ the determinants of $\boldsymbol{F}$, $\boldsymbol{F}_{\mathrm{e}}$, and $\boldsymbol{F}_{\gamma}$, respectively. In particular, we prescribe the condition $J_{\gamma} = 1$ since, in our present work and for the considered time scales, the processes described by $\boldsymbol{F}_{\gamma}$ concern solely the isochoric alteration of the structural properties of the extracellular matrix. Indeed, we assume here that the fibers do not grow, are not reabsorbed, and do not undergo internal processes. Clearly, each of these processes does occur, and are studied elsewhere [4, 44]. In this respect, our modeling choice is dictated solely by simplicity and has the purpose of focusing on the main point of our work, which is the stochastic description of the fiber reorientation.

Once $\boldsymbol{F}_{\gamma}$ is introduced, it is possible to characterize the "natural —or relaxed— state" of the biological medium under study as $\mathcal{N}(t) = \cup_{X\in\mathscr{B}}\big(\{X\}\times\mathcal{N}_X(t)\big)$, where, at a given instant of time t, $\mathcal{N}_X(t) := \boldsymbol{F}_{\gamma}(X,t)T_X\mathscr{B}$ is the relaxed state of the *"material neighborhood"* [40] of X (*"body element"*, in the terminology of [63]), identified with the tangent space of the body's reference placement $\mathscr{B}$ at the point X, i.e., $T_X\mathscr{B}$ (see also [64] for a discussion on this issue). Here, the notation "$\boldsymbol{F}_{\gamma}(X,t)T_X\mathscr{B}$" means that $\boldsymbol{F}_{\gamma}(X,t)$ is applied to the whole tangent space $T_X\mathscr{B}$, while the terminology "relaxed state" indicates that $\mathcal{N}_X(t)$ is free of residual stresses due, e.g., to the formation of geometric incompatibilities. Here, however, by adhering to the approach developed in [65], we consider the simplified setting in which $\mathcal{N}_X(t)$ is viewed as the relaxed "version" of $T_X\mathscr{B}$ itself.

We complete the geometric setting that acts as background in our work (see e.g. [66]) by introducing the metric tensors $\boldsymbol{G}$, $\boldsymbol{\eta}$, and $\boldsymbol{g}$, associated with the reference placement, with the natural state, and with the current placement, respectively. Although it is often assumed to work within a Cartesian setting, from a conceptual point of view, the introduction of an underlying geometric setting, along with the covariant formalism, allows us to "put order" in the presentation of the forthcoming results.

For future use, we also introduce the volumetric fractions associated with the matrix, fibers, and interstitial fluid measured per unit volume of the relaxed state and of the reference placement $\mathscr{B}$. Hence, in general, we write $\Phi_{0s\nu} := J_{\mathrm{e}}\varphi_{0s}$ and $\Phi_{1s\nu} := J_{\mathrm{e}}\varphi_{1s}$ for the pull-backs of the volumetric fractions of the matrix and of the fibers to the natural state, and we write $\Phi_{0s} := J\varphi_{0s} = J_{\gamma}\Phi_{0s\nu}$ and $\Phi_{1s} := J\varphi_{1s} = J_{\gamma}\Phi_{1s\nu}$ for the same quantities expressed per unit volume of the reference placement. For the volumetric fraction of the fluid, we write $\Phi_{\mathrm{f}} := J\varphi_{\mathrm{f}}$ and $\Phi_{\mathrm{f}\nu} := J_{\mathrm{e}}\varphi_{\mathrm{f}}$, while we set $\Phi_{\mathrm{s}} := J\varphi_{\mathrm{s}}$ and $\Phi_{\mathrm{s}\nu} := J_{\mathrm{e}}\varphi_{\mathrm{s}}$ for the solid. In fact, since $J_{\gamma}(X,t)$ is equal to unity at all points $X\in\mathscr{B}$ and at all times, the following identities apply: $\Phi_{0s}\equiv\Phi_{0s\nu}$, $\Phi_{1s}\equiv\Phi_{1s\nu}$, and $\Phi_{\mathrm{f}}\equiv\Phi_{\mathrm{f}\nu}$.

2.2 Revisited Principle of Virtual Power

In this section, we adhere to the formulation proposed by [51, 52] to revisit the Principle of Virtual Power (PVP) for the case of the dynamics of a mixture made of intrinsically incompressible phases. For this purpose, we regard the saturation condition, the mass balance of each phase, and the shared kinematics of fibers and matrix as constraints. In fact, from here on, the extracellular matrix and the fibers are assumed to have the same velocity $\boldsymbol{V}_{0s} = \boldsymbol{V}_{1s} = \boldsymbol{V}_{\mathrm{s}}$, which characterizes the homogenized kinematics of the mixture.

Because of incompressibility, the mass balance laws of the constituents of the mixture become balance equations for the volumetric fractions of the constituents themselves. Furthermore, these balance laws are viewed as constraints relating the evolution of the volumetric fractions with the velocities of the solid and of the fluid phase. In particular, such constraints are combined so as to re-obtain the relations $\Phi_{0s} = J\varphi_{0s}$ and $\Phi_{1s} = J\varphi_{1s}$ for the solid constituents, and a relation between $\dot{J}$ and the material divergence of the material filtration velocity $\boldsymbol{Q} := \Phi_{\mathrm{f}}(\boldsymbol{V}_{\mathrm{f}} - \boldsymbol{V}_{\mathrm{s}})\boldsymbol{F}^{-\mathrm{T}}$, i.e., $\dot{J} + \mathrm{Div}\boldsymbol{Q} = 0$.

We consider the constraints of saturation, of "shared" kinematics $\boldsymbol{V}_{0s} = \boldsymbol{V}_{1s} = \boldsymbol{V}_{\mathrm{s}}$, and of the mass balances of the solid constituents in explicit form, so that the constrained quantities are expressed in

terms of the "free" ones, whereas the mass balance of the mixture as a whole and the isochoricity of the remodeling distortions are handled implicitly. With this wording, we mean here that these constraints are studied by the Lagrange multiplier technique.

To this end, we consider the *virtual* velocity fields $(\boldsymbol{V}_{\mathrm{vs}}, \boldsymbol{V}_{\mathrm{vf}}, \boldsymbol{\mathcal{V}}_{\mathrm{v}\gamma})$, defined over the medium's reference placement and associated with the kinematic descriptors $(\boldsymbol{V}_{\mathrm{s}}, \boldsymbol{V}_{\mathrm{f}}, \dot{\boldsymbol{F}}_{\gamma})$. Moreover, by introducing the generalized forces that are power-conjugate with $(\boldsymbol{V}_{\mathrm{vs}}, \boldsymbol{V}_{\mathrm{vf}}, \boldsymbol{\mathcal{V}}_{\mathrm{v}\gamma})$, we write the real-valued functionals of the internal and external virtual powers (see [67])

$$\mathcal{W}_{\mathrm{v}}^{(\mathrm{int})}(\boldsymbol{V}_{\mathrm{vs}}, \boldsymbol{V}_{\mathrm{vf}}, \boldsymbol{\mathcal{V}}_{\mathrm{v}\gamma}) := -\int_{\mathscr{B}} \left\{ \sum_{\alpha} J\, \boldsymbol{m}_{\alpha} \boldsymbol{V}_{\mathrm{v}\alpha} + \sum_{\alpha} \boldsymbol{P}_{\alpha} : \mathrm{Grad} \boldsymbol{V}_{\mathrm{v}\alpha} \right\} - \int_{\mathscr{B}} \boldsymbol{F}_{\gamma}^{-\mathrm{T}} \boldsymbol{Y}_{\mathrm{u}} : \boldsymbol{\mathcal{V}}_{\mathrm{v}\gamma}, \tag{3a}$$

$$\mathcal{W}_{\mathrm{v}}^{(\mathrm{ext})}(\boldsymbol{V}_{\mathrm{vs}}, \boldsymbol{V}_{\mathrm{vf}}, \boldsymbol{\mathcal{V}}_{\mathrm{v}\gamma}) := \int_{\mathscr{B}} \sum_{\alpha} J \rho_{\alpha} \boldsymbol{f}\, \boldsymbol{V}_{\mathrm{v}\alpha} + \int_{\partial\mathscr{B}} \sum_{\alpha} \xi_{\alpha} \boldsymbol{\tau} \boldsymbol{V}_{\mathrm{v}\alpha} + \int_{\mathscr{B}} \boldsymbol{F}_{\gamma}^{-\mathrm{T}} \boldsymbol{Z} : \boldsymbol{\mathcal{V}}_{\mathrm{v}\gamma}, \tag{3b}$$

where the sum over the index α must be understood on the set $\{\mathrm{s}, \mathrm{f}\}$. In Equation (3a), $\boldsymbol{P}_{\alpha}$ is the active part of the stress tensor associated with the αth phase; $J\boldsymbol{m}_{\alpha}$ is the density, per unit volume of the reference placement, of the linear momentum exchanged between the solid phase as a whole (matrix and fibers) and the fluid phase; $\boldsymbol{F}_{\gamma}^{-\mathrm{T}} \boldsymbol{Y}_{\mathrm{u}}$ is the generalized force that is power-conjugate with $\boldsymbol{\mathcal{V}}_{\mathrm{v}\gamma}$. In Equation (3b), $J\rho_{\alpha}\boldsymbol{f}$ is the αth contribution, with $\alpha \in \{\mathrm{s}, \mathrm{f}\}$, of the external body force densities acting on the mixture and expressed per unit volume of the reference placement, while ρ_{α} is the apparent mass density of the αth phase, which is defined as the product $\rho_{\alpha} = \varphi_{\alpha}\varrho_{\alpha}$, with ϱ_{α} being the "true", or intrinsic, mass density; $\xi_{\alpha}\boldsymbol{\tau}$ is the contact force on the portion of $\partial\mathscr{B}$ with area fraction ξ_{α} of the αth component; $\boldsymbol{F}_{\gamma}^{-\mathrm{T}}\boldsymbol{Z}$ is the external generalized force dual to $\boldsymbol{\mathcal{V}}_{\mathrm{v}\gamma}$ [68, 63, 51, 52, 69].

To study the constraints handled in implicit form, we follow the procedure described in [51, 52], and we write them in differential form as

$$\hat{C}_{\mathrm{tot}} \circ (\boldsymbol{F}, \boldsymbol{F}_{\gamma}, \boldsymbol{V}_{\mathrm{s}}, \boldsymbol{V}_{\mathrm{f}}) = \mathrm{Div}\left[J_{\gamma} (\Phi_{\mathrm{s}\nu} \boldsymbol{V}_{\mathrm{s}} + \Phi_{\mathrm{f}\nu} \boldsymbol{V}_{\mathrm{f}}) \boldsymbol{F}^{-\mathrm{T}} \right] = 0, \tag{4a}$$

$$\hat{C}_{\gamma} \circ (\boldsymbol{F}_{\gamma}, \dot{\boldsymbol{F}}_{\gamma}) = \boldsymbol{F}_{\gamma}^{-\mathrm{T}} : \dot{\boldsymbol{F}}_{\gamma} = \boldsymbol{I}^{\mathrm{T}} : \boldsymbol{F}_{\gamma}^{-1} \dot{\boldsymbol{F}}_{\gamma} = 0. \tag{4b}$$

Note that, since Equations (4a) and (4b) are linear in the velocities, the Chetaev forms [70, 71, 72] of the constraints (4a) and (4b) can be obtained by replacing $\boldsymbol{V}_{\mathrm{s}}$, $\boldsymbol{V}_{\mathrm{f}}$, and $\dot{\boldsymbol{F}}_{\gamma}$ with their virtual counterparts. Hence, after introducing the Lagrange multipliers P and μ_{γ} associated with the constraints, and by following the procedure depicted in [51, 52], we write the augmented form of the internal virtual power as

$$\begin{aligned} &\mathcal{W}_{\mathrm{v}}^{(\mathrm{int,a})}(\boldsymbol{V}_{\mathrm{vs}}, \boldsymbol{V}_{\mathrm{vf}}, \boldsymbol{\mathcal{V}}_{\mathrm{v}\gamma}, P_{\mathrm{v}}, \mu_{\mathrm{v}\gamma}) \\ &:= \mathcal{W}_{\mathrm{v}}^{(\mathrm{int})}(\boldsymbol{V}_{\mathrm{vs}}, \boldsymbol{V}_{\mathrm{vf}}, \boldsymbol{\mathcal{V}}_{\mathrm{v}\gamma}) + \int_{\mathscr{B}} \left\{ P[\hat{C}_{\mathrm{tot}} \circ (\boldsymbol{F}, \boldsymbol{F}_{\gamma}, \boldsymbol{V}_{\mathrm{vs}}, \boldsymbol{V}_{\mathrm{vf}})] - \mu_{\gamma}[\hat{C}_{\gamma} \circ (\boldsymbol{F}_{\gamma}, \boldsymbol{\mathcal{V}}_{\mathrm{v}\gamma})] \right\} \\ &\quad + \int_{\mathscr{B}} \left\{ P_{\mathrm{v}}[\hat{C}_{\mathrm{tot}} \circ (\boldsymbol{F}, \boldsymbol{F}_{\gamma}, \boldsymbol{V}_{\mathrm{s}}, \boldsymbol{V}_{\mathrm{f}})] - \mu_{\mathrm{v}\gamma}[\hat{C}_{\gamma} \circ (\boldsymbol{F}_{\gamma}, \dot{\boldsymbol{F}}_{\gamma})] \right\}. \end{aligned} \tag{5}$$

Next, we impose the Principle of Virtual Power, thereby requiring the total virtual power, obtained as the sum of the augmented internal virtual power and the external virtual power, to be null for any arbitrary set of virtual fields $(\boldsymbol{V}_{\mathrm{vs}}, \boldsymbol{V}_{\mathrm{vf}}, \boldsymbol{\mathcal{V}}_{\mathrm{v}\gamma}, P_{\mathrm{v}}, \mu_{\mathrm{v}\gamma})$, i.e.,

$$\mathcal{W}_{\mathrm{v}}^{(\mathrm{int,a})}(\boldsymbol{V}_{\mathrm{vs}}, \boldsymbol{V}_{\mathrm{vf}}, \boldsymbol{\mathcal{V}}_{\mathrm{v}\gamma}, P_{\mathrm{v}}, \mu_{\mathrm{v}\gamma}) + \mathcal{W}_{\mathrm{v}}^{(\mathrm{ext})}(\boldsymbol{V}_{\mathrm{vs}}, \boldsymbol{V}_{\mathrm{vf}}, \boldsymbol{\mathcal{V}}_{\mathrm{v}\gamma}) = 0. \tag{6}$$

Hence, standard arguments permit to write the dynamic equations and the implicit constraints in the reference placement $\mathscr{B}$, i.e.,

$$\mathrm{Div}\boldsymbol{P}_{\alpha} - J\boldsymbol{m}_{\alpha} - J_{\gamma}\Phi_{\alpha\nu}\boldsymbol{F}^{-\mathrm{T}}\mathrm{Grad}P + J_{\gamma}\varrho_{\alpha}\Phi_{\alpha\nu}\boldsymbol{f} = \boldsymbol{0}, \qquad \text{with } \alpha \in \{\mathrm{s}, \mathrm{f}\}, \tag{7a}$$

$$\mathrm{Div}\left[J_{\gamma}\boldsymbol{F}^{-1}(\Phi_{\mathrm{s}\nu}\boldsymbol{V}_{\mathrm{s}} + \Phi_{\mathrm{f}\nu}\boldsymbol{V}_{\mathrm{f}}) \right] = 0, \tag{7b}$$

$$\boldsymbol{Y}_{\mathrm{u}} + \mu_{\gamma}\boldsymbol{I}^{\mathrm{T}} - \boldsymbol{Z} = \boldsymbol{O}, \tag{7c}$$

$$\boldsymbol{F}_\gamma^{-\mathrm{T}} : \dot{\boldsymbol{F}}_\gamma = 0, \tag{7d}$$

which are accompanied by boundary and initial conditions of the type [67]

$$(\boldsymbol{P}_\alpha - J_\gamma \Phi_{\alpha\nu} P \boldsymbol{F}^{-\mathrm{T}})\boldsymbol{N} = \xi_\alpha \boldsymbol{\tau}, \qquad \text{with } \alpha \in \{\mathrm{s},\mathrm{f}\}, \qquad \text{on } \partial_{\mathrm{N}}\mathscr{B}, \tag{8a}$$

$$\chi = \chi_{\mathrm{b}}, \qquad \text{on } \partial_{\mathrm{D}}\mathscr{B}, \tag{8b}$$

$$\boldsymbol{V}_{\mathrm{f}} = \boldsymbol{V}_{\mathrm{fb}}, \qquad \text{on } \partial_{\mathrm{D}}\mathscr{B}, \tag{8c}$$

$$\chi(X, t_{\mathrm{in}}) = \chi_{\mathrm{in}}(X), \qquad \text{in } \mathscr{B}, \tag{8d}$$

$$\boldsymbol{F}_\gamma(X, t_{\mathrm{in}}) = \boldsymbol{F}_{\gamma\mathrm{in}}(X), \qquad \text{in } \mathscr{B}. \tag{8e}$$

These conditions are purely formal at this stage, and have to be specialized for the problems to be solved (see section 5). Since the mass balance laws for the constituents of the solid phase reduce to the equations $\dot{\Phi}_{0\nu\mathrm{s}} = 0$ and $\dot{\Phi}_{1\nu\mathrm{s}} = 0$ because of the isochoricity constraint $J_\gamma = 1$, the volumetric fractions in the natural state read $\Phi_{0\mathrm{s}\nu}(X,t) = \Phi_{0\mathrm{in}}(X)$ and $\Phi_{1\mathrm{s}\nu}(X,t) = \Phi_{1\mathrm{in}}(X)$ at all times and for all $X \in \mathscr{B}$, where $\Phi_{0\mathrm{in}}(X)$ and $\Phi_{1\mathrm{in}}(X)$ define the initial volumetric fractions of the matrix and of the fibers.

We notice, in addition, that the volumetric fractions in the reference placement are $\Phi_{0\mathrm{s}}(X,t) = \Phi_{0\mathrm{s}\nu}(X,t) = \Phi_{0\mathrm{in}}(X)$ and $\Phi_{1\mathrm{s}}(X,t) = \Phi_{1\mathrm{s}\nu}(X,t) = \Phi_{1\mathrm{in}}(X)$, for all $X \in \mathscr{B}$.

We remark that, in Equation (7a), $\boldsymbol{P}_\alpha$ can be identified with the *constitutive* first Piola–Kirchhoff stress tensor of the αth phase, whereas $\boldsymbol{m}_\alpha$ is the dissipative part of the exchange of linear momentum between the fluid phase and the solid phase as a whole. Moreover, we assume that the mixture is closed under exchange of linear momentum, so that $\boldsymbol{m}_{\mathrm{s}} + \boldsymbol{m}_{\mathrm{f}} = \boldsymbol{0}$ [73, 74, 75, 76, 7, 77]. Finally, a suitable constitutive characterization of $\boldsymbol{m}_{\mathrm{f}}$ extracts Darcy's Law (see e.g. [2]) from Equation (7a), written for $\alpha = \mathrm{f}$.

We notice that we can split Equation (7c) in its spherical and deviatoric parts, the former of which gives an expression for the *a posteriori* determination of μ_γ [51], i.e.,

$$\mu_\gamma = -\tfrac{1}{3}\mathrm{tr}(\boldsymbol{Y}_{\mathrm{u}}) + \tfrac{1}{3}\mathrm{tr}(\boldsymbol{Z}), \qquad \text{in } \mathscr{B}, \tag{9a}$$

$$\mathrm{dev}\boldsymbol{Y}_{\mathrm{u}} - \mathrm{dev}\boldsymbol{Z} = \boldsymbol{O}, \qquad \text{in } \mathscr{B}. \tag{9b}$$

By adding together Equation (7a) over $\alpha \in \{\mathrm{s},\mathrm{f}\}$, setting $\varrho = \varphi_{\mathrm{s}}\varrho_{\mathrm{s}} + \varphi_{\mathrm{f}}\varrho_{\mathrm{f}}$, and exploiting the relation $\boldsymbol{m}_{\mathrm{s}} + \boldsymbol{m}_{\mathrm{f}} = \boldsymbol{0}$ as well as Piola's identity [66], we obtain the set of equations

$$\mathrm{Div}(\boldsymbol{P}_{\mathrm{s}} + \boldsymbol{P}_{\mathrm{f}}) - J\boldsymbol{F}^{-\mathrm{T}}\mathrm{Grad}P + J\varrho\boldsymbol{f} = \boldsymbol{0}, \tag{10a}$$

$$\mathrm{Div}\boldsymbol{P}_{\mathrm{f}} - J\boldsymbol{m}_{\mathrm{f}} - J_\gamma\Phi_{\mathrm{f}\nu}\boldsymbol{F}^{-\mathrm{T}}\mathrm{Grad}P + J_\gamma\varrho_{\mathrm{f}}\Phi_{\mathrm{f}\nu}\boldsymbol{f} = \boldsymbol{0}, \tag{10b}$$

$$\mathrm{Div}\left[J_\gamma\boldsymbol{F}^{-1}(\Phi_{\mathrm{s}\nu}\boldsymbol{V}_{\mathrm{s}} + \Phi_{\mathrm{f}\nu}\boldsymbol{V}_{\mathrm{f}})\right] = 0, \tag{10c}$$

$$\mathrm{dev}\boldsymbol{Y}_{\mathrm{u}} - \mathrm{dev}\boldsymbol{Z} = \boldsymbol{O}, \tag{10d}$$

$$\boldsymbol{F}_\gamma^{-\mathrm{T}} : \dot{\boldsymbol{F}}_\gamma = 0, \tag{10e}$$

in which μ_γ does not appear because Equation (9a) allows to determine it after the dynamic equations are solved. For this reason, μ_γ can be eliminated from the set of the unknowns of the problem. Moreover, since we are considering explicitly the mass balance of the solid constituents, the volumetric fractions of the matrix and of the fibers are determined by $\varphi_{0\mathrm{s}} = J^{-1}\Phi_{0\mathrm{in}}$ and $\varphi_{1\mathrm{s}} = J^{-1}\Phi_{1\mathrm{in}}$, with $\varphi_{\mathrm{s}} = J^{-1}(\Phi_{0\mathrm{in}} + \Phi_{1\mathrm{in}})$. Therefore, also $\varphi_{0\mathrm{s}}$ and $\varphi_{1\mathrm{s}}$ can be removed from the set of unknowns.

In conclusion, the unknowns featuring in Equations (10a)–(10e) consists of 46 variables: 3 for the components of the motion χ; 3 for the components of the fluid velocity $\boldsymbol{V}_{\mathrm{f}}$; 9 for the components of $\boldsymbol{P}_{\mathrm{s}}$; 9 for the components of $\boldsymbol{P}_{\mathrm{f}}$; 3 for the components of $\boldsymbol{m}_{\mathrm{f}}$; 9 for the components of $\boldsymbol{F}_\gamma$; 9 for the components of $\boldsymbol{Y}_{\mathrm{u}}$; and 1 for the Lagrange multiplier P, associated with the mass balance of the mixture as a whole. Since $\boldsymbol{f}$, $\boldsymbol{\tau}$, and $\boldsymbol{Z}$ are external forces assigned from the outset, from now on we consider them as given quantities, with an expression that depends on the case to which the model is specialized. In the following sections, we supply the constitutive expressions of $\boldsymbol{P}_{\mathrm{s}}$, $\boldsymbol{P}_{\mathrm{f}}$, $\boldsymbol{m}_{\mathrm{f}}$, and $\boldsymbol{Y}_{\mathrm{u}}$, thereby adding 30 scalar equations. Hence, the model consists of 46 scalar equations for 46 macroscopic variables.

However, at the mesoscopic scale, the biological tissue is characterized by the presence of fibers, and the mechanical properties of the medium are heavily influenced by their orientations. In this framework, we will describe the probability distribution that a fiber is aligned along a certain direction as the solution of a prototype evolutionary law [50], thereby considering it as an additional unknown of the problem, coupled with the deformation at the macroscale, but determined by its own dynamics.

2.3 Stochastic dynamics of the fiber angle distribution

Following a standard notation in continuum mechanics [24, 8, 12, 13, 14, 15, 16, 17, 25, 26, 10, 18, 27, 28, 29, 19, 30, 20, 31, 32, 35, 33, 78, 79], for each point $X \in \mathscr{B}$, we define the *set of all directions* in the reference placement $\mathscr{B}$ as

$$\mathbb{S}^2_X\mathscr{B} := \big\{\boldsymbol{M}_X \in T_X\mathscr{B} : \|\boldsymbol{M}_X\| = 1\big\}, \tag{11}$$

where $T_X\mathscr{B}$ is the tangent space of $\mathscr{B}$ at $X \in \mathscr{B}$ [66]. The tangent bundle of $\mathscr{B}$ is $T\mathscr{B} := \cup_{X\in\mathscr{B}}(\{X\} \times T_X\mathscr{B})$. In the sequel, we denote by $(T_X\mathscr{B})^*$ the cotangent space of $\mathscr{B}$ at X, i.e., the dual space of $T_X\mathscr{B}$, and by $(T\mathscr{B})^*$ the cotangent bundle. We also define the bundle $\mathbb{S}^2\mathscr{B} = \cup_{X\in\mathscr{B}}(\{X\} \times \mathbb{S}^2_X\mathscr{B})$ along with the field of unit vectors $\boldsymbol{M} : \mathscr{B} \mapsto \mathbb{S}^2\mathscr{B}$, such that $\boldsymbol{M}(X) := (X, \boldsymbol{M}_X) \in (\{X\} \times \mathbb{S}^2_X\mathscr{B})$ and $\boldsymbol{M}_X \in \mathbb{S}^2_X\mathscr{B}$. Together with $\mathbb{S}^2_X\mathscr{B}$ and $\mathbb{S}^2\mathscr{B}$, we introduce $(\mathbb{S}^2_X\mathscr{B})^*$ and $(\mathbb{S}^2\mathscr{B})^*$ as the subsets of $(T_X\mathscr{B})^*$ and $(T\mathscr{B})^*$ generated by all the real-valued linear and bounded maps defined over $\mathbb{S}^2_X\mathscr{B}$ and $\mathbb{S}^2\mathscr{B}$, respectively.

By employing local spherical coordinates, a generic element $\boldsymbol{M}_X \in \mathbb{S}^2_X\mathscr{B}$ can be expressed through the parameterization

$$\hat{\boldsymbol{M}}_X : [0,\pi] \times [0, 2\pi[\to \mathbb{S}^2_X\mathscr{B}, \tag{12a}$$

$$\boldsymbol{M}_X = \hat{\boldsymbol{M}}_X(\Theta,\Phi) = \sin\Theta\cos\Phi\,\boldsymbol{E}_1 + \sin\Theta\sin\Phi\,\boldsymbol{E}_2 + \cos\Theta\,\boldsymbol{E}_3, \tag{12b}$$

where $\{\boldsymbol{E}_1, \boldsymbol{E}_2, \boldsymbol{E}_3\} \in T_X\mathscr{B}$ is an orthonormal vector basis of $T_X\mathscr{B}$ (to make the notation lighter, we omit the subscript "X" in the specification of the unit vectors $\boldsymbol{E}_A$, for $A = 1, 2, 3$).

In the "classical" literature on fiber-reinforced media (see e.g. [24, 8, 12, 13, 14, 15, 16, 17, 25, 26, 10, 18, 27, 28, 29, 19, 30, 20, 31, 32, 35, 33, 78, 79]), the directions of fiber reinforcement $\boldsymbol{M}_X$ undergo no evolution in time apart from the passive one $\boldsymbol{M}_X \mapsto \boldsymbol{F}(X,t)\boldsymbol{M}_X$, since each $\boldsymbol{M}_X$ describes a preferred direction in the reference placement of the body. Quite differently, however, in some other works on *remodeling*, the generic $\boldsymbol{M}_X$ is endowed with its own kinematics (see e.g. [56]). The purpose of this modeling choice is to capture the capability of the fibers of changing their orientation not only in response to deformation or to stress, but also as a result of their inherent dynamics. To the best of our understanding, it is in this sense that one speaks of "active evolution" when referring to the remodeling of the fibers, since this remodeling is, in fact, a manifestation of the fibers' intrinsic evolution. In this respect, we emphasize that, in our work, we have two types of remodeling: the one described by $\boldsymbol{F}_\gamma$, and the one expressed by the intrinsic capability of the fibers to reorient.

Whereas models of the type mentioned above remind of Cosserat media (see e.g. [80]), a different point of view, suggested in [81] and, later, in [6, 82, 31, 32], applies to fiber-reinforced composite media with statistical distribution of orientation of the fibers. In these papers, it is assumed that the probability density distribution of fiber alignment at a given point of the composite medium under study depends on the most probable direction of orientation, the latter being regarded as an independent kinematic variable subjected to its own remodeling dynamics ("active" evolution). More specifically, the probability density distribution is assigned from the outset, while the evolution of the most probable orientation solves an initial- and boundary-value problem (IBVP) [31, 32] coupled with the deformation and, when considered, with other forms of remodeling [32]. In the present work, however, we propose another perspective, which expands the previous ones in that the probability density distribution *is not* given a priori, but is rather an unknown of the model and is determined by solving a Fokker–Planck equation. In fact, this idea was suggested in [6], but not developed therein, and it has recently been expanded in [83, 50]. The main ingredients of this latter perspective can be summarized as follows.

To account for the evolution of the preferred direction associated with the generic $\boldsymbol{M}_X \in \mathbb{S}^2_X\mathscr{B}$, we hypothesize that $\boldsymbol{M}_X$ can be seen as the imagine of a function of time obtained by composition of $\hat{\boldsymbol{M}}_X$ with the unknown angular functions

$$\theta : [t_{\text{in}}, t_{\text{fin}}] \to \mathbb{R}, \qquad \phi : [t_{\text{in}}, t_{\text{fin}}] \to \mathbb{R}, \tag{13}$$

defined over the time window $[t_{\text{in}}, t_{\text{fin}}]$ over which the considered system is observed, and we write

$$\boldsymbol{M}_X = \hat{\boldsymbol{M}}_X(\theta(t), \phi(t)) = \check{\boldsymbol{M}}_X(t), \qquad \check{\boldsymbol{M}}_X := \hat{\boldsymbol{M}}_X \circ (\theta, \phi) : [t_{\text{in}}, t_{\text{fin}}] \to \mathbb{S}^2_X\mathscr{B}. \tag{14}$$

Since the time change of $\check{\boldsymbol{M}}_X$ is expressed in terms of θ and ϕ through Equation (14), we regard these two functions as generalized Lagrangian parameters of our theory (see e.g. [56]), and we prescribe that they evolve in time as dictated by a suitable *local* force balance taking on the form (see [56, 83, 50])

$$\gamma_\Theta \dot{\theta} = \frac{\partial \hat{\mathcal{W}}}{\partial \Theta} \circ (\boldsymbol{F}, \boldsymbol{F}_\gamma, \theta, \phi, \mathcal{X}) + \underbrace{\mathcal{F}^{\text{ext,det}}_\Theta + \mathcal{F}^{\text{ext,noise}}_\Theta}_{\equiv \mathcal{F}^{\text{ext}}_\Theta}, \tag{15a}$$

$$\gamma_\Phi \dot{\phi} = \frac{1}{\sin\theta} \frac{\partial \hat{\mathcal{W}}}{\partial \Phi} \circ (\boldsymbol{F}, \boldsymbol{F}_\gamma, \theta, \phi, \mathcal{X}) + \underbrace{\mathcal{F}^{\text{ext,det}}_\Phi + \mathcal{F}^{\text{ext,noise}}_\Phi}_{\equiv \mathcal{F}^{\text{ext}}_\Phi}, \tag{15b}$$

where γ_Θ and γ_Φ are damping coefficients, with units $\mathrm{N}\cdot\mathrm{s}/\mathrm{m}^2$, here assumed to be strictly positive and coincident $\gamma_\Theta = \gamma_\Phi = \gamma$, and defining the dissipative nature of the generalized forces $\gamma\dot{\theta}$ and $\gamma\dot{\phi}$; $\hat{\mathcal{W}}$ is the solid medium's strain energy function per unit volume, while $\mathcal{F}^{\text{ext}}_\Theta := \mathcal{F}^{\text{ext,det}}_\Theta + \mathcal{F}^{\text{ext,noise}}_\Theta$ and $\mathcal{F}^{\text{ext}}_\Phi := \mathcal{F}^{\text{ext,det}}_\Phi + \mathcal{F}^{\text{ext,noise}}_\Phi$ are generalized forces, conceived as external (see the discussion reported in section 4.2, in which they will be expressed explicitly), that feature both the deterministic terms $\mathcal{F}^{\text{ext,det}}_\Theta$ and $\mathcal{F}^{\text{ext,det}}_\Phi$, and the *stochastic* terms $\mathcal{F}^{\text{ext,noise}}_\Theta$ and $\mathcal{F}^{\text{ext,noise}}_\Phi$. Note that $\hat{\mathcal{W}}$ is composed also with the map $\mathcal{X}$, such that $\mathcal{X}(X,t) = X$ for all $(X,t) \in \mathscr{B} \times \mathscr{I}$, where $\mathscr{I}$ is the time line, to highlight that the material is inhomogeneous in general. Finally, the derivatives of $\hat{\mathcal{W}}$ with respect to Θ and Φ are non-dissipative contributions to generalized forces power-conjugate with $\dot{\theta}$ and $\dot{\phi}$.

Since Equations (15a) and (15b) express the process of reorientation of a fiber embedded in the extracellular matrix, the non-dissipative contributions due to the interactions with the matrix, given by the derivatives of $\hat{\mathcal{W}}$ with respect to Θ and Φ, have to be regarded as external generalized forces. In fact, these terms describe the agency of the extracellular matrix on the fibers embedded in it, and represent a deterministic drift term guiding the fiber reorientation.

We emphasize here that stochastic models of fiber reorientation have been recently proposed in [83] for a problem of cell reorientation and in [50] within a study on fiber reinforced composite materials. It is also important to mention that, beyond some "technical" differences between the model presented in the sequel and the one proposed in [56] (these essentially referring to the way in which $\hat{\mathcal{W}}$ and the forces $\mathcal{F}^{\text{ext}}_\Theta$ and $\mathcal{F}^{\text{ext}}_\Phi$ are constructed), the most relevant features of the theory discussed in our work are as follows:

- On the trail of an idea put forward in [6], and by elaborating the framework presented in [83, 50], we introduce stochastic sources $\mathcal{F}^{\text{ext,noise}}_\Theta$ and $\mathcal{F}^{\text{ext,noise}}_\Phi$ that drive the dynamics of the angle functions θ and ϕ, thereby interpreting Equations (15a) and (15b) as Langevin-like evolution laws for θ and ϕ. Hence, whereas in [56] $\mathcal{F}^{\text{ext}}_\Theta$ and $\mathcal{F}^{\text{ext}}_\Phi$ are related to the deterministic concept of *"target angle"* [17, 56] only, we *presume* here that the reorientation of the fibers is influenced also by reciprocal interactions that, understood as the easiest type of "collisions", may be described through a *white noise*. On the basis of these considerations, and by employing a well-established procedure in the field of stochastic processes, we replace Equations (15a) and (15b), which are valid at the scale of a single fiber (or of a family of fibers aligned along the same direction), with the resulting Fokker–Planck equation in the associated probability density distribution [6, 83, 50]. This distribution,

denoted by $\hat{f}_{\mathrm{R}}$ when expressed with respect to the reference placement $\mathscr{B}$ of the composite, must thus satisfy the Fokker–Planck equation on the boundary of the sphere associated with $\mathbb{S}^2_X\mathscr{B}$, i.e.,

$$\partial_t \hat{f}_{\mathrm{R}} = -\frac{1}{\sin\Theta}\frac{\partial}{\partial\Theta}\left[\frac{1}{\gamma}\left(\mathcal{F}_{\Theta}^{\mathrm{ext,det}} + \frac{\partial\hat{\mathcal{W}}}{\partial\Theta}\right)\sin\Theta\,\hat{f}_{\mathrm{R}}\right] - \frac{1}{\sin\Theta}\frac{\partial}{\partial\Phi}\left[\frac{1}{\gamma}\left(\mathcal{F}_{\Phi}^{\mathrm{ext,det}} + \frac{1}{\sin\Theta}\frac{\partial\hat{\mathcal{W}}}{\partial\Phi}\right)\hat{f}_{\mathrm{R}}\right] + D\frac{1}{\sin\Theta}\frac{\partial}{\partial\Theta}\left[\sin\Theta\frac{\partial\hat{f}_{\mathrm{R}}}{\partial\Theta}\right] + D\frac{1}{(\sin\Theta)^2}\frac{\partial^2\hat{f}_{\mathrm{R}}}{\partial\Phi^2}, \tag{16}$$

where the explicit dependence of $\partial_\Theta\hat{\mathcal{W}}$ and $\partial_\Phi\hat{\mathcal{W}}$ on their arguments has been omitted for the sake of a lighter notation; $D \in \mathbb{R}^+$ is referred to as *diffusion coefficient* and has units of $\mathrm{rad}^2/\mathrm{s}$; and $\hat{f}_{\mathrm{R}}$ is defined through the identification $\hat{f}_{\mathrm{R}}(X,\Theta,\Phi,t) \equiv f_{\mathrm{R}}(X,\boldsymbol{M}_X,t)$, with the probability density distribution f_{R} being such that

$$f_{\mathrm{R}} : \mathbb{S}^2\mathscr{B}\times\mathscr{I} \to \mathbb{R}^+, \tag{17a}$$

$$(X,\boldsymbol{M}_X,t) \mapsto f_{\mathrm{R}}(X,\boldsymbol{M}_X,t) = f_{\mathrm{R}}(X,\hat{\boldsymbol{M}}_X(\Theta,\Phi),t) \equiv \hat{f}_{\mathrm{R}}(X,\Theta,\Phi,t) \in \mathbb{R}^+. \tag{17b}$$

Since f_{R} is a probability density distribution, it has to be normalized, i.e.,

$$\int_{\mathbb{S}^2_X\mathscr{B}} f_{\mathrm{R}}(X,\boldsymbol{M}_X,t) = \int_0^{2\pi}\int_0^{\pi} \hat{f}_{\mathrm{R}}(X,\Theta,\Phi,t)\sin\Theta\,\mathrm{d}\Theta\,\mathrm{d}\Phi = 1, \tag{18}$$

for all $X \in \mathscr{B}$ and $t \in [t_{\mathrm{in}}, t_{\mathrm{fin}}]$. We emphasize that, in Equation (16), the dependence of $\hat{f}_{\mathrm{R}}$ on the point X has to be regarded as parametric, since Equation (16) has to be solved at each $X \in \mathscr{B}$ for varying time and with the angular distribution of $\hat{f}_{\mathrm{R}}$ resolved through its dependence on Θ and Φ. In addition, it should be noticed that, in general, the quantity D may depend on X, while the energy $\hat{\mathcal{W}}$ and the driving forces $\mathcal{F}_{\Theta}^{\mathrm{ext,det}}$ and $\mathcal{F}_{\Phi}^{\mathrm{ext,det}}$ may depend explicitly on X and time.

- Although Equation (16) is similar to the one studied in [83], we deviate from the model presented therein in that our Fokker–Planck equation is formulated in two dimensions (in fact, on the spherical surface parameterized by Θ and Φ), and because our *drift terms* are defined by $\mathcal{F}_{\Theta}^{\mathrm{ext,det}} + \partial_\Theta\hat{\mathcal{W}}$ and $\mathcal{F}_{\Phi}^{\mathrm{ext,det}} + (\sin\Theta)^{-1}\partial_\Phi\hat{\mathcal{W}}$, rather than by the derivatives of the strain energy density, only. The forces $\mathcal{F}_{\Theta}^{\mathrm{ext,det}}$ and $\mathcal{F}_{\Phi}^{\mathrm{ext,det}}$, in turn, will be defined on the basis of the introduction of histological target angles [17, 56]. Furthermore, our model considers, along with the stochastic reorientation of the fibers, also the other type of remodeling due to the development of anelastic distortions in the tissue, described by $\boldsymbol{F}_\gamma$. Finally, as will be shown in the forthcoming sections, we study a fully coupled problem accounting for the influence both of fiber reorientation and of anelastic distortions on the flow of the tissue's interstitial fluid.

3 Strain energy density and permeability

In this section, we briefly recall the procedure for the construction of the strain energy density function and of the permeability tensor field of the fiber reinforced medium under study. To this end, we will have recourse to the formulation presented in [31, 32], which, in turn, is largely based on the models developed in [25, 26, 84, 27, 28, 29]. We emphasize that, although much of the information reported in this section is known in the literature, we find it important to summarize it here both for the sake of completeness and in order to highlight some deviations of our present formulation from the previous ones.

The first step is the introduction of the *directional average* [24] of a generic physical quantity $\mathfrak{F}$. As done in [31], but with some notational differences from [31], at each instant of time $t \in \mathscr{I}$ and point $X \in \mathscr{B}$, we evaluate $\mathfrak{F}$ at $\boldsymbol{M}_X \in \mathbb{S}^2_X\mathscr{B}$, which identifies the direction along which a single rectified fiber is aligned. In the most general case, the arguments of $\mathfrak{F}$ are also $\boldsymbol{F}$, $\boldsymbol{F}_\gamma$, and all the model

parameters evaluated at X and t. However, to simplify the notation, we shall write $\mathfrak{F}(X, \boldsymbol{M}_X, t, \ldots)$, and, upon considering the probability density distribution f_{R} solving Equation (16), we *define* the directional average of $\mathfrak{F}$ as

$$\begin{aligned}\langle\!\langle \mathfrak{F} \rangle\!\rangle(X, t, \ldots) &= \int_{\mathbb{S}^2_X\mathscr{B}} \mathfrak{F}(X, \boldsymbol{M}_X, t, \ldots) f_{\mathrm{R}}(X, \boldsymbol{M}_X, t) \\ &= \int_0^{2\pi} \int_0^{\pi} \hat{\mathfrak{F}}(X, \Theta, \Phi, \ldots) \hat{f_{\mathrm{R}}}(X, \Theta, \Phi, t) \sin\Theta \, \mathrm{d}\Theta \, \mathrm{d}\Phi, \end{aligned} \tag{19}$$

with $\hat{\mathfrak{F}}(X, \Theta, \Phi, t, \ldots) := \mathfrak{F}(X, \boldsymbol{M}_X, t, \ldots)$. Note that $\langle\!\langle \mathfrak{F} \rangle\!\rangle$ is a "functional" of f_{R} (while $\langle\!\langle \mathfrak{F} \rangle\!\rangle$ is a true functional when $\mathfrak{F}$ is scalar-valued, we use this terminology in generalized sense when $\mathfrak{F}$ is a vector or a tensor field). We also remark that the expression of directional average provided in Equation (19) has to be understood as a definition, since we do not discuss here the ergodicity of the system under study.

As recalled in [85, 86, 31] and in the references therein, $\mathfrak{F}(X, \boldsymbol{M}_X, t, \ldots)$ is assumed to enjoy the invariance property $\mathfrak{F}(X, -\boldsymbol{M}_X, t, \ldots) = \mathfrak{F}(X, \boldsymbol{M}_X, t, \ldots)$, which has to hold for all $X \in \mathscr{B}$, $t \in \mathscr{I}$, and $\boldsymbol{M}_X \in \mathbb{S}^2_X\mathscr{B}$. In terms of $\hat{\mathfrak{F}}$, this writes $\hat{\mathfrak{F}}(X, \pi - \Theta, \Phi + \pi, t, \ldots) = \hat{\mathfrak{F}}(X, \Theta, \Phi, t, \ldots)$, for all $(\Theta, \Phi) \in [0, \pi] \times [0, 2\pi[$. In the literature on fiber reinforced composite materials with statistical orientation of the fibers, the same symmetry property is prescribed to apply also to the fiber probability density distribution f_{R}, which is thus defined in such a way that it complies with the condition $f_{\mathrm{R}}(X, -\boldsymbol{M}_X, t) = f_{\mathrm{R}}(X, \boldsymbol{M}_X, t)$ for all $\boldsymbol{M}_X \in \mathbb{S}^2_X\mathscr{B}$ (or, $\hat{f_{\mathrm{R}}}(X, \pi - \Theta, \Phi + \pi, t) = \hat{f_{\mathrm{R}}}(X, \Theta, \Phi, t)$, for all $(\Theta, \Phi) \in [0, \pi] \times [0, 2\pi[$, uniformly with respect to $X \in \mathscr{B}$ and $t \in \mathscr{I}$. In our approach, however, this property is not imposed from the outset. Rather, it should be inherited from the drift terms featuring in the Fokker–Planck equation (16), when they are defined in such a way that f_{R} solving Equation (16) fulfills the requirement $f_{\mathrm{R}}(X, -\boldsymbol{M}_X, t) = f_{\mathrm{R}}(X, \boldsymbol{M}_X, t)$.

The physical quantity $\mathfrak{F}$ must also reflect the material symmetries of the composite material under study. If, as done in [86, 31], the matrix of the composite is isotropic, and the fiber parallel to $\boldsymbol{M}_X$ is transversely isotropic with respect to this direction, then the material is transversely isotropic at X with respect to the same direction. Then, by denoting by Orth^+ the group of all proper rotations, and by $\mathcal{G}_X(\boldsymbol{M}_X) := \{\boldsymbol{H} \in \mathrm{Orth}^+ : \boldsymbol{H}\boldsymbol{M}_X = \boldsymbol{M}_X\}$ the group of all proper rotations about $\boldsymbol{M}_X$, for all $\boldsymbol{H} \in \mathcal{G}_X(\boldsymbol{M}_X)$ it must hold true that[1]

$$\mathfrak{F}(X, \boldsymbol{H}\boldsymbol{M}_X, t, \boldsymbol{F}(X,t)\boldsymbol{H}, \boldsymbol{F}_\gamma(X,t)\boldsymbol{H}, \ldots) = \mathfrak{F}(X, \boldsymbol{M}_X, t, \boldsymbol{F}(X,t), \boldsymbol{F}_\gamma(X,t), \ldots). \tag{20}$$

3.1 Strain energy density

The considerations discussed so far are now applied to the definition of the strain energy density function of the composite material. Following [26, 27, 28, 86, 31, 87, 61], we write the strain energy density function of the solid phase associated with the single family of fibers aligned along $\boldsymbol{M}_X$ at $X \in \mathscr{B}$, and written per unit volume of the reference placement $\mathscr{B}$, as

$$\begin{aligned}\mathcal{W} &= \check{\mathcal{W}}(X, \boldsymbol{M}_X, \boldsymbol{F}, \boldsymbol{F}_\gamma) \\ &= \Phi_{\mathrm{s}}\hat{\mathcal{U}}(X, J, J_\gamma) + \Phi_{0\mathrm{s}}\hat{\mathcal{W}}_0(X, \boldsymbol{F}, \boldsymbol{F}_\gamma) + \Phi_{1\mathrm{s}}\big[\hat{\mathcal{W}}_{1\mathrm{i}}(X, \boldsymbol{F}, \boldsymbol{F}_\gamma) + \check{\mathcal{W}}_{1\mathrm{a}}(X, \boldsymbol{M}_X, \boldsymbol{F}, \boldsymbol{F}_\gamma)\big] \\ &= \Phi_{\mathrm{s}}\hat{\mathcal{U}}(X, J, J_\gamma) + \Phi_{0\mathrm{s}}\hat{\mathcal{W}}_0(X, \boldsymbol{F}, \boldsymbol{F}_\gamma) + \Phi_{1\mathrm{s}}\big[\hat{\mathcal{W}}_{1\mathrm{i}}(X, \boldsymbol{F}, \boldsymbol{F}_\gamma) + \hat{\mathcal{W}}_{1\mathrm{a}}(X, \Theta, \Phi, \boldsymbol{F}, \boldsymbol{F}_\gamma)\big], \end{aligned} \tag{21}$$

where the volumetric fractions are expressed as $\Phi_{\mathrm{s}} = J_\gamma\Phi_{\mathrm{s}\nu}$, $\Phi_{0\mathrm{s}} = J_\gamma\Phi_{0\mathrm{s}\nu}$, and $\Phi_{1\mathrm{s}} = J_\gamma\Phi_{1\mathrm{s}\nu}$, with $\Phi_{\mathrm{s}\nu}$, $\Phi_{0\mathrm{s}\nu}$, and $\Phi_{1\mathrm{s}\nu}$ evaluated at $X \in \mathscr{B}$; $\boldsymbol{F}$, $\boldsymbol{F}_\gamma$, J, and J_γ are evaluated in the pair $(X, t) \in \mathscr{B} \times \mathscr{I}$, although this dependence has been omitted for the sake of brevity; the term $\hat{\mathcal{W}}_0$ is the strain energy

[1] We would like to rephrase here the way in which this statement was given in [31], where the invariance property in Equation (20) was formulated as *"[...] the symmetry condition $\mathfrak{F}_X(\boldsymbol{H}\boldsymbol{M}_X) = \mathfrak{F}_X(\boldsymbol{M}_X)$, for all proper rotation tensors $\boldsymbol{H}$ such that $\boldsymbol{H}\boldsymbol{M}_X = \pm\boldsymbol{M}_X$."* [31].

density of the matrix; $\hat{\mathcal{W}}_{1\mathrm{i}}$ and $\hat{\mathcal{W}}_{1\mathrm{a}}$ are the isotropic and anisotropic contributions of the fibers to the overall strain energy density, respectively; and $\hat{\mathcal{U}}$ is defined by [28]

$$\hat{\mathcal{U}}(X, J, J_\gamma) = \alpha_0(X)\mathcal{H}_-(J_{\mathrm{cr}}(X) - J_{\mathrm{e}})\frac{[J_{\mathrm{e}} - J_{\mathrm{cr}}(X)]^{2q}}{[J_{\mathrm{e}} - \Phi_{\mathrm{s}\nu}(X)]^r}, \qquad \text{with} \quad J_{\mathrm{e}} = \frac{J}{J_\gamma}. \tag{22}$$

The function $\hat{\mathcal{U}}$ plays the role of a *"penalty"* [86, 31] that prevents compaction by diverging in the limit in which $J_{\mathrm{e}}(X,t)$ approaches $\Phi_{\mathrm{s}\nu}(X)$ from above. Moreover, $\alpha_0(X)$ is a point-dependent elastic property of the composite; $J_{\mathrm{cr}}(X)$ represents a *"critical value"* [28, 88] of J_{e}, below which $\hat{\mathcal{U}}$ is activated by the Heaviside function $\mathcal{H}_-(J_{\mathrm{cr}}(X) - J_{\mathrm{e}}(X,t))$[2]; q is a strictly positive integer[3], taken to be $q \geq 2$, and $r \in]0,1]$; and the inequality $J_{\mathrm{e}}(X,t) > \Phi_{\mathrm{s}\nu}(X)$ must be respected at all times and at all points. Finally, following [27, 28, 29, 86, 31, 32, 61], $\hat{\mathcal{W}}_0$, $\hat{\mathcal{W}}_{1\mathrm{i}}$, and $\hat{\mathcal{W}}_{1\mathrm{a}}$ are given by

$$\hat{\mathcal{W}}_0(X, \boldsymbol{F}, \boldsymbol{F}_\gamma) = \alpha_0(X)\left[\frac{\exp\left(\alpha_1(X)[I_{1\mathrm{e}} - 3] + \alpha_2(X)[I_{2\mathrm{e}} - 3]\right)}{[I_{3\mathrm{e}}]^{\alpha_3(X)}} - 1\right], \tag{23a}$$

$$\hat{\mathcal{W}}_{1\mathrm{i}}(X, \boldsymbol{F}, \boldsymbol{F}_\gamma) = \alpha_{0\mathrm{i}}(X)\left[\frac{\exp\left(\alpha_{1\mathrm{i}}(X)[I_{1\mathrm{e}} - 3] + \alpha_{2\mathrm{i}}(X)[I_{2\mathrm{e}} - 3]\right)}{[I_{3\mathrm{e}}]^{\alpha_{3\mathrm{i}}(X)}} - 1\right], \tag{23b}$$

$$\hat{\mathcal{W}}_{1\mathrm{a}}(X, \Theta, \Phi, \boldsymbol{F}, \boldsymbol{F}_\gamma) = \mathcal{H}_-(I_{4\mathrm{e}} - 1)\frac{k_1}{2k_2}\left[\exp\left(k_2[I_{4\mathrm{e}} - 1]^2\right) - 1\right]. \tag{23c}$$

The quantities $I_{\alpha\mathrm{e}}$, with $\alpha = 1, 2, 3$, are the three principal invariants of the *elastic* right Cauchy–Green stretch tensor $\boldsymbol{C}_{\mathrm{e}} = \boldsymbol{F}_{\mathrm{e}}^{\mathrm{T}}\boldsymbol{g}\boldsymbol{F}_{\mathrm{e}} = \boldsymbol{F}_\gamma^{-\mathrm{T}}\boldsymbol{C}\boldsymbol{F}_\gamma^{-1}$ ($\boldsymbol{C} = \boldsymbol{F}^{\mathrm{T}}\boldsymbol{g}\boldsymbol{F}$ being the right Cauchy–Green stretch tensor) [62], and are defined as

$$I_{1\mathrm{e}} := \mathrm{tr}\boldsymbol{C}_{\mathrm{e}} = \mathrm{tr}(\boldsymbol{C}\boldsymbol{B}_\gamma), \tag{24a}$$

$$I_{2\mathrm{e}} := \tfrac{1}{2}\{I_{1\mathrm{e}}^2 - \mathrm{tr}(\boldsymbol{C}_{\mathrm{e}}^2)\} = \tfrac{1}{2}\{\mathrm{tr}(\boldsymbol{C}\boldsymbol{B}_\gamma)^2 - \mathrm{tr}(\boldsymbol{C}\boldsymbol{B}_\gamma\boldsymbol{C}\boldsymbol{B}_\gamma)\}, \tag{24b}$$

$$I_{3\mathrm{e}} := \det\boldsymbol{C}_{\mathrm{e}} = J_\gamma^{-2}\det\boldsymbol{C}, \tag{24c}$$

where $\boldsymbol{B}_\gamma = \boldsymbol{C}_\gamma^{-1}$ is the inverse of the *anelastic* right Cauchy–Green stretch tensor $\boldsymbol{C}_\gamma = \boldsymbol{F}_\gamma^{\mathrm{T}}\boldsymbol{\eta}\boldsymbol{F}_\gamma$. Moreover, $\alpha_1(X)$, $\alpha_2(X)$, and $\alpha_3(X) \equiv \alpha_1(X) + 2\alpha_2(X)$ are the non-dimensional elastic parameters characterizing the isotropic material response of the matrix, together with $\alpha_0(X)$ (which, however, has the physical dimension of a volumetric energy density). Similarly, $\alpha_{0\mathrm{i}}(X)$, $\alpha_{1\mathrm{i}}(X)$, $\alpha_{2\mathrm{i}}(X)$, and $\alpha_{3\mathrm{i}}(X) \equiv \alpha_{1\mathrm{i}}(X) + 2\alpha_{2\mathrm{i}}(X)$ determine the elastic properties of the isotropic contribution of the fibers to the overall strain energy density. As in [3, 29], we set $\alpha_3(X) = 1$ and $\alpha_{3\mathrm{i}}(X) = 1$. Finally, the elastic parameters k_1 and k_2 featuring in $\hat{\mathcal{W}}_{1\mathrm{a}}$ are assumed here to be constant for the sake of simplicity, and, following [8, 56], $\hat{\mathcal{W}}_{1\mathrm{a}}$ is prescribed as a function of the invariant $I_{4\mathrm{e}}$, which can be written here as

$$I_{4\mathrm{e}} = \boldsymbol{C}_{\mathrm{e}} : \frac{\boldsymbol{F}_\gamma\boldsymbol{M}_X}{\|\boldsymbol{F}_\gamma\boldsymbol{M}_X\|} \otimes \frac{\boldsymbol{F}_\gamma\boldsymbol{M}_X}{\|\boldsymbol{F}_\gamma\boldsymbol{M}_X\|} = \frac{\boldsymbol{C} : \boldsymbol{M}_X \otimes \boldsymbol{M}_X}{\boldsymbol{C}_\gamma : \boldsymbol{M}_X \otimes \boldsymbol{M}_X} \equiv \frac{I_4}{I_{4\gamma}} =: \hat{I}_{4\mathrm{e}}(\boldsymbol{C}, \boldsymbol{C}_\gamma, \Theta, \Phi), \tag{25}$$

where $I_4 := \boldsymbol{C} : \boldsymbol{M}_X \otimes \boldsymbol{M}_X$ is the fourth invariant of $\boldsymbol{C}$, and $I_{4\gamma} := \boldsymbol{C}_\gamma : \boldsymbol{M}_X \otimes \boldsymbol{M}_X$ the fourth invariant of $\boldsymbol{C}_\gamma$. Both I_4 and $I_{4\gamma}$ are defined with respect to the direction $\boldsymbol{M}_X$ associated with the reference placement of the composite material.

It is important to notice that, although a more detailed and realistic description of transverse isotropy would require making $\hat{\mathcal{W}}_{1\mathrm{a}}$ to depend also on the fifth invariant $I_{5\mathrm{e}}$ [89, 90], we neglect it for this study. However, we notice that, if written in terms of $\boldsymbol{C}$ and $\boldsymbol{C}_\gamma$, $I_{5\mathrm{e}}$ reads

$$I_{5\mathrm{e}} = \boldsymbol{C}_{\mathrm{e}}^2 : \frac{\boldsymbol{F}_\gamma\boldsymbol{M}_X}{\|\boldsymbol{F}_\gamma\boldsymbol{M}_X\|} \otimes \frac{\boldsymbol{F}_\gamma\boldsymbol{M}_X}{\|\boldsymbol{F}_\gamma\boldsymbol{M}_X\|} = \frac{\boldsymbol{C}\boldsymbol{C}_\gamma^{-1}\boldsymbol{C} : \boldsymbol{M}_X \otimes \boldsymbol{M}_X}{\boldsymbol{C}_\gamma : \boldsymbol{M}_X \otimes \boldsymbol{M}_X} \equiv \frac{\tilde{I}_5}{I_{4\gamma}} =: \hat{I}_{5\mathrm{e}}(\boldsymbol{C}, \boldsymbol{C}_\gamma, \Theta, \Phi), \tag{26}$$

[2] Here, the Heaviside function is defined as $\mathcal{H}_-(y) = 1$, for $y > 0$, and $\mathcal{H}_-(y) = 0$, for $y \leq 0$.

[3] In [86, 31], it has been omitted to specify that q is an integer, although it must be so in order for the numerator $[J_{\mathrm{e}} - J_{\mathrm{cr}}(X)]^{2q}$ in Equation (22) to be well-defined.

where we introduced the notation $\tilde{I}_5 := \boldsymbol{C}\boldsymbol{C}_\gamma^{-1}\boldsymbol{C} : \boldsymbol{M}_X \otimes \boldsymbol{M}_X$. For a discussion on a peculiar definition of functions of the invariants $I_1, \dots, I_5$, which are particularly suitable for modeling transversely isotropic composite materials, the reader is referred, e.g., to [15]. As remarked in [91] referring to [92], the expressions obtained for $I_{4\mathrm{e}}$ and $I_{5\mathrm{e}}$ in Equations (25) and (26) allow to write each of these quantities as a function of $\boldsymbol{C}$ and $\boldsymbol{C}_\gamma$, thereby making it possible to re-define $\hat{\mathcal{W}}_{1\mathrm{a}}$ as a function of the same tensor variables as well as of the material points X and of the direction of fiber alignment through $\boldsymbol{M}_X = \hat{\boldsymbol{M}}_X(\Theta, \Phi)$.

As long as the Fokker–Planck equation is concerned, the derivatives of the strain energy density function with respect to the angles determining the point-wise direction of fiber alignment involve only the anisotropic contribution $\hat{\mathcal{W}}_{1\mathrm{a}}$ to $\mathcal{W}$, as defined in Equation (21). However, to study the mechanical response of the tissue, one has to account for the fact that the strain energy density function of the composite material is the directional average of $\mathcal{W}$. Thus, since the terms $\hat{\mathcal{U}}$, $\hat{\mathcal{W}}_0$, and $\hat{\mathcal{W}}_{1\mathrm{i}}$ do not depend on the fiber direction $\boldsymbol{M}_X$, only $\hat{\mathcal{W}}_{1\mathrm{a}}$ is effectively averaged. Hence, using Equation (19) and the normalization condition (18), we obtain

$$\langle\!\langle \mathcal{W} \rangle\!\rangle = \Phi_{\mathrm{s}}\hat{\mathcal{U}} + \Phi_{0\mathrm{s}}\hat{\mathcal{W}}_0 + \Phi_{1\mathrm{s}}\hat{\mathcal{W}}_{1\mathrm{i}} + \Phi_{1\mathrm{s}}\langle\!\langle \hat{\mathcal{W}}_{1\mathrm{a}} \rangle\!\rangle, \tag{27}$$

where we omitted to specify the arguments of each addend for the sake of a lighter notation.

3.2 Permeability

In this work, the macroscopic permeability tensor $\boldsymbol{K}$ in the reference placement of a porous, fiber-reinforced material is given by [25, 84, 28]

$$\boldsymbol{K} = \hat{\boldsymbol{K}}(X, \boldsymbol{C}) = \hat{k}_0(J)\frac{(J-\Phi_{1\mathrm{s}})^2}{J}\boldsymbol{C}^{-1} + \hat{k}_0(J)\frac{(J-\Phi_{1\mathrm{s}})\Phi_{1\mathrm{s}}}{J}\left\langle\!\!\left\langle \frac{\boldsymbol{M}_X \otimes \boldsymbol{M}_X}{\boldsymbol{C} : \boldsymbol{M}_X \otimes \boldsymbol{M}_X} \right\rangle\!\!\right\rangle, \tag{28}$$

and the scalar quantity $\hat{k}_0(J)$ is expressed constitutively as [3]

$$\hat{k}_0(X, J) = k_{0\mathrm{R}}(X)\left[\frac{J-\Phi_{\mathrm{s}}}{1-\Phi_{\mathrm{s}}}\right]^{m_0}\exp\left(\frac{m_1}{2}[J^2-1]\right), \tag{29}$$

where m_0, m_1 are material parameters and $k_{0\mathrm{R}}$ is a reference permeability (for other permeability laws see, e.g., [7]). Note that in Equations (28) and (29) the dependence on X is also through the volumetric fractions and, when needed, through the material coefficients, although it has not been explicitly reported for the sake of conciseness. Moreover, in the case of articular cartilage, $k_{0\mathrm{R}}$ exhibits a dependence on the material points that is given, for example, in [93]. We emphasize that, throughout this thesis, the term "permeability" is understood as a synonym of "hydraulic conductivity".

We identify the anisotropic contribution to the macroscopic permeability tensor with

$$\boldsymbol{K}_{\mathrm{a}} = \hat{\boldsymbol{K}}_{\mathrm{a}}(X, \boldsymbol{C}) = \hat{k}_0(J)\frac{(J-\Phi_{1\mathrm{s}})\Phi_{1\mathrm{s}}}{J}\left\langle\!\!\left\langle \frac{\boldsymbol{M}_X \otimes \boldsymbol{M}_X}{\boldsymbol{C} : \boldsymbol{M}_X \otimes \boldsymbol{M}_X} \right\rangle\!\!\right\rangle. \tag{30}$$

4 Constitutive assignments and remodeling laws

In this section, we recall the usual constitutive assignments in the framework of porous, fluid-saturated, fiber-reinforced media, and the remodeling law for the plastic distortions obtained from the Dissipation inequality [74, 76, 94, 6, 31], which is recalled but not discussed.

In Section 2.22, we have identified the first Piola–Kirchhoff stress tensor of a given phase with its constitutive characterization, which we provide in accordance with the residual dissipation. In particular, the behavior of the solid phase is that of a fiber-reinforced, elasto-plastic material (where "plastic" refers to the anelastic distortions due to remodeling); the fluid phase is assumed to bear only equilibrium hydrostatic stresses, while $\boldsymbol{m}_{\mathrm{f}}$ plays a relevant role in the dissipative processes concerning the fluid. The

residual dissipation, as studied in [74, 76, 94, 32], is satisfied with the following constitutive assignments [27, 28, 29, 32]

$$\boldsymbol{P}_{\mathrm{s}} := J_{\gamma}\frac{\partial\langle\!\langle \mathcal{W}\rangle\!\rangle}{\partial \boldsymbol{F}_{\mathrm{e}}}\boldsymbol{F}_{\gamma}^{-\mathrm{T}}, \tag{31a}$$

$$\boldsymbol{P}_{\mathrm{f}} := \boldsymbol{O}, \tag{31b}$$

$$J\boldsymbol{m}_{\mathrm{f}} := J_{\gamma}\Phi_{\mathrm{f}\nu}\boldsymbol{F}^{-\mathrm{T}}\boldsymbol{K}^{-1}\boldsymbol{Q}, \tag{31c}$$

where $\boldsymbol{Q}$ is the material filtration velocity and $\boldsymbol{K}$ is the material permeability tensor in Equation (28).

As customary in this framework, neglecting gravity (which amounts to dropping $\boldsymbol{f}$ from Equations (10a) and (10b)), and substituting Equations (31b) and (31c) into Equation (10b) lead to Darcy's Law in the form $\boldsymbol{Q} = -\boldsymbol{K}\mathrm{Grad}P$, while Equations (10a)–(10e) can be "condensed" in the system

$$\mathrm{Div}\boldsymbol{P}_{\mathrm{s}} - J\boldsymbol{F}^{-\mathrm{T}}\mathrm{Grad}P = \boldsymbol{0}, \tag{32a}$$

$$\dot{J} - \mathrm{Div}(\boldsymbol{K}\mathrm{Grad}P) = 0, \tag{32b}$$

$$\mathrm{dev}\boldsymbol{Y}_{\mathrm{u}} - \mathrm{dev}\boldsymbol{Z} = \boldsymbol{O}, \tag{32c}$$

$$\boldsymbol{F}_{\gamma}^{-\mathrm{T}} : \dot{\boldsymbol{F}}_{\gamma} = 0, \tag{32d}$$

where we have combined Equations (10b) and (10c) to obtain Equation (32b).

By considering the strain energy density function expressed in Equation (27) for a case in which $\hat{\mathcal{U}}$ is not activated, i.e., whenever the porous medium is not approaching compaction, the constitutive first Piola–Kirchhoff stress tensor can be expressed as

$$\boldsymbol{P}_{\mathrm{s}} = 2\Phi_{\mathrm{s}}\big[(b_1 + b_2 I_{1\mathrm{e}})\boldsymbol{g}\boldsymbol{F}\boldsymbol{B}_{\gamma} - b_2\boldsymbol{g}\boldsymbol{F}\boldsymbol{B}_{\gamma}\boldsymbol{C}\boldsymbol{B}_{\gamma} + b_3 I_{3\mathrm{e}}\boldsymbol{F}^{-\mathrm{T}}\big] + 2\Phi_{1\mathrm{s}}\boldsymbol{g}\boldsymbol{F}\langle\!\langle\frac{b_4}{I_{4\gamma}}(\boldsymbol{M}_X\otimes\boldsymbol{M}_X)\rangle\!\rangle, \tag{33}$$

where $\zeta_i b_i = \frac{\partial\hat{\mathcal{W}}}{\partial I_{i\mathrm{e}}}$, $i = 1,...,4$, are constitutive functions of the invariants of $\boldsymbol{C}_{\mathrm{e}}$; $\zeta_k = \Phi_{\mathrm{s}}$ and $b_k = \partial\mathcal{W}_0/\partial I_{k\mathrm{e}}$ for $k = 1,2,3$; $\zeta_4 = \Phi_{1\mathrm{s}}$ and $b_4 = \partial\mathcal{W}_{1\mathrm{a}}/\partial I_{4\mathrm{e}}$ (note that these definitions of ζ_k descend from taking in our model $\alpha_0 \equiv \alpha_{0\mathrm{i}}$, $\alpha_1 \equiv \alpha_{1\mathrm{i}}$, and $\alpha_2 \equiv \alpha_{2\mathrm{i}}$). It is worth noticing that the Heaviside function that appears in Equation (23c) is contained within b_4. In particular, we identify the anisotropic contribution to the constitutive first Piola–Kirchhoff stress tensor associated with the solid phase as

$$\boldsymbol{P}_{\mathrm{sa}} = 2\Phi_{1\mathrm{s}}\boldsymbol{g}\boldsymbol{F}\langle\!\langle\frac{b_4}{I_{4\gamma}}(\boldsymbol{M}_X\otimes\boldsymbol{M}_X)\rangle\!\rangle. \tag{34}$$

4.1 Remodeling law

Following the study of the dissipation inequality conducted in [51, 95], and adapting it to the case of isochoric inelastic distortions developed in our present work, we provide the following identification for the deviatoric part of the stress-like tensor $\boldsymbol{Y}_{\mathrm{u}}$, power-conjugate with the traceless anelastic rate $\boldsymbol{F}_{\gamma}^{-1}\dot{\boldsymbol{F}}_{\gamma}$:

$$\mathrm{dev}\boldsymbol{Y}_{\mathrm{u}} = -\mathrm{dev}\boldsymbol{\Sigma}_{\mathrm{s}}(\boldsymbol{F},\boldsymbol{F}_{\gamma}) + \mathrm{dev}\boldsymbol{Y}_{\mathrm{u,d}}, \tag{35}$$

with $\boldsymbol{\Sigma}_{\mathrm{s}} = \boldsymbol{F}^{\mathrm{T}}\boldsymbol{P}_{\mathrm{s}}$ being the constitutive Mandel stress tensor associated with the solid phase and $\boldsymbol{Y}_{\mathrm{u,d}} \equiv \mathrm{dev}\boldsymbol{Y}_{\mathrm{u,d}}$ representing the *dissipative* part of $\mathrm{dev}\boldsymbol{Y}_{\mathrm{u}}$. In particular, following the study of the residual dissipation [51, 95], $\mathrm{dev}\boldsymbol{Y}_{\mathrm{u,d}}$ can be prescribed as

$$\mathrm{dev}\boldsymbol{Y}_{\mathrm{u,d}} = \mathbb{A}(\boldsymbol{F},\boldsymbol{F}_{\gamma}) : \boldsymbol{F}_{\gamma}^{-1}\dot{\boldsymbol{F}}_{\gamma}, \tag{36}$$

where $\mathbb{A}$ is a positive semi-definite fourth-order tensor.

From here on we make the strong hypothesis that remodeling is "confined" to the matrix of the medium under study (we recall that the matrix is isotropic) and that it is independent of the local direction of fiber alignment. In short, we shall say that remodeling is isotropic in the sense that Equation

(36) is covariant under transformations of the type $\boldsymbol{F} \mapsto \boldsymbol{F}\boldsymbol{H}$ and $\boldsymbol{F}_\gamma \mapsto \boldsymbol{F}_\gamma\boldsymbol{H}$, for any proper rotation tensor $\boldsymbol{H}$, which yield $\boldsymbol{F}_\gamma^{-1}\dot{\boldsymbol{F}}_\gamma \mapsto \boldsymbol{H}^{-1}(\boldsymbol{F}_\gamma^{-1}\dot{\boldsymbol{F}}_\gamma)\boldsymbol{H}$, $\mathbb{A}(\boldsymbol{F}\boldsymbol{H}, \boldsymbol{F}_\gamma\boldsymbol{H}) = \boldsymbol{H}^{\mathrm{T}}\underline{\otimes}\boldsymbol{H}^{-1} : \mathbb{A}(\boldsymbol{F}, \boldsymbol{F}_\gamma) : \boldsymbol{H}\underline{\otimes}\boldsymbol{H}^{-\mathrm{T}}$, and $\mathrm{dev}\boldsymbol{Y}_{\mathrm{u,d}} \mapsto \boldsymbol{H}^{\mathrm{T}}(\mathrm{dev}\boldsymbol{Y}_{\mathrm{u,d}})\boldsymbol{H}^{-\mathrm{T}}$. Hence, we prescribe $\mathbb{A}$ in such a way that the preceding transformation laws are satisfied and, for this purpose, we adapt the definition in [96] to our case (see also [51, 95]), that is

$$\mathbb{A}(\boldsymbol{F}, \boldsymbol{F}_\gamma) = J_\gamma \mathfrak{b}_\nu \left[\boldsymbol{C}\underline{\otimes}\boldsymbol{C}^{-1} + \boldsymbol{I}^{\mathrm{T}}\overline{\otimes}\boldsymbol{I}\right] + J_\gamma \mathfrak{c}_\nu \left[\boldsymbol{C}\underline{\otimes}\boldsymbol{C}^{-1} - \boldsymbol{I}^{\mathrm{T}}\overline{\otimes}\boldsymbol{I}\right], \tag{37}$$

where $\mathfrak{b}_\nu$ and $\mathfrak{c}_\nu$ are material parameters such that $\mathfrak{b}_\nu \geq 0$ and $\mathfrak{c}_\nu \geq 0$ (we recall that, in all these expressions above, J_γ is equal to unity). We remark that $\mathbb{A}$ only gives rise to an isotropic contribution in the remodeling law, whereas the fiber-reinforced composite is regarded at least as a transversely isotropic material, if not orthotropic [97]. In this regard, an enriched description of remodeling should take into account two separate contributions, one from the matrix and one from the fibers themselves. The latter form of remodeling could be framed as put forward in [6], i.e., by taking $\mathbb{A}$ in the space of the transversely isotropic tensors, the basis of which is identified with a combination of tensor products between $\boldsymbol{A}_{\mathrm{X}} = \boldsymbol{M}_X \otimes \boldsymbol{M}_X$ and $\boldsymbol{B}_{\mathrm{X}} = \boldsymbol{I} - \boldsymbol{M}_X \otimes \boldsymbol{M}_X$. However, in this work we resort to the characterization of $\mathbb{A}$ expressed in Equation (37) of isotropic remodeling, while we set the goal of studying anisotropic remodeling in future works.

By enforcing Equations (35) and (37), we can rewrite Equation (32c) and extract its skew-symmetric and symmetric part. Moreover, by assuming $\boldsymbol{Z} = \boldsymbol{O}$, we can write the equations for the evolution of $\boldsymbol{F}_\gamma$ as

$$2J_\gamma \mathfrak{b}_\nu \mathrm{Dev}_{\boldsymbol{C}}\mathrm{Sym}(\boldsymbol{F}_\gamma^{-1}\dot{\boldsymbol{F}}_\gamma\boldsymbol{C}^{-1}) - \mathrm{Dev}_{\boldsymbol{C}}(\boldsymbol{C}^{-1}\boldsymbol{\Sigma}_{\mathrm{s}}) = \boldsymbol{O}, \tag{38a}$$

$$2J_\gamma \mathfrak{c}_\nu \mathrm{Skew}(\boldsymbol{F}_\gamma^{-1}\dot{\boldsymbol{F}}_\gamma\boldsymbol{C}^{-1}) = \boldsymbol{O}, \tag{38b}$$

where, for any second-order tensor $\boldsymbol{T}$ with contravariant material indices, the notation $\mathrm{Dev}_{\boldsymbol{C}}\boldsymbol{T}$ means $\mathrm{Dev}_{\boldsymbol{C}}\boldsymbol{T} := \boldsymbol{T} - \frac{1}{3}\mathrm{tr}(\boldsymbol{C}\boldsymbol{T})\boldsymbol{C}^{-1}$ [51].

Equations (38a) and (38b) are understood as the dynamic equations that drive the onset and evolution of the remodeling distortions. In particular, Equation (38b) retrieves the condition of null plastic spin as a consequence of the model, rather than imposing it, as often done in the literature.

4.2 "Target angle" and fiber reorientation

Following [47, 81, 17, 56, 32], we introduce the concept of "target" angle, i.e., the angle corresponding to the most probable direction along which fibers tend to align themselves. Various approaches are present in the literature to couple the evolution of the target angle with the mechanical state of the tissue. For example, the evolution of the target angle is driven by the mechanical stress in [17, 56], while it depends on the deformation in [47, 81]. A similar approach is followed also in [31, 32], in which the most probable fiber angle is driven by the target angle, the target angle is treated as a kinematic variable and its evolution is described in terms of external remodeling forces.

In this work, we adhere to the conceptual framework put forward in [32], and, by considering the Fokker–Planck equation (16), we expand the approach of Crevacore et al. [32] to describe the time evolution of the probability density distribution f_{R}. Hence, even though we speak of *"target angle"*, we search for the identification of a *target probability distribution*, in which the most probable angle of orientation defines the "target angle" of our model. That being said, we follow the same conceptual trail of [31, 32], and we consider $\mathcal{F}_\Theta^{\mathrm{ext,det}}$ and $\mathcal{F}_\Phi^{\mathrm{ext,det}}$ as the driving generalized forces associated with a potential $\Pi = \hat{\Pi}(X, \Theta, \Phi)$. In particular, we assume that all the information regarding the preferred directions along which the fibers align in the absence of elastic and anelastic distortions is stored in Π, and that Π does not vary during the tissue's evolution. In this setting, Π may represent biochemical, genetic, and/or epigenetic factors that can play a relevant role in shaping the tissue's mesoscopic structure.

Notice that, if we assume the existence of Π and that no other external action is exerted on f_{R}, the external forces $\mathcal{F}_{\Theta}^{\mathrm{ext,det}}$ and $\mathcal{F}_{\Phi}^{\mathrm{ext,det}}$ consist only of the contributions that read

$$\mathcal{F}_{\Theta}^{\mathrm{ext,det}} = [\mathrm{Grad}\hat{\Pi}]_{\Theta} = \frac{\partial \hat{\Pi}}{\partial \Theta}, \qquad \mathcal{F}_{\Phi}^{\mathrm{ext,det}} = [\mathrm{Grad}\hat{\Pi}]_{\Phi} = \frac{1}{\sin\Theta}\frac{\partial \hat{\Pi}}{\partial \Phi}, \tag{39}$$

and Equation (16) becomes

$$\partial_t \hat{f}_{\mathrm{R}} = -\frac{1}{\sin\Theta}\frac{\partial}{\partial\Theta}\left[\sin\Theta\left(\frac{1}{\gamma}\frac{\partial(\hat{\Pi}+\hat{\mathcal{W}})}{\partial\Theta}\hat{f}_{\mathrm{R}} - D\frac{\partial \hat{f}_{\mathrm{R}}}{\partial\Theta}\right)\right] - \frac{1}{(\sin\Theta)^2}\frac{\partial}{\partial\Phi}\left[\frac{1}{\gamma}\frac{\partial(\hat{\Pi}+\hat{\mathcal{W}})}{\partial\Phi}\hat{f}_{\mathrm{R}} - D\frac{\partial \hat{f}_{\mathrm{R}}}{\partial\Phi}\right]. \tag{40}$$

Hence, we can identify the components of a flux vector $\boldsymbol{\jmath} = \hat{\boldsymbol{\jmath}}(X, \Theta, \Phi, \boldsymbol{F}, \boldsymbol{F}_\gamma)$ as

$$[\hat{\boldsymbol{\jmath}}]_{\Theta} = \frac{1}{\gamma}\frac{\partial(\hat{\Pi}+\hat{\mathcal{W}})}{\partial\Theta}\hat{f}_{\mathrm{R}} - D\frac{\partial \hat{f}_{\mathrm{R}}}{\partial\Theta}, \qquad [\hat{\boldsymbol{\jmath}}]_{\Phi} = \frac{1}{\sin\Theta}\left(\frac{1}{\gamma}\frac{\partial(\hat{\Pi}+\hat{\mathcal{W}})}{\partial\Phi}\hat{f}_{\mathrm{R}} - D\frac{\partial \hat{f}_{\mathrm{R}}}{\partial\Phi}\right), \tag{41}$$

so that Equation (40) becomes

$$\partial_t \hat{f}_{\mathrm{R}} = -\mathrm{Div}_{\mathbb{S}^2}\hat{\boldsymbol{\jmath}}, \tag{42}$$

with $\mathrm{Div}_{\mathbb{S}^2}$ being the divergence operator on the sphere, returning the right-hand side of Equation (40).

It is well known that Equation (40) admits a unique stationary solution [98, 99], that is

$$\hat{f}_{\mathrm{SR}} := \frac{1}{\mathcal{Z}}\exp\left(\beta\hat{\Pi} + \beta\hat{\mathcal{W}}\right), \qquad \mathcal{Z} := \int_0^{2\pi}\int_0^{\pi}\exp\left(\beta\hat{\Pi} + \beta\hat{\mathcal{W}}\right)\sin\Theta\,\mathrm{d}\Theta\mathrm{d}\Phi, \tag{43}$$

where $\beta := (D\gamma)^{-1} > 0$ is the inverse of a characteristic energy density. Out of this result for the stationary solution, we make the following remarks. Equation (43) defines our target probability density distribution.

Remark 1 ((The spherical von Mises distribution as a particular solution of the Fokker–Planck equation)). In the absence of deformation and plastic-like distortions, we consider the case in which Π is given by $\Pi = \Pi_0 \boldsymbol{\mu}_{\mathrm{X}}\boldsymbol{M}_X$, where $\Pi_0 > 0$ is a coefficient independent of the angles Θ and Φ, and having the units of energy per unit volume, $\boldsymbol{M}_X \in \mathbb{S}^2_X\mathscr{B}$ is a generic direction along which a rectified fiber is aligned, $\boldsymbol{\mu}_{\mathrm{X}} \in (\mathbb{S}^2_X\mathscr{B})^*$ is a *constant* linear map (i.e., a covector), and the juxtaposition $\boldsymbol{\mu}_{\mathrm{X}}\boldsymbol{M}_X$ is a shorthand notation for expressing the duality product $\langle\boldsymbol{\mu}_{\mathrm{X}}|\boldsymbol{M}_X\rangle \equiv \boldsymbol{\mu}_{\mathrm{X}}\boldsymbol{M}_X$. Hence, the stationary solution reads

$$f_{\mathrm{VM}} := \frac{1}{\mathcal{Z}_0}\exp\left(\beta\Pi_0\boldsymbol{\mu}_{\mathrm{X}}\boldsymbol{M}_X\right), \qquad \mathcal{Z}_0 := \int_{\mathbb{S}^2_X\mathscr{B}}\exp\left(\beta\Pi_0\boldsymbol{\mu}_{\mathrm{X}}\boldsymbol{M}_X\right), \tag{44}$$

which coincides with the von Mises distribution on the sphere. In particular, if $\boldsymbol{\mu}_X$ is taken as the covector associated with the specific unit vector $\bar{\boldsymbol{M}}_X = \sin\bar{\Theta}\cos\Phi\boldsymbol{E}_1 + \sin\bar{\Theta}\sin\Phi\boldsymbol{E}_2 + \cos\bar{\Theta}\boldsymbol{E}_3$, where $\bar{\Theta} \in [0, \pi]$ is a preferred value of the colatitude, then Equation (44) becomes

$$\hat{f}_{\mathrm{VM}} := \frac{1}{\mathcal{Z}_0}\exp\left(\beta\Pi_0\cos(\Theta - \bar{\Theta})\right), \qquad \mathcal{Z}_0 := 2\pi\int_0^{\pi}\exp\left(\beta\Pi_0\cos(\Theta - \bar{\Theta})\right)\sin\Theta\,\mathrm{d}\Theta. \tag{45}$$

However, the distribution in Equation (44) does not satisfy the condition $f_{\mathrm{R}}(X, -\boldsymbol{M}_X, t) = f_{\mathrm{R}}(X, \boldsymbol{M}_X, t)$ for all $\boldsymbol{M}_X \in \mathbb{S}^2_X\mathscr{B}$ and fixed $\boldsymbol{\mu}_X$, which was discussed at the beginning of Section 3, when introducing the directional average of a generic physical quantity $\mathfrak{F}$.

The most immediate way to obtain this invariance is to require Π to depend on $\boldsymbol{M}_X$ through the structure tensor $\boldsymbol{A}_{\mathrm{X}} := \boldsymbol{M}_X \otimes \boldsymbol{M}_X$, which is invariant under the transformation $\boldsymbol{M}_X \mapsto -\boldsymbol{M}_X$. We provide, thus, the following form for the potential Π:

$$\Pi = \Pi_0[\boldsymbol{\mu}_{\mathrm{X}} \otimes \boldsymbol{\mu}_{\mathrm{X}}](\boldsymbol{M}_X \otimes \boldsymbol{M}_X) = \Pi_0(\boldsymbol{\mu}_{\mathrm{X}}\boldsymbol{M}_X)^2, \tag{46}$$

so that the stationary solution associated with Equation (46) is

$$f_{\mathrm{SVM}} := \frac{1}{\mathcal{Z}_0}\exp\big(\beta\Pi_0(\boldsymbol{\mu}_X\boldsymbol{M}_X)^2\big), \qquad \mathcal{Z}_0 := \int_{\mathbb{S}^2_X\mathscr{B}} \exp\big(\beta\Pi_0(\boldsymbol{\mu}_X\boldsymbol{M}_X)^2\big). \tag{47}$$

Therefore, we recover a symmetric, bimodal von Mises distribution as the stationary probability density distribution associated with the reorientation process described by Equations (15a) and (15b) (see, e.g., the comparison in Figure 1). In particular, if, as before, $\boldsymbol{\mu}_X$ is associated with the specific unit vector $\bar{\boldsymbol{M}}_X = \sin\bar{\Theta}\cos\Phi\boldsymbol{E}_1 + \sin\bar{\Theta}\sin\Phi\boldsymbol{E}_2 + \cos\bar{\Theta}\boldsymbol{E}_3$, then Equation (46) yields

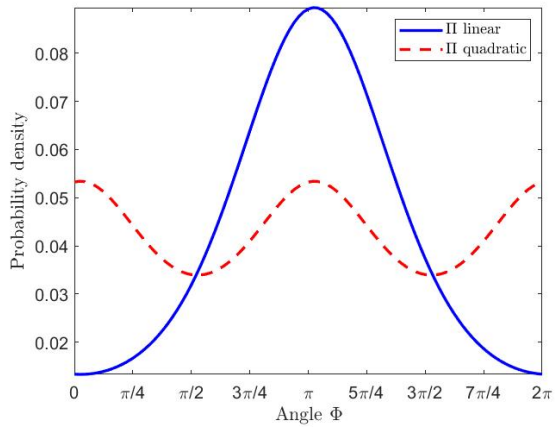
$$\hat{\Pi}(\Theta) = \Pi_0[\cos(\Theta-\bar{\Theta})]^2 = \Pi_0\frac{\cos(2[\Theta-\bar{\Theta}])+1}{2} = \frac{\Pi_0}{2}\big\{\cos(2[\Theta-\bar{\Theta}])+1\big\}. \tag{48}$$

Accordingly, Equation (47) becomes

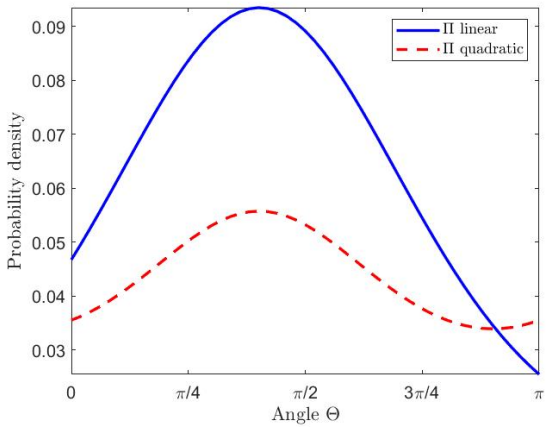
$$f_{\mathrm{SVM}} := \frac{1}{\mathcal{Z}_0}\exp\Big(\beta\Pi_0\big[\cos(\Theta-\bar{\Theta})\big]^2\Big) = \frac{1}{\mathcal{Z}_0}\exp\left(\frac{\beta\Pi_0}{2}\big\{\cos(2[\Theta-\bar{\Theta}])+1\big\}\right), \tag{49a}$$

$$\begin{aligned}\mathcal{Z}_0 &:= 2\pi\int_0^{\pi}\exp\Big(\beta\Pi_0\big[\cos(\Theta-\bar{\Theta})\big]^2\Big)\sin\Theta\,\mathrm{d}\Theta\\ &= \frac{2\pi\sqrt{\pi}\cos\bar{\Theta}}{\sqrt{\beta\Pi_0}}\mathrm{erfi}\big(\sqrt{\beta\Pi_0}\cos\bar{\Theta}\big) + \frac{2\pi\sqrt{\pi}\sin\bar{\Theta}}{\sqrt{\beta\Pi_0}}\mathrm{e}^{\beta\Pi_0}\mathrm{erf}\big(\sqrt{\beta\Pi_0}\sin\bar{\Theta}\big),\end{aligned} \tag{49b}$$

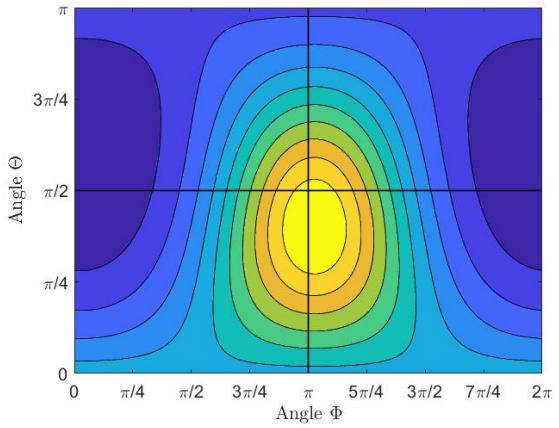
where $\mathrm{erfi}(\kappa)$ is the imaginary Error function, defined by $\mathrm{erfi}(\kappa) = -i\,\mathrm{erf}(i\kappa)$, with $\kappa \in \mathbb{C}$ and i being the imaginary unit. Before proceeding, it is worth noticing that $\bar{\boldsymbol{M}}_X$ has been defined for a fixed $\bar{\Theta}$ and variable Φ (thereby identifying a half cone). Thus, $\bar{\boldsymbol{M}}_X$ and $\hat{\boldsymbol{M}}_X$ are parameterized by different angles $\bar{\Theta}$ and Θ, but by the same angle Φ. This is the reason why the potential Π prescribed in Equation (46) takes on the functional form given in Equation (48). Consequently, neither the potential $\hat{\Pi}$ nor the probability density distribution f_{SVM} in Equation (49a) are symmetric under the transformation $(\Theta,\Phi) \mapsto (\pi-\Theta,\Phi+\pi)$. Indeed, given $\boldsymbol{\mu}_X\boldsymbol{M}_X = \bar{\boldsymbol{M}}_X(\bar{\Theta},\Phi)\cdot\hat{\boldsymbol{M}}_X(\Theta,\Phi)$, the expression $\bar{\boldsymbol{M}}_X(\bar{\Theta},\Phi+\pi)\cdot\hat{\boldsymbol{M}}_X(\pi-\Theta,\Phi+\pi) = -\cos(\Theta+\bar{\Theta})$ is not equivalent to $\bar{\boldsymbol{M}}_X(\bar{\Theta},\Phi)\cdot\hat{\boldsymbol{M}}_X(\pi-\Theta,\Phi+\pi) = -\cos(\Theta-\bar{\Theta})$. Rather, both the potential and the distribution are symmetric with respect to the transformation $(\Theta-\bar{\Theta},\Phi) \mapsto (\pi-(\Theta-\bar{\Theta}),\Phi+\pi)$. This transformation, in turn, becomes trivially identical to the previous one for $\bar{\Theta}=0$ and for $\bar{\Theta}=\pi$, since $\bar{\boldsymbol{M}}_X$ coincides with $\boldsymbol{E}_3$ and $-\boldsymbol{E}_3$, respectively. However, if $\bar{\boldsymbol{M}}_X$ is taken as $\bar{\boldsymbol{M}}_X = \sin\bar{\Theta}\cos\bar{\Phi}\boldsymbol{E}_1 + \sin\bar{\Theta}\sin\bar{\Phi}\boldsymbol{E}_2 + \cos\bar{\Theta}\boldsymbol{E}_3$, i.e., with fixed $\bar{\Theta}$ and $\bar{\Phi}$, then the potential Π becomes $\Pi = \Pi_0(\boldsymbol{\mu}_X\boldsymbol{M}_X)^2 = \Pi_0(\bar{\boldsymbol{M}}_X\cdot\boldsymbol{M}_X)^2 = \Pi_0[\sin\bar{\Theta}\sin\Theta\cos(\Phi-\bar{\Phi})+\cos\bar{\Theta}\cos\Theta]^2$. Then, it is invariant under the transformation $(\Theta,\Phi) \mapsto (\pi-\Theta,\Phi+\pi)$, and so is also f_{SVM} (see Figure 1). In particular, for $\bar{\Theta}=0$ and $\bar{\Theta}=\pi$, one obtains $\Pi = \Pi_0[\cos\Theta]^2$, and f_{SVM} equals the more "familiar" von Mises distribution used, e.g., in [27].



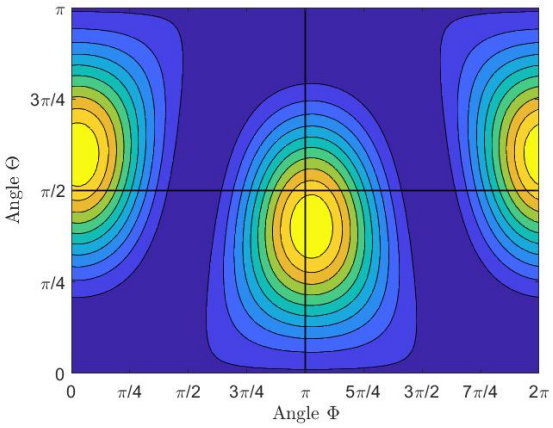
(a) Comparison between f_{VM} and f_{SVM} for $\Theta = \pi/2$.



(b) Comparison between f_{VM} and f_{SVM} for $\Phi = 0$.



(c) Plot of f_{VM} over $[0, 2\pi[\times [0, \pi]$.



(d) Plot of f_{SVM} over $[0, 2\pi[\times [0, \pi]$.

Figure 1: Comparison between the stationary solutions of Equation (42) for a linear and a quadratic potential Π in $\boldsymbol{M}_X$ (see Equations (44) and (47), respectively), with $\beta = 1$, $\Pi_0 = 1$ and $\boldsymbol{\mu}_X = -0.9495\boldsymbol{E}^1 - 0.0792\boldsymbol{E}^2 + 0.3036\boldsymbol{E}^3$ (here, the coefficients of $\boldsymbol{\mu}_X$ are taken randomly with respect to the unit covectors $\boldsymbol{E}^A$, with $A = 1, 2, 3$, of the canonical basis of $(T_X\mathscr{B})^*$). Figures 1a and 1b show f_{VM} and f_{SVM} evaluated for $\Theta = \pi/2$ and for $\Phi = 0$. Figures 1c and 1d show ten level sets of f_{VM} and f_{SVM} plotted on the domain $[0, 2\pi[\times [0, \pi]$. As expected, f_{SVM} respects the symmetry condition $\hat{f}_{\mathrm{SVM}}(X, \pi - \Theta, \Phi + \pi) = \hat{f}_{\mathrm{SVM}}(X, \Theta, \Phi)$, while f_{VM} does not.

Remark 2 ((Fibers orientation in articular cartilage)).
In the absence of deformation, articular cartilage shows a very clear histological pattern in the distribution of the fibers [100, 101, 102, 14]. To see how this histological information can be used to construct the stationary probability density distribution through the potential Π, we consider a cylindrical specimen of cartilage, and we assume it to be *"transversely isotropic and transversely homogeneous"* [14] with respect to the geometric symmetry axis of the specimen itself. Then, by choosing a global reference frame with the $\boldsymbol{E}_3$-axis coincident with the specimen's symmetry axis, the probability density distribution is taken independent of the longitude, i.e., independent of the angle Φ, and dependent on the co-latitude, i.e., on the angle Θ. The histological orientation of the fibers is characterized by the *histological* angle Θ_{hi}, which determines the most probable angle that the collagen fibers form with $\boldsymbol{E}_3$. The histological angle Θ_{hi} varies with the axial coordinate of the specimen, but remains constant in each transverse section of the specimen. More specifically, it can be observed that Θ_{hi} ranges from $\Theta_{\mathrm{hi}} = 0$ at the bottom of the specimen to $\Theta_{\mathrm{hi}} = \pi/2$ at the upper surface of the specimen. Note that, in this description, the bottom surface represents the interface between cartilage and bone, while the upper surface corresponds

to the articular surface, i.e., the surface that is in contact with the cartilage covering the extremity of the opposing bone in a synovial joint [103]. In the middle, or transitional, region of the specimen, the fibers exhibit greater variance in the histological angle Θ_{hi}. It is worth noticing that, in spite of the description given so far, some works in the literature relax the hypothesis of transverse isotropy and assume the probability density distribution to be a bi-variate, spherical von Mises distribution, depending both on Θ and on Φ [19, 30, 33].

In our framework, we encode the fiber histological pattern described by Θ_{hi} in the target probability density distribution of the tissue, and, by recurring to Equation (43), we couple it with the body's strain energy density per unit volume of the reference placement. However, only the anisotropic term (23c) concurs to shaping f_{SR}, whereas the other energetic contributions do not, since they are independent of Θ and Φ.

To proceed with the target probability density distribution, we prescribe the potential Π as

$$\hat{\Pi}(\Theta;\Theta_{\text{hi}},\omega) = \hat{\Pi}_0(\omega)[\cos(\Theta-\Theta_{\text{hi}})]^2 = \frac{\Pi_{\text{c}}}{\omega^2}[\cos(\Theta-\Theta_{\text{hi}})]^2, \qquad \hat{\Pi}_0(\omega) := \frac{\Pi_{\text{c}}}{\omega^2}, \tag{50}$$

where the histological fibers' angle Θ_{hi} depends solely on the coordinate X^3, ω is a dimensionless strictly positive quantity associated with the variance of the fiber distribution and depending only on X^3, and Π_{c} is a constant, strictly positive referential value of the potential. Note that, with respect to the potential introduced in Equation (48), the new definition of $\hat{\Pi}$ in Equation (50) is given to rescale the amplitude of the potential with ω^2. Clearly, this requires reformulating the normalization factor $\mathcal{Z}_0$ through the substitution $\Pi_0 \mapsto \hat{\Pi}_0(\omega) = \Pi_{\text{c}}/\omega^2$, which, in the absence of deformation, yields

$$\hat{f}_{\text{SR}}(\Theta,\Phi;\Theta_{\text{hi}},\omega) = \hat{f}_{\text{SVM}}(\Theta;\Theta_{\text{hi}},\omega) = \frac{1}{\mathcal{Z}_0}\exp\left(\frac{\beta\Pi_{\text{c}}}{\omega^2}[\cos(\Theta-\Theta_{\text{hi}})]^2\right), \tag{51a}$$

$$\begin{aligned}\mathcal{Z}_0 &:= 2\pi\int_0^{\pi}\exp\left(\frac{\beta\Pi_{\text{c}}}{\omega^2}\big[\cos(\Theta-\Theta_{\text{hi}})\big]^2\right)\sin\Theta\,\mathrm{d}\Theta \\ &= \frac{2\pi\sqrt{\pi}\,\omega\cos\Theta_{\text{hi}}}{\sqrt{\beta\Pi_{\text{c}}}}\operatorname{erfi}\left(\frac{\sqrt{\beta\Pi_{\text{c}}}}{\omega}\cos\Theta_{\text{hi}}\right) + \frac{2\pi\sqrt{\pi}\,\omega\sin\Theta_{\text{hi}}}{\sqrt{\beta\Pi_{\text{c}}}}\mathrm{e}^{\beta\Pi_{\text{c}}/\omega^2}\operatorname{erf}\left(\frac{\sqrt{\beta\Pi_{\text{c}}}}{\omega}\sin\Theta_{\text{hi}}\right).\end{aligned} \tag{51b}$$

In particular, following [14], we take:

$$\Theta_{\text{hi}}(X^3) := \frac{\pi}{2}\left\{1-\cos\left(\frac{\pi}{2}\left[-\frac{2}{3}\left(\frac{X^3}{H}\right)^2+\frac{5}{3}\frac{X^3}{H}\right]\right)\right\}, \tag{52a}$$

$$\omega(X^3) := 10^3\left[\left(1-\frac{X^3}{H}\right)\frac{X^3}{H}\right]^4 + 0.03, \tag{52b}$$

where H is the height of the cartilage sample. Note that, according to Equation (50), Π is defined as a function of Θ parameterized by Θ_{hi} and ω. We prefer this definition instead of expressing Π as a function of Θ and X^3 in order to highlight that the dependence of Π on X^3 is through the parameters Θ_{hi} and ω that characterize the model of tissue under investigation. It is also important to emphasize that, differently from the expression of Π given in Equation (48), ω^2 plays a modulating role on the strength of the drift exerted by Π on the probability density distribution.

Also the volumetric fractions of the extracellular matrix and of the fibers depend on X^3, and are obtained by means of a polynomial fit of experimental data. For example, following [104, 105, 94], we use

$$\Phi_{0\text{s}}(X^3) = 0.046 + 0.038\frac{X^3}{H} - 0.062\left(\frac{X^3}{H}\right)^2, \tag{53a}$$

$$\Phi_{1\text{s}}(X^3) = 0.204 - 0.138\frac{X^3}{H} + 0.062\left(\frac{X^3}{H}\right)^2. \tag{53b}$$

Therefore, for articular cartilage, we obtain the following stationary probability density distribution

$$\begin{aligned}\hat{f}_{\mathrm{SR}}(\Theta,\Phi;\boldsymbol{F},\boldsymbol{F}_\gamma,\Theta_{\mathrm{hi}},\omega,\Phi_{1\mathrm{s}}) &:= \frac{1}{\mathcal{Z}}\exp(\beta\hat{\Pi}+\beta\hat{\mathcal{W}})\\ &= \frac{1}{\mathcal{Z}_{\mathrm{a}}}\exp\left(\frac{\beta\Pi_{\mathrm{c}}}{\omega^2}\left[\cos(\Theta-\Theta_{\mathrm{hi}})\right]^2+\beta\Phi_{1\mathrm{s}}\hat{\mathcal{W}}_{1\mathrm{a}}(\Theta,\Phi,\boldsymbol{F},\boldsymbol{F}_\gamma)\right),\end{aligned}\tag{54}$$

in which $\mathcal{Z}_{\mathrm{a}}$ is the normalization constant associated with the sole anisotropic terms of the model, i.e.,

$$\begin{aligned}\mathcal{Z}_{\mathrm{a}} &:= \int_{\mathbb{S}^2_X\mathscr{B}}\exp(\beta\Pi+\beta\Phi_{1\mathrm{s}}\mathcal{W}_{1\mathrm{a}})\\ &= \int_0^{2\pi}\int_0^{\pi}\exp\left(\frac{\beta\Pi_{\mathrm{c}}}{\omega^2}[\cos(\Theta-\Theta_{\mathrm{hi}})]^2\right)\exp\left(\beta\Phi_{1\mathrm{s}}\hat{\mathcal{W}}_{1\mathrm{a}}(\Theta,\Phi,\boldsymbol{F},\boldsymbol{F}_\gamma)\right)\sin\Theta\,\mathrm{d}\Theta\mathrm{d}\Phi,\end{aligned}\tag{55}$$

where the quantities ω, Θ_{hi}, and $\Phi_{1\mathrm{s}}$ are functions of the axial coordinate $X^3\in[0,H]$, the dependence of $\hat{\mathcal{W}}_{1\mathrm{a}}$ on X has been suppressed, since its material coefficients are assumed to be homogeneous, and $\hat{f}_{\mathrm{SR}}$ is made dependent parametrically also on $\Phi_{1\mathrm{s}}$.

Remark 3 ((Change of measure)).
Equation (54) permits to introduce the equivalent expression of $\hat{f}_{\mathrm{SR}}$ given by

$$\hat{f}_{\mathrm{SR}}(\Theta,\Phi;\boldsymbol{F},\boldsymbol{F}_\gamma,\Theta_{\mathrm{hi}},\omega,\Phi_{1\mathrm{s}}) := \frac{1}{\mathcal{Z}_f}\hat{f}_{1\mathrm{a}}(\Theta,\Phi;\boldsymbol{F},\boldsymbol{F}_\gamma,\Phi_{1\mathrm{s}})\hat{f}_{\mathrm{SVM}}(\Theta;\Theta_{\mathrm{hi}},\omega),\tag{56}$$

where the new distribution $\hat{f}_{1\mathrm{a}}$ and the new normalization factors $\mathcal{Z}_f$ and $\mathcal{Z}_{1\mathrm{a}}$ are defined by

$$\hat{f}_{1\mathrm{a}}(\Theta,\Phi;\boldsymbol{F},\boldsymbol{F}_\gamma,\Phi_{1\mathrm{s}}) := \frac{1}{\mathcal{Z}_{1\mathrm{a}}}\exp\big(\beta\Phi_{1\mathrm{s}}\hat{\mathcal{W}}_{1\mathrm{a}}(\Theta,\Phi,\boldsymbol{F},\boldsymbol{F}_\gamma)\big),\tag{57a}$$

$$\mathcal{Z}_f := \int_0^{2\pi}\int_0^{\pi}\hat{f}_{1\mathrm{a}}(\Theta,\Phi;\boldsymbol{F},\boldsymbol{F}_\gamma,\Phi_{1\mathrm{s}})\hat{f}_{\mathrm{SVM}}(\Theta;\Theta_{\mathrm{hi}},\omega)\ \sin\Theta\,\mathrm{d}\Theta\mathrm{d}\Phi,\tag{57b}$$

$$\mathcal{Z}_{1\mathrm{a}} := \int_0^{2\pi}\int_0^{\pi}\exp\big(\beta\Phi_{1\mathrm{s}}\hat{\mathcal{W}}_{1\mathrm{a}}(\Theta,\Phi,\boldsymbol{F},\boldsymbol{F}_\gamma)\big)\sin\Theta\,\mathrm{d}\Theta\mathrm{d}\Phi.\tag{57c}$$

We remark that the identity $\mathcal{Z}_{\mathrm{a}}=\mathcal{Z}_0\mathcal{Z}_{1\mathrm{a}}\mathcal{Z}_f$ applies, where $\mathcal{Z}_0$ and $\mathcal{Z}_{\mathrm{a}}$ are defined in Equations (51b) and (55), respectively. Therefore, when the directional average of a given physical quantity g is performed, one can write

$$\begin{aligned}\langle\!\langle g\rangle\!\rangle &= \int_0^{2\pi}\int_0^{\pi}g(X,\Theta,\Phi,\ldots)\hat{f}_{\mathrm{SR}}(\Theta,\Phi;\boldsymbol{F},\boldsymbol{F}_\gamma,\Theta_{\mathrm{hi}},\omega,\Phi_{1\mathrm{s}})\sin\Theta\mathrm{d}\Theta\mathrm{d}\Phi\\ &= \frac{1}{\mathcal{Z}_f}\int_0^{2\pi}\int_0^{\pi}g(X,\Theta,\Phi,\ldots)\hat{f}_{1\mathrm{a}}(\Theta,\Phi;\boldsymbol{F},\boldsymbol{F}_\gamma,\Phi_{1\mathrm{s}})\hat{f}_{\mathrm{SVM}}(\Theta;\Theta_{\mathrm{hi}},\omega)\sin\Theta\mathrm{d}\Theta\mathrm{d}\Phi,\end{aligned}\tag{58}$$

and $\langle\!\langle g\rangle\!\rangle$ can be rephrased either as the average of g with respect to the distribution $\hat{f}_{1\mathrm{a}}$ and the Von Mises measure $\mathrm{d}\mathfrak{m}_{\mathrm{SVM}}:=(\mathcal{Z}_f)^{-1}\hat{f}_{\mathrm{SVM}}(\Theta;\Theta_{\mathrm{hi}},\omega)\sin\Theta\mathrm{d}\Theta\mathrm{d}\Phi$ or, equivalently, as the average of g with respect to the distribution $\hat{f}_{\mathrm{SVM}}$ and the deformational measure $\mathrm{d}\mathfrak{m}_{1\mathrm{a}}:=(\mathcal{Z}_f)^{-1}\hat{f}_{1\mathrm{a}}(\Theta,\Phi;\boldsymbol{F},\boldsymbol{F}_\gamma,\Phi_{1\mathrm{s}})\sin\Theta\mathrm{d}\Theta\mathrm{d}\Phi$. In the first case, $\hat{f}_{\mathrm{SVM}}$ does not change in time, and encompasses the histological information associated with Θ_{hi} and ω; in the second case, $\hat{f}_{1\mathrm{a}}$ depends on the constitutive representation of the anisotropic part of the material's strain energy density, evolves in time through $\boldsymbol{F}$ and $\boldsymbol{F}_\gamma$, and is modulated by $\Phi_{1\mathrm{s}}$.

To conclude this section, we examine the inverse problem, i.e., a procedure to find Π when a given stationary probability density distribution of the fibers is known either by experimental evidence or because it is assigned from the outset. For instance, one can select the probability density distribution at the time conventionally taken as initial for a given benchmark problem. If, in addition, one assumes that neither deformations nor anelastic distortions have occurred at this initial time (in our setting, this

amounts to taking $\mathcal{W} = 0$), then, upon identifying the stationary probability density distribution f_{SR} with the initial one $f_{\mathrm{R,in}}$, i.e., $f_{\mathrm{SR}} \equiv f_{\mathrm{R,in}}$, Equation $(43)_1$ yields

$$f_{\mathrm{SR}} \equiv f_{\mathrm{R,in}} = \frac{1}{\mathcal{Z}_0}\exp(\beta\Pi) \qquad \Longrightarrow \qquad \Pi = \frac{1}{\beta}\log\left(\mathcal{Z}_0 f_{\mathrm{SR}}\right). \tag{59}$$

Hence, the deterministic external forces $\mathcal{F}_{\Theta}^{\mathrm{ext,det}}$ and $\mathcal{F}_{\Phi}^{\mathrm{ext,det}}$ can be interpreted as the driving forces that lead the system's probability density distribution towards f_{SR}, and that can be written as

$$\mathcal{F}_{\Theta}^{\mathrm{ext,det}} = \frac{\partial\hat{\Pi}}{\partial\Theta} = \frac{1}{\beta\hat{f}_{\mathrm{SR}}}\frac{\partial\hat{f}_{\mathrm{SR}}}{\partial\Theta}, \qquad \mathcal{F}_{\Phi}^{\mathrm{ext,det}} = \frac{1}{\sin\Theta}\frac{\partial\hat{\Pi}}{\partial\Phi} = \frac{1}{\sin\Theta}\frac{1}{\beta\hat{f}_{\mathrm{SR}}}\frac{\partial\hat{f}_{\mathrm{SR}}}{\partial\Phi}. \tag{60}$$

Let us assume now that a mechanical action is applied from the outset in such a way that the system remains in elastic regime (i.e., $\boldsymbol{F}_\gamma$ remains equal to the identity tensor). Then, the probability density distribution evolves in time and deviates from the initial one, $\hat{f}_{\mathrm{R,in}}$. However, if the system is (elastically) unloaded and brought back to the initial state, then the probability density distribution attained at the end of the unloading phase will be equal to $\hat{f}_{\mathrm{SR}} \equiv \hat{f}_{\mathrm{R,in}}$, and the terms $\mathcal{F}_{\Theta}^{\mathrm{ext,det}}$ and $\mathcal{F}_{\Phi}^{\mathrm{ext,det}}$ in Equation (60) can be interpreted as the forces that maintain the original probability density distribution.

If anelastic distortions are present at the instant of time taken as initial, then the body is not stress-free in this initial state [106], and the energetic contribution featuring in Equation $(43)_1$, which we indicate as $\hat{\mathcal{W}}_{\mathrm{1a,in}}(X,\Theta,\Phi) = \hat{\mathcal{W}}_{\mathrm{1a}}(\Theta,\Phi;\boldsymbol{F}_{\mathrm{in}}(X),\boldsymbol{F}_{\gamma\mathrm{in}}(X))$, is not null in general. Consequently, the initial probability density distribution and its associated potential would read

$$f_{\mathrm{SR}} \equiv f_{\mathrm{R,in}} = \frac{1}{\mathcal{Z}_{\mathrm{a}}}\exp\left(\beta\Pi + \beta\Phi_{1\mathrm{s}}\mathcal{W}_{\mathrm{1a,in}}\right) \qquad \Longrightarrow \qquad \Pi = \frac{1}{\beta}\log\left(\mathcal{Z}_{\mathrm{a}} f_{\mathrm{SR}}\right) - \Phi_{1\mathrm{s}}\mathcal{W}_{\mathrm{1a,in}}. \tag{61}$$

Hence, the deterministic external forces would be characterized by the expressions

$$\mathcal{F}_{\Theta}^{\mathrm{ext,det}}(X,\Theta,\Phi) = \frac{1}{\beta\hat{f}_{\mathrm{SR}}(X,\Theta,\Phi)}\frac{\partial\hat{f}_{\mathrm{SR}}}{\partial\Theta}(X,\Theta,\Phi) - \Phi_{1\mathrm{s}}(X)\frac{\partial\hat{\mathcal{W}}_{\mathrm{1a,in}}}{\partial\Theta}(X,\Theta,\Phi), \tag{62a}$$

$$\mathcal{F}_{\Phi}^{\mathrm{ext,det}}(X,\Theta,\Phi) = \frac{1}{\sin\Theta}\left(\frac{1}{\beta\hat{f}_{\mathrm{SR}}(X,\Theta,\Phi)}\frac{\partial\hat{f}_{\mathrm{SR}}}{\partial\Phi}(X,\Theta,\Phi) - \Phi_{1\mathrm{s}}(X)\frac{\partial\hat{\mathcal{W}}_{\mathrm{1a,in}}}{\partial\Phi}(X,\Theta,\Phi)\right). \tag{62b}$$

5 Summary of the model and description of the benchmarks

In this section, we describe two initial- and boundary-value problems that we simulate with the aid of the software COMSOL Multiphysics®, version 5.3. To compute the directional averages, we recur to the Spherical Design Algorithm [107, 27], suitably implemented in COMSOL [87]. With these numerical experiments we aim at investigating the capabilities of the model presented in the previous sections. In particular, we are interested in showing how the mesoscopic description of the reorientation of the fibers, accounted for by means of the Fokker–Planck Equation (40), influences the behavior of the tissue at the macroscale. For these purposes, we examine our model for the following two benchmarks:

1) Uni-axial stretch test of a slice of articular cartilage, taken from the surface region, i.e., the region in which the fibers most likely lie on the transverse plane of the tissue's considered specimen (this corresponds to $\Theta_{\mathrm{hi}}(H) = \pi/2$, where H is the specimen's thickness);

2) Uni-axial compression-maintenance test of a cylindrical specimen of a hypothetical fiber-reinforced tissue that borrows its properties from articular cartilage.

In both of these benchmarks, we consider a *quasi-stationary* evolution of the Fokker–Planck equation for the fibers' probability density distribution, thereby directly employing Equation (54) to describe the fibers' reorientation, instead of enforcing a pseudo-Gaussian or a symmetrized, bi-variate von Mises distribution [19, 32, 33] from the outset. While this approach is justified for the first benchmark, since

it aims at recovering some experimental curves in stationary conditions, for the second benchmark the hypothesis of a quasi-stationary evolution of the fibers is a simplifying assumption. However, in spite of this simplification, our procedure yields results similar to the non-stationary Fokker–Planck equation, and requires less computational resources. To be more specific, we are using the general result, based on the spectral analysis of linear operators, according to which the solution of the Fokker–Planck equation with a drift term generated by a potential converges exponentially to the stationary solution [108]. Clearly, the *quasi-stationary* approach reduces significantly the computational burden when the Fokker–Planck equation has to be solved together with Equations (32a)–(32d). Indeed, solving the non-stationary Fokker–Planck Equation (40) would require finding, for each point $X \in \mathscr{B}$, and at each time t, the probability density distribution $\hat{f}_{\mathrm{R}}$ as a function of Θ and Φ. In other words, this approach would require solving, at each time $t \in [t_{\mathrm{in}}, t_{\mathrm{fin}}]$, the Fokker–Planck equation, coupled with the full system (32a)–(32d), for each triplet of coordinates identifying a point $X \in \mathscr{B}$, and for each pair of spherical coordinates (Φ, Θ) identifying a direction $\boldsymbol{M}_X \in \mathbb{S}^2_X\mathscr{B}$. Instead, directly using Equation (54), i.e., invoking the quasi-stationary solution of the Fokker–Planck equation, partially decouples the remodeling of the fibers (described through the evolution of their probability density distribution) from the determination of the deformation and anelastic distortions of the extracellular matrix and from the pressure of the interstitial fluid. The decoupling is only partial for the following reason: on the one hand, the probability density distribution is needed, at each time, to evaluate the directional averages of the strain energy density and of the permeability, which are necessary for solving the "macroscopic" problem described by Equations (32a)–(32d); on the other hand, the strain energy density —in particular $\hat{\mathcal{W}}_{1\mathrm{a}}$— is needed, at each time, to determine the quasi-stationary probability density distribution through Equation (54).

5.1 Uni-axial stretch test of a slice of articular cartilage

We specialize the model to portray the experimental setting used in the work of Mansfield et al. [109]. In the aforementioned paper, the harvested articular cartilage is sliced at various depths, and, in each sample, the reorientation of the fibers under mechanical load is studied by imposing uni-axial stretch. Each slice can be thought of as a parallepiped with thickness much smaller than the other characteristic lengths. Two opposing sides of the lateral boundary of the cuboid are clamped to the experimental apparatus. The experiment is conducted in displacement control, and the orientation of the fibers in a specific zone at the center of the sample itself is measured by studying the scattering of light after the sample reaches the mechanical equilibrium. Under these conditions, the problem can be considered static for each of the imposed displacements assigned in the aforementioned paper [109].

We specialize our model to a purely elastic case, i.e., by assuming *no remodeling*, and we neglect the dynamic contribution of the fluid, which, for sufficiently long times (after relaxation), is characterized by a uniformly null pressure field. Thus, we solve the dynamic equation

$$\mathrm{Div}\boldsymbol{P}_{\mathrm{s}} = \boldsymbol{0} \qquad \text{in } \mathscr{B}. \tag{63}$$

The boundary is partitioned as $\partial\mathscr{B} = \Gamma_1 \cup \Gamma_2 \cup \Gamma_3 \cup \Gamma_4 \cup \Gamma_5 \cup \Gamma_6$, where, for $i = 1, 2, 3, 4, 5, 6$, each Γ_i represents a face of the parallelepiped. We select a Cartesian basis $\{\boldsymbol{E}_1, \boldsymbol{E}_2, \boldsymbol{E}_3\}$ such that the unit vector $\boldsymbol{E}_1$ is perpendicular to the faces Γ_1 and Γ_4; $\boldsymbol{E}_2$ is perpendicular to the faces Γ_2 and Γ_5; and $\boldsymbol{E}_3$ is perpendicular to the faces Γ_3 and Γ_6 (see Figure 2a). For simulations, we employ a parallelepiped of length $L = 1.5\,\mathrm{mm}$, width $W = 1.0\,\mathrm{mm}$, and thickness $H = 0.1\mathrm{mm}$. Thus, we prescribe the boundary conditions

$$\chi(X,t) = X, \qquad \text{on } \Gamma_1, \tag{64a}$$

$$\chi^1(X,t) = (1+\varepsilon)L, \quad \chi^2(X,t) = X^2, \quad \chi^3(X,t) = X^3, \qquad \text{on } \Gamma_4, \tag{64b}$$

$$\boldsymbol{P}_{\mathrm{s}}\boldsymbol{N}_2 = \boldsymbol{0}, \qquad \text{on } \Gamma_2, \tag{64c}$$

$$\boldsymbol{P}_{\mathrm{s}}\boldsymbol{N}_5 = \boldsymbol{0}, \qquad \text{on } \Gamma_5, \tag{64d}$$

$$\boldsymbol{P}_{\mathrm{s}}\boldsymbol{N}_3 = \boldsymbol{0}, \qquad \text{on } \Gamma_3, \tag{64e}$$

$$\boldsymbol{P}_{\mathrm{s}}\boldsymbol{N}_6 = \boldsymbol{0}, \qquad \text{on } \Gamma_6, \tag{64f}$$

where $\varepsilon \in \{0.00, 0.04, 0.08, 0.12, 0.16\}$ is the imposed strain.

Since the slice is taken from the superficial zone of the tissue, we consider that all the fibers have the same orientation $\Theta = \pi/2$. This amounts to imposing that the probability density distribution is a Dirac Delta centered at $\Theta_{\mathrm{hi}} = \pi/2$, as can be recovered from the expressions of the initial probability density distribution $\hat{f}_{\mathrm{R,in}}$ and of the normalization factor $\mathcal{Z}_0$ supplied in Equations (51a) and (51b) by setting $\Theta_{\mathrm{hi}} = \pi/2$ and $\omega \to 0^+$ (this limit, in fact, is approximated by the value $\omega(H) = 0.03$, assumed in Equation (52b) consistently with [14]). Indeed, for $\Theta_{\mathrm{hi}} = \pi/2$, and ω in a (right) neighborhood of zero, $\mathcal{Z}_0$ becomes

$$\mathcal{Z}_0 = \frac{2\pi\sqrt{\pi}\,\omega}{\sqrt{\beta\Pi_{\mathrm{c}}}} \mathrm{e}^{\beta\Pi_{\mathrm{c}}/\omega^2} \mathrm{erf}\left(\frac{\sqrt{\beta\Pi_{\mathrm{c}}}}{\omega}\right), \tag{65}$$

and the probability density distribution takes on the form

$$\hat{f}_{\mathrm{R,in}}(\Theta; \pi/2, \omega) = \frac{1}{2\pi\sqrt{\pi}\,\dfrac{\omega}{\sqrt{\beta\Pi_{\mathrm{c}}}}\,\mathrm{erf}\left(\dfrac{\sqrt{\beta\Pi_{\mathrm{c}}}}{\omega}\right)} \exp\left(-\frac{\beta\Pi_{\mathrm{c}}}{\omega^2}[\sin(\Theta - \pi/2)]^2\right). \tag{66}$$

Thus, in the limit $\omega \to 0^+$, $\hat{f}_{\mathrm{R,in}}(\Theta; \pi/2, \omega)$ converges towards zero whenever Θ is different from $\pi/2$, while it diverges positively for $\Theta = \pi/2$. In conclusion, for $\omega \to 0^+$, $\hat{f}_{\mathrm{R,in}}(\Theta; \pi/2, \omega)$ converges, in distributional sense, to the Dirac Delta distribution divided by 2π, i.e., to $\frac{1}{2\pi}\delta(\Theta - \pi/2)$.

Lastly, in the experiments by Mansfield et al. [109], the initial distribution of the fibers is not uniform with respect to Φ (i.e., the slices are not transversely isotropic). However, since we do not posses enough information on the whole tissue, we approximate this initial datum with a uniform distribution in Φ (i.e., the Dirac Delta centered in $\Theta = \pi/2$ and normalized by 2π) in order to calculate the deformations. Afterwards, we use the calculated deformations in conjunction with the initial distribution of the fibers, as shown in section 4.2, to reconstruct the experimental data collected in [109].

For what concerns the numerical implementation, we used quadratic Lagrange elements for solving the displacement and the pressure field, whereas no remodeling is accounted for in this benchmark. The overall system consists of 14937 degrees of freedom, with 5106 internal.

5.2 Uni-axial compression test of a cylindrical specimen

We consider the case of the uni-axial compression test of a cylindrical sample of cartilage of radius $R = 1.5\,\mathrm{mm}$ and height $H = 1\,\mathrm{mm}$, modeled as a saturated, soft, fiber-reinforced material undergoing a stress-driven remodeling process and reorientation of the fibers. The experimental setup consists of a chamber, filled with warm water to maintain temperature at about 20°C, in the interior of which the sample is confined at the top and at the bottom by two non-adhesive, impermeable plates characterized by a stiffness much higher than that of cartilage. The experiment is in displacement control by prescribing the compressive ramp [29, 86, 110]

$$\chi^3_{\mathrm{U}}(X^1, X^2, t) \equiv \chi^3(X^1, X^2, H, t) := \begin{cases} H - u_{\mathrm{T}}\dfrac{t - t_{\mathrm{in}}}{t_{\mathrm{ramp}} - t_{\mathrm{in}}}, & t \in [t_{\mathrm{in}}, t_{\mathrm{ramp}}], \\ H - u_{\mathrm{T}}, & t \in]t_{\mathrm{ramp}}, t_{\mathrm{fin}}], \end{cases} \tag{67}$$

where, for $t > t_{\mathrm{ramp}}$, the apparatus keeps fixed the imposed displacement on the sample. For our study, we consider $t_{\mathrm{in}} = 0\,\mathrm{s}$, $t_{\mathrm{ramp}} = 20\,\mathrm{s}$ and $t_{\mathrm{fin}} = 30\,\mathrm{s}$.

For the simulations, rather of speaking of articular cartilage, we speak of a hypothetical tissue "borrowing" some material properties from articular cartilage, including the histological profile of the fibers, because we aim at describing a broader class of tissues that may be of interest from the point of view of bio-engineered materials. For instance, as done for other studies on cartilage (see, e.g., [29]), we

assume the referential permeability of the tissue to be a function of X^3, normalized with respect to the height H of the sample [93], and we prescribe it to be

$$k_{0\mathrm{R}} \equiv k_{0\mathrm{R}}^{(0)} \left[\frac{e_{\mathrm{R}}(X^3/H)}{e_{\mathrm{R}}^{(0)}} \right]^{m_0} \exp\left\{ \frac{m_1}{2} \left[\left(\frac{1+e_{\mathrm{R}}(X^3/H)}{1+e_{\mathrm{R}}^{(0)}} \right)^2 - 1 \right] \right\}, \tag{68}$$

with $e_{\mathrm{R}} = (1-\Phi_{\mathrm{s}})/\Phi_{\mathrm{s}}$ being the void ratio, and $e_{\mathrm{R}}^{(0)}$ being the referential void ratio (we recall that the hypothesis of isochoric remodeling implies $J_\gamma = 1$, and, thus, $\Phi_{\mathrm{s}\nu} = \Phi_{\mathrm{s}}$).

We perform the simulations by solving the equations

$$\begin{aligned}
&\mathrm{Div}\boldsymbol{P}_{\mathrm{s}} - J\boldsymbol{F}^{-\mathrm{T}}\mathrm{Grad}P = \boldsymbol{0} && \text{in } \mathscr{B}, && (69a)\\
&\dot{J} - \mathrm{Div}(\boldsymbol{K}\mathrm{Grad}P) = 0 && \text{in } \mathscr{B}, && (69b)\\
&2\mathfrak{b}_\nu \mathrm{DevSym}(\boldsymbol{F}_\gamma^{-1}\dot{\boldsymbol{F}}_\gamma\boldsymbol{C}^{-1}) - \mathrm{Dev}(\boldsymbol{C}^{-1}\boldsymbol{\Sigma}_{\mathrm{s}}) = \boldsymbol{O} && \text{in } \mathscr{B}, && (69c)\\
&\mathrm{Skew}(\boldsymbol{F}_\gamma^{-1}\dot{\boldsymbol{F}}_\gamma\boldsymbol{C}^{-1}) = \boldsymbol{O} && \text{in } \mathscr{B}, && (69d)\\
&\boldsymbol{F}_\gamma^{-\mathrm{T}} : \dot{\boldsymbol{F}}_\gamma = 0 && \text{in } \mathscr{B}, && (69e)
\end{aligned}$$

in a cylindrical domain $\mathscr{B}$, with symmetry axis aligned along $\boldsymbol{E}_3$. We partition the boundary $\partial\mathscr{B}$ as $\partial\mathscr{B} = \Gamma_{\mathrm{U}} \cup \Gamma_{\mathrm{L}} \cup \Gamma_{\mathrm{B}}$, where Γ_{U} is the upper surface, Γ_{L} is the lateral surface, and Γ_{B} is the bottom surface. The co-normal of a given surface is indicated by adopting the same subscript, so that $\boldsymbol{N}_{\mathrm{U}}$, $\boldsymbol{N}_{\mathrm{L}}$, and $\boldsymbol{N}_{\mathrm{B}}$ are the fields of co-normals associated with Γ_{U}, Γ_{L} and Γ_{B}, respectively (see Figure 2b). Hence, for every time $t \in [t_{\mathrm{in}}, t_{\mathrm{fin}}]$, we prescribe the boundary conditions as

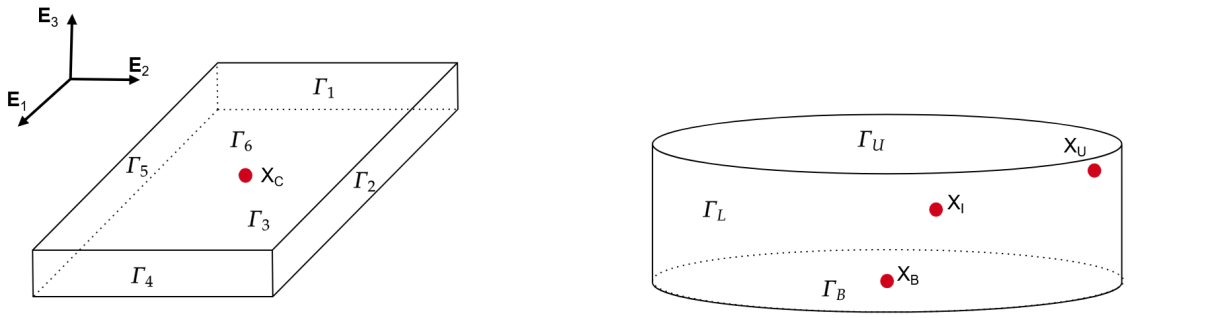
$$\begin{aligned}
&\chi^3(X,t) = \chi_{\mathrm{U}}^3(X_1,X_2,t), \quad [(\boldsymbol{P}_{\mathrm{s}} - J\boldsymbol{P}\boldsymbol{F}^{-\mathrm{T}})\boldsymbol{N}_{\mathrm{U}}]\boldsymbol{E}_1 = 0, \quad [(\boldsymbol{P}_{\mathrm{s}} - J\boldsymbol{P}\boldsymbol{F}^{-\mathrm{T}})\boldsymbol{N}_{\mathrm{U}}]\boldsymbol{E}_2 = 0, && \text{on } \Gamma_{\mathrm{U}}, && (70a)\\
&\boldsymbol{Q}\boldsymbol{N}_{\mathrm{U}} = 0, && \text{on } \Gamma_{\mathrm{U}}, && (70b)\\
&(\boldsymbol{P}_{\mathrm{s}} - J\boldsymbol{P}\boldsymbol{F}^{-\mathrm{T}})\boldsymbol{N}_{\mathrm{L}} = \boldsymbol{0}, && \text{on } \Gamma_{\mathrm{L}}, && (70c)\\
&P = 0, && \text{on } \Gamma_{\mathrm{L}}, && (70d)\\
&\chi(X,t) = (X^1, X^2, 0), && \text{on } \Gamma_{\mathrm{B}}, && (70e)\\
&\boldsymbol{Q}\boldsymbol{N}_{\mathrm{B}} = 0, && \text{on } \Gamma_{\mathrm{B}}. && (70f)
\end{aligned}$$

Finally, the initial conditions for the IBVP are

$$\begin{aligned}
&\chi(X,t_{\mathrm{in}}) = \chi_{\mathrm{in}}(X), && \text{in } \mathscr{B}, && (71a)\\
&P(X,t_{\mathrm{in}}) = 0, && \text{in } \mathscr{B}, && (71b)\\
&\boldsymbol{F}_\gamma(X,t_{\mathrm{in}}) = \boldsymbol{I}, && \text{in } \mathscr{B}, && (71c)\\
&\hat{f}_{\mathrm{R,in}}(\Theta;\Theta_{\mathrm{hi}},\omega) = \frac{1}{\mathcal{Z}_0}\exp\left(\frac{\beta\Pi_{\mathrm{c}}}{\omega^2}\left[\cos(\Theta-\Theta_{\mathrm{hi}})\right]^2\right), && \text{in } \mathbb{S}^2\mathscr{B}, && (71d)
\end{aligned}$$

where we set $\chi_{\mathrm{in}}(X) = (X^1, X^2, X^3)$, $\boldsymbol{I}$ is the identity tensor in the reference placement, and $\mathcal{Z}_0$ is defined in Equation (47). Note that the dependence of $\hat{f}_{\mathrm{R,in}}$ on X —in fact, on X^3— is through Θ_{hi} and ω according to the expressions (52a) and (52b), respectively. Consequently, also $\mathcal{Z}_0$ depends on X^3 through these quantities, as can be deduced from Equation (51b). Moreover, because of lack of better information, and to fall within an already established framework [27], we set $\Pi_{\mathrm{c}} = 1/\beta$ in Equation (71d). By doing so, the quantity $1/\omega^2$ in the argument of the exponential function in Equation (71d) can be identified with $1/\omega^2 \equiv 2b$, where b is the parameter of the von Mises distribution used for the "Model B" of Federico and Gasser [27].

Also for this benchmark we used quadratic Lagrange elements for solving the displacement and the pressure field, whereas the remodeling variable is solved in the Gauss points used for integration. In the case of the cylinder, the overall system consists of 34580 degrees of freedom (plus 7128 internal degrees of freedom introduced by COMSOL).



(a) Geometry of the cuboid sample for benchmark 1.

(b) Geometry of the cylindrical sample for benchmark 2.

Figure 2: Geometries of the two benchmarks. The point X_{C} in the first geometry is taken in the middle of the cuboid, at Cartesian coordinates $(0.5, 0.75, 0.05)$, expressed in millimeters. The points X_{U}, X_{I} and X_{B} in the second geometry are taken at Cartesian coordinates $(0.0, 1.35, 0.9)$, $(0.0, 0.375, 0.5)$ and $(0.0, 0.0, 0.0)$, respectively, expressed in millimeters.

6 Results and discussion

In this section, we report and discuss the results of the two benchmarks described previously, and we examine the influence of the fibers on the overall behavior of the medium.

6.1 Fiber orientation under uni-axial stretch of a slice of cartilage

By following the procedure depicted at the end of section 4.2, and by approximating the deformation as written in section 5.1, we aim to recover some experimental curves presented in the work of Mansfield et al. [109]. In particular, we simulate the evolution of the probability density distribution in the cases of uni-axial stretch of superficial slices of cartilage for the two initial data

$$\hat{f}^{(i)}_{\mathrm{R,in}}(\Theta,\Phi) = \frac{1}{2\pi}\delta\left(\Theta-\frac{\pi}{2}\right)\frac{1}{C_0^{(i)}}\hat{h}^{(i)}(\Phi), \qquad i\in\{1,2\}, \tag{72}$$

where $\hat{h}^{(1)}(\Phi)$ and $\hat{h}^{(2)}(\Phi)$ are given by

$$\hat{h}^{(1)}(\Phi) = \exp\left(3.4\left[\cos\left(\Phi-\frac{\pi}{12}\right)\right]^2\right), \tag{73a}$$

$$\hat{h}^{(2)}(\Phi) = \exp\left(6.4\left[\cos\left(\Phi-\frac{11}{24}\pi\right)\right]^2\right) + 0.5\exp\left(6.2\left[\cos\left(\Phi-\frac{\pi}{18}\right)\right]^2\right), \tag{73b}$$

and the normalizing constants $C_0^{(i)}$ coincide with their averages over $[0, 2\pi]$, i.e.,

$$C_0^{(i)} = \frac{1}{2\pi}\int_0^{2\pi} h^{(i)}(\Phi)\mathrm{d}\Phi, \qquad i\in\{1,2\}. \tag{74}$$

For $i = 1, 2$, $\hat{f}^{(i)}_{\mathrm{R,in}}$ fits the experimental curves for the distribution of the fiber orientation without applied stretch [109], and the overall normalization constants are identified by the equalities $\mathcal{Z}_0^{(i)} = 2\pi C_0^{(i)}$.

We are able to predict the evolution of the probability density distributions obtained as solutions of the Fokker–Planck Equation (40) starting from $\hat{f}^{(1)}_{\mathrm{R,in}}$ and $\hat{f}^{(2)}_{\mathrm{R,in}}$. In particular, for these initial distributions, the corresponding potentials $\Pi^{(1)}$ and $\Pi^{(2)}$ are assigned in such a way that $\hat{f}^{(1)}_{\mathrm{R,in}}$ and $\hat{f}^{(2)}_{\mathrm{R,in}}$ coincide with the stationary solutions of the Fokker–Planck equation in the absence of deformation (see Equation $(59)_2$). After stretching, the stationary solutions can be recast in the form

$$\hat{f}^{(i)}_{\mathrm{SR}}(\Theta,\Phi) = \frac{\mathcal{Z}_0^{(i)}}{\mathcal{Z}_{\mathrm{a}}^{(i)}}\hat{f}^{(i)}_{\mathrm{R,in}}(\Theta,\Phi)\mathrm{e}^{\beta\Phi_{1\mathrm{s}}(H)\hat{W}_{1\mathrm{a}}(\Theta,\Phi,\boldsymbol{F}(H))}, \tag{75a}$$

Parameter	Symbol	Numerical value	Unit of measure	Reference
Density fluid phase	ϱ_{f}	$1 \cdot 10^3$	$\mathrm{kg/m^3}$	[111]
Density solid phase	ϱ_{s}	$1 \cdot 10^3$	$\mathrm{kg/m^3}$	[111]
Critical J	J_{cr}	$0.1 + \Phi_{\mathrm{s}\nu}$	-	[32]
Coefficient of $\mathcal{U}$	q	2	-	[32]
Coefficient of $\mathcal{U}$	r	0.5	-	[32]
Elastic property	$\alpha_0 = \alpha_{0i}$	0.125	MPa	[29]
Elastic property	$\alpha_1 = \alpha_{1i}$	0.778	-	[29]
Elastic property	$\alpha_2 = \alpha_{2i}$	0.111	-	[29]
Elastic property	k_1	7.5	MPa	[112, 29]
Elastic property	k_2	0.5	-	-
Characteristic energy density	β	$2.71 \cdot 10^{-4}$	$\mathrm{Pa^{-1}}$	-
Reference hydraulic conductivity	$k_{0\mathrm{R}}^{(0)}$	$3.7729 \cdot 10^{-3}$	$\mathrm{mm^4/(N \cdot s)}$	[86]
Material parameter	m_0	0.0848	-	[113]
Material parameter	m_1	4.6380	-	[113]
Referential void ratio	$e_{\mathrm{R}}^{(0)}$	4.0	–	[29]
Remodeling rate	b_ν	25.0	$\mathrm{N \cdot s/mm^2}$	-

Table 1: Values of the material parameters used for the numerical simulations.

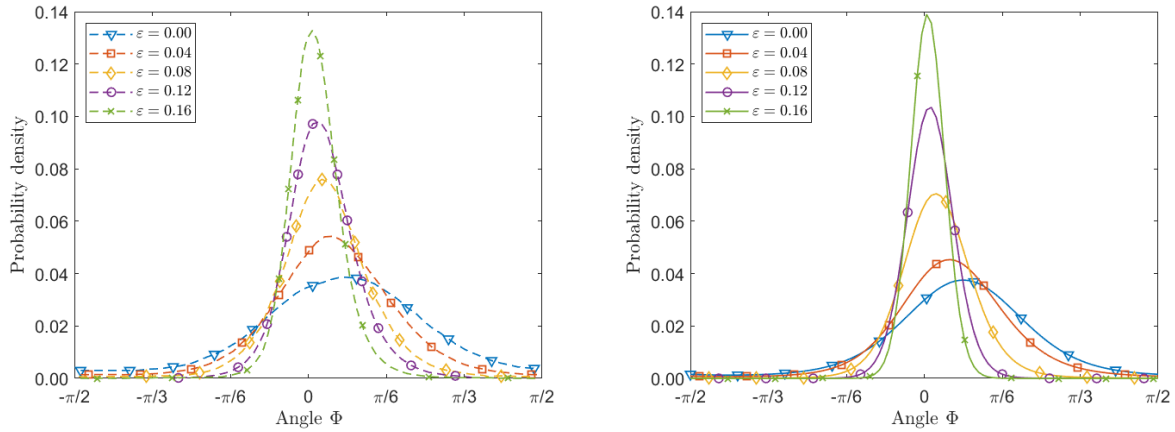
$$\frac{\mathcal{Z}_{\mathrm{a}}^{(i)}}{\mathcal{Z}_0^{(i)}} = \int_0^{2\pi}\int_0^{\pi} \hat{f}_{\mathrm{R,in}}^{(i)}(\Theta,\Phi)\mathrm{e}^{\beta\Phi_{1\mathrm{s}}(H)\hat{\mathcal{W}}_{1\mathrm{a}}(\Theta,\Phi,\boldsymbol{F}(H))}\sin\Theta\,\mathrm{d}\Theta\mathrm{d}\Phi$$
$$= \frac{1}{2\pi C^{(i)}}\int_0^{2\pi} \hat{h}^{(i)}(\Phi)\mathrm{e}^{\beta\Phi_{1\mathrm{s}}(H)\hat{\mathcal{W}}_{1\mathrm{a}}(\pi/2,\Phi,\boldsymbol{F}(H))}\mathrm{d}\Phi, \tag{75b}$$

where the explicit dependence of $\hat{\mathcal{W}}_{1\mathrm{a}}$ on $\boldsymbol{F}_\gamma$ and on X has been suppressed because, for this benchmark test, no remodeling is considered, and because the parameters k_1 and k_2 are assumed to be constant (see Table 1).

In particular, the parameters k_2 and β are assigned by fitting the experimental findings. It is worth noticing that the last integral in Equation (75b) amounts to performing the change of measure $\mathrm{d}\Phi \mapsto (2\pi C^{(i)})^{-1}\hat{h}^{(i)}(\Phi)\mathrm{d}\Phi$ (see Remark 3).

In Figures 3a and 4a, we report a selected collection of data, extracted for "Figure 9a (ii)" of Mansfield et al. [109] and replotted in radians for comparison with our numerical results, as shown in Figures 3b and 4b. In these figures, with the same convention adopted in [109], the directions identified by $(\Theta,\Phi) = (\pi/2, 0)$ are parallel to the Cartesian unit vector $\boldsymbol{E}_1$, along which the tissue is stretched. Note that, in order to directly compare our numerical results with the experimental findings of Mansfield et al. [109], we redefined $\hat{f}_{\mathrm{SR}}^{(i)}$ so as to exploit the symmetry condition $\hat{f}_{\mathrm{SR}}^{(i)}(\Theta,\Phi) = \hat{f}_{\mathrm{SR}}^{(i)}(\pi-\Theta,\Phi+\pi)$ to restrict the plot of $\hat{f}_{\mathrm{SR}}^{(i)}$ along Φ on the subdomain $[-\pi/2,\pi/2] \subset [-\pi,\pi[$. The agreement between the experimental data and the probability densities of our model is particularly good for strains equal to, or greater than, the 8% of the overall length L of the slice. However, for smaller strains, the probability densities computed numerically differ quantitatively from the experimental ones in appreciable way, although their trend is still in agreement with the experimental data.

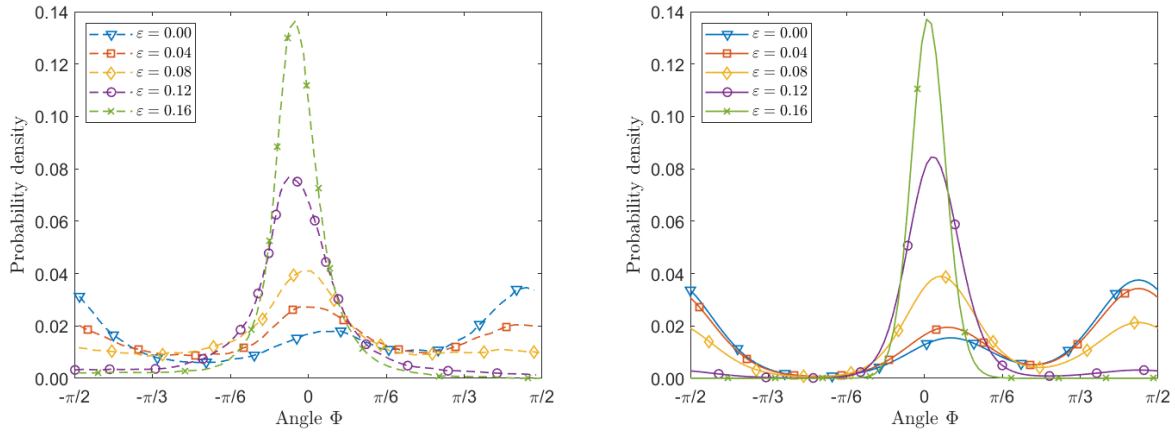
A similar detachment of our numerical results from the experimental ones of Mansfield et al. [109] occurs in correspondence to the "tails" of the bi-variate distribution in Figure 4b, i.e., for the values attained by $\hat{f}_{\mathrm{SR}}^{(2)}$ as Φ approaches both $-\pi/2$ and $\pi/2$. In fact, in the experiment the number of fibers aligned in the direction perpendicular to the one along which the strain is applied decreases for small strains (i.e., from $\varepsilon = 0.00$ to $\varepsilon = 0.04$) more markedly than predicted by our simulations. In our opinion, this would suggest some form of self-interactions among the collagen fibers, which is not considered in the present model, and that could improve the accuracy in the modeling of the fiber reorientation process. With respect to the viewpoint expressed in [115], the behavior observed in Figure 4a, and, to a smaller



(a) Experimental finding, surface slice

(b) Numerical simulation

Figure 3: Comparison between the experimental findings of Mansfield et al. [109] (Figure 3a, adapted from "Figure 9a (ii)" [109]) and our numerically simulated curves for an imposed deformation $\varepsilon = 0.04n$, for $n = 0, 1, 2, 3, 4$ (Figure 3b). The experimental data points of Mansfield et al.[109] have been extracted from their "Figure 9a (ii)" by using the online software `WebPlotDigitizer` [114], and have been replotted vs radians (degrees are used in the original image) as shown in Figure 3a.



(a) Experimental finding, surface slice

(b) Numerical simulation

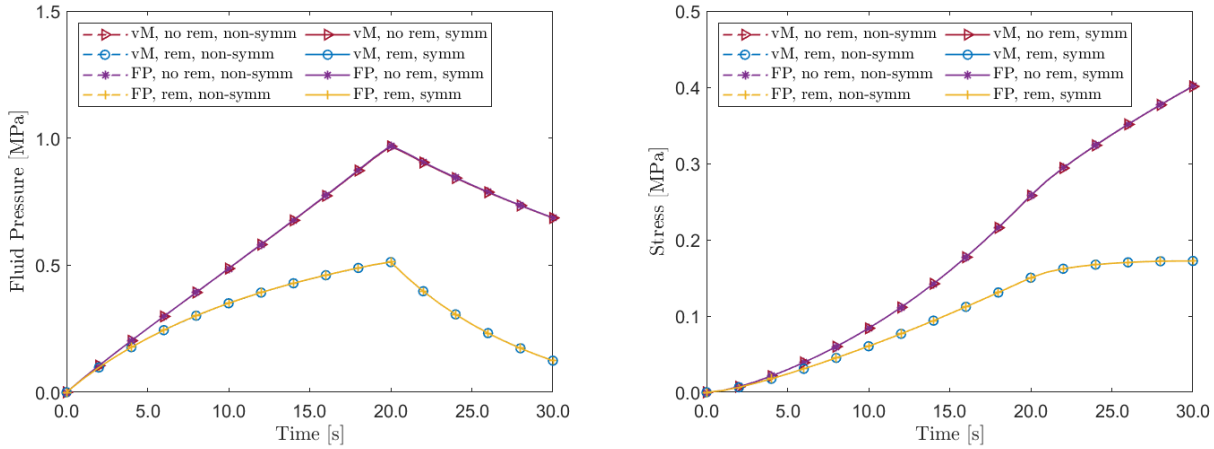
Figure 4: Comparison between the experimental findings of Mansfield et al. [109] (Figure 4a, adapted from "Figure 9b (ii)" [109]) and our numerically simulated curves for an imposed deformation $\varepsilon = 0.04n$, for $n = 0, 1, 2, 3, 4$ (Figure 4b). The experimental data points of Mansfield et al.[109] have been extracted from their "Figure 9b (ii)" by using the online software `WebPlotDigitizer` [114], and have been replotted vs radians (degrees are used in the original image) as shown in Figure 4a.

extent, in Figure 3a, could constitute a clue that there are cross-links between collagen fibers.

We remark that the hypothesis of transverse isotropy is not respected, since not only are the initial distributions of fibers nonuniform with respect to Φ, but, in addition, the subsequent mechanical action reorients the fibers significantly, even for moderate strains.

Finally, we observe that the fitting of the experimental curves returns very different numerical values for β and k_2 depending on the considered experiment (as indicated in Table 1, we take k_1 from the literature). This difference could be interpreted as a material heterogeneity of the cartilage under examination, or as a byproduct of a remodeling process that took place and altered irreversibly the mechanical behavior. In particular, from the fitting of Figure 3a we obtain $\beta = 2.71 \cdot 10^{-4}\,\mathrm{Pa}^{-1}$ and

$k_2 = 0.5$, while from the fitting of Figure 4a we obtain $\beta = 1.042 \cdot 10^{-4}\,\mathrm{Pa}^{-1}$ and $k_2 = 8$. We took the former values of β and k_2 as a reference for Table 1 since the initial distribution $\hat{f}_{\mathrm{SR}}^{(1)}$ exhibits less deviation from a uniform distribution with respect to $\hat{f}_{\mathrm{SR}}^{(2)}$.



(a) Fluid pressure, point X_{B}.

(b) Constitutive stress, point X_{B}.

Figure 5: Comparison between the time evolution of pressure field (figure on the left) and of the constitutive normal stresses (figure on the right) under different remodeling processes, evaluated at the point X_{B}. The curves associated with the label "non-symm" refer to the simulations obtained with the initial probability density distribution given in Equation (71d), while the curves associated with the label "symm" adopt the symmetric probability density distribution discussed in the conclusions (cf. Equation (80)) as initial condition.

6.2 Compression of a cylindrical specimen

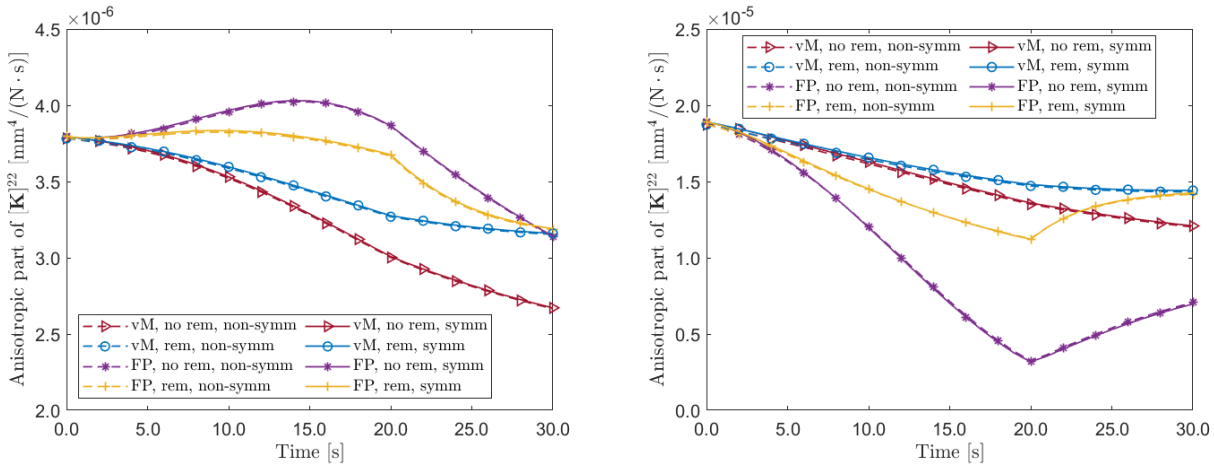
In this section, we report the results of the numerical simulations of the benchmark described in section 5.2, and we discuss their possible physical interpretation. In particular, we address the relevance of the two types of remodeling considered in our work, i.e., the reorientation of the fibers and the isotropic structural reorganization of the matrix, in the characterization of the medium's behavior under compressive loading.

We consider the following different simulations: (i) the one in which no remodeling is considered; (ii) the one in which both types of remodeling are present; (iii) and the two intermediate cases, with one active and the other switched off. To compare the data, we take measurements in three points of the specimen: one placed near the intersection between the upper surface and the lateral one, denominated X_{U}; one placed at half of the height of the cylinder, near the symmetry axis, and denominated X_{I}; the last one is placed in the center of the bottom surface, denominated X_{B}. For brevity, we refer to the anelastic distortions developed in the material as "remodeling" and we distinguish the case in which the anelastic distortions are deactivated (marked in the figures as "no remodeling") from the one in which they are active (indicated by "remodeling").

As expected, the fluid pressure and the overall constitutive stresses in X_{B} in direction $\boldsymbol{E}_3$ (i.e., $[\boldsymbol{P}_{\mathrm{s}}]_3{}^3$), shown in Figures 5a and 5b, respectively, are largely influenced by the onset of remodeling distortions, while the reorientation of the fibers does not alter significantly their values. In fact, since the fibers are aligned perpendicularly to the lower surface and, thus, are compressed by the loading, they do not provide any contribution, and the production of anelastic distortions is the dominant mechanism of remodeling.

Next, we examine the behavior of the porous medium at X_{I} and X_{U}, and we focus on the anisotropic contributions to stress and permeability. In particular, we want to relate the obtained values with the evolution at the mesoscale of the fibers' probability density distributions. We remark that, since the points X_{I} and X_{U} have null X_1-coordinate, they belong to the plane spanned by $\boldsymbol{E}_2$ (oriented radially)

and $\boldsymbol{E}_3$ (symmetry axis). Moreover, for this particular choice of coordinates the 22-components of $\boldsymbol{K}_\mathrm{a}$ and $\boldsymbol{P}_\mathrm{sa}$ evaluated at X_I and X_U are representative of the radial components of $\boldsymbol{K}_\mathrm{a}$ and$\boldsymbol{P}_\mathrm{sa}$, since the problem describing this benchmark is axial-symmetric. As highlighted in Figures 6a and 6b, the reorientation of the fibers heavily impacts the anisotropic term in the hydraulic conductivity[4], whereas the isotropic remodeling (i.e., the anelastic distortions) influences slightly less the anisotropic contribution to the hydraulic conductivity. Indeed, the increase or decrease in the hydraulic conductivity is due to the process of alignment of the fibers along the radial and circumferential directions, since the compression is unconfined and the solid matrix can spread radially and guide the fibers embedded in it. The reorientation of the fibers results in an increase of the radial permeability in the interior point X_I, whereas it results in a decrease of this quantity at X_U. However, since this quantity is already a correction to the isotropic hydraulic conductivity, it does not alter significantly the fluid efflux (data not shown).



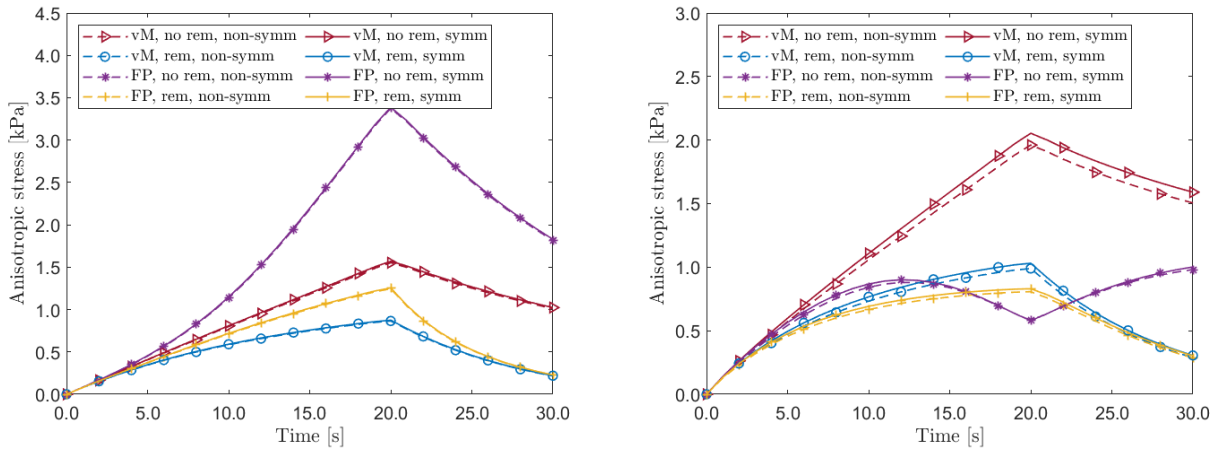
(a) 22-Component of the anisotropic hydraulic conductivity $\boldsymbol{K}_\mathrm{a}$, point X_I.

(b) 22-Component of the anisotropic hydraulic conductivity $\boldsymbol{K}_\mathrm{a}$, point X_U.

Figure 6: Comparison between the time evolution of the anisotropic contribution to the component $[\boldsymbol{K}_\mathrm{a}]_{22}$ of the permeability tensor evaluated at the points X_I (figure on the left) and X_U (figure on the right). We remark that, at these points, the radial direction coincides with the Cartesian direction $\boldsymbol{E}_2$. The curves associated with the label "non-symm" refer to the simulations obtained with the initial probability density distribution given in Equation (71d), while the curves associated with the label "symm" adopt the symmetric probability density distribution discussed in the conclusions (cf. Equation (80)) as initial condition.

A much more nuanced situation appears when examining the 22-component of the anisotropic stress, which is shown in Figures 7a and 7b. We consider first the case in which the anelastic distortions are switched off. In this situation, the anisotropic stresses $[\boldsymbol{P}_\mathrm{sa}]_2{}^2$ registered in X_I when the probability density distribution is the stationary solution of the Fokker–Planck equation, with the drift term featuring both Π and $\mathcal{W}_\mathrm{1a}$, are higher than those obtained for the von Mises distribution, which considers only $\beta\Pi$ as drift term. This is because $[\boldsymbol{P}_\mathrm{sa}]_2{}^2$, being a directional average, depends on the probability density distribution. This distribution, in turn, evolves in time under the guidance of $\mathcal{W}_\mathrm{1a}$ and deviates considerably from the von Mises distribution, taken as initial datum. In particular, the probability density distribution driven by $\mathcal{W}_\mathrm{1a}$ weighs the fibers in a way that depends on both angles Θ and Φ (see Figures 8a and 8b). Moreover, if no anelastic distortions are considered, the radial stress registered at X_I increases for $t \in [t_\mathrm{in}, t_\mathrm{ramp}[$ and decreases for $t > t_\mathrm{ramp}$, i.e., when the imposed deformation is kept fixed. However, at X_U the value of the radial anisotropic contribution to the first Piola–Kirchhoff stress computed by solving

[4]When we speak of "hydraulic conductivity", we mean here the ratio between the permeability of the medium, expressed in m^2, and the viscosity of the fluid, expressed in $\mathrm{N}\cdot\mathrm{s}/\mathrm{m}^2$. Note, however, that in the literature on porous media the wording "hydraulic conductivity" usually refers to the ratio $k\varrho g/\mu$, where k is a constant referential value of permeability, ϱ is the constant true density of water, and g the magnitude of the gravity acceleration vector.



(a) 22-Component of the anisotropic stress, point X_{I}.

(b) 22-Component of the anisotropic stress, point X_{U}.

Figure 7: Comparison between the time evolution of the 22-component of the anisotropic contribution of the first Piola–Kirchhoff stress tensor of the solid phase, evaluated at the points X_{I} (figure on the left) and X_{U} (figure on the right). At these points, the radial direction coincides with the Cartesian direction $\boldsymbol{E}_2$. The curves associated with the label "non-symm" refer to the simulations obtained with the initial probability density distribution given in Equation (71d), while the curves associated with the label "symm" adopt the symmetric probability density distribution discussed in the conclusions (cf. Equation (80)) as initial condition.

the Fokker–Planck equation exhibits a different, non-monotonic behavior in $t \in [t_{\mathrm{in}}, t_{\mathrm{ramp}}[$. At first it increases, but it reaches the peak before the compressive ramp attains the maximum compression. The difference in the examined behaviors can be explained by looking at the evolution of the fiber probability density distributions (see in particular Figures 9a and 9b).

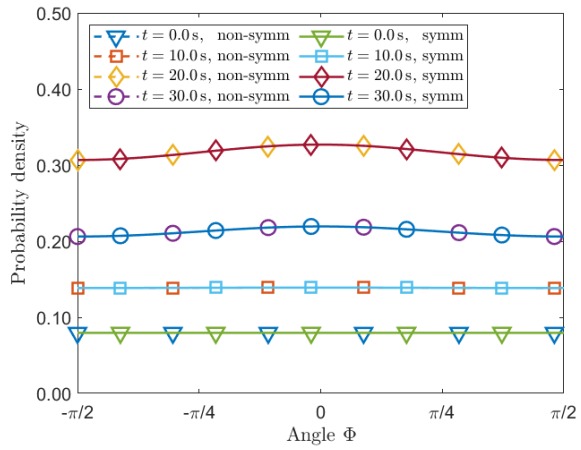
We report the evolution of the fiber probability density distributions at X_{I} in Figure 8, where Figures 8a and 8b refer to the case of no anelastic distortions ("no remodeling"), and Figures 8c and 8d refer to the case in which anelastic distortions are switched on ("remodeling"). In Figure 9, we report the probability density distributions at X_{U}, with Figures 9a and 9b reporting the case of no remodeling, and Figures 9c and 9d the case in which remodeling is switched on.

In our model, in the absence of remodeling distortions, the fibers tend to align themselves along the direction of higher deformation. In X_{I}, the radial deformation, which coincides with the deformation along the Cartesian direction $\boldsymbol{E}_2$, is lower than the circumferential deformation during the whole simulation. In fact, the probability density registered along the radial direction, individuated by $\Theta = \pi/2$ and $\Phi = \pm\pi/2$, increases with the application of the compressive ramp, i.e., up to 20 s(see e.g. Figure 8a and 8b), which means that it is more likely to find fibers that have reoriented in parallel with the transversal plane and along the radial direction. However, at X_{U}, a similar trend takes place: the deformation along the circumferential direction is greater than the radial one, and the fibers tend to align in parallel with the transversal plane, but orthogonally to the radial deformation. Hence, at X_{U} the anisotropic contributions to permeability and to the stress computed by solving the stationary Fokker–Planck equation are lower than those computed with the von Mises distribution, since the fibers reorient mostly in the direction orthogonal to the radial displacement, which does not coincide with the direction of maximum deformation.

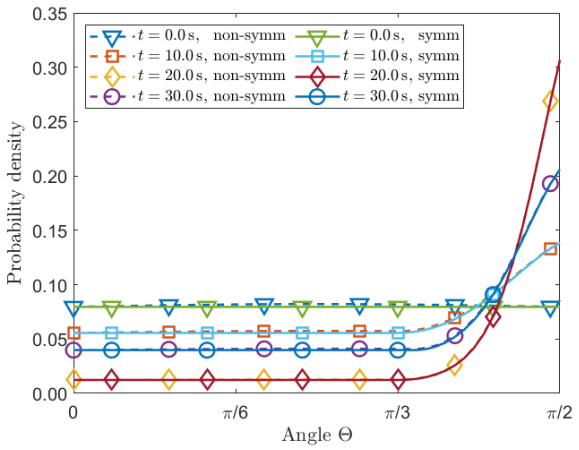
However, if the extracellular matrix undergoes isotropic remodeling, the radial anisotropic permeabilities are lower in the case of no remodeling, as shown in Figure 6b, and, for the von Mises distribution, they decrease even after the compressive ramp reaches the maximum displacement, while, for the Fokker–Planck distribution, they increase for $t > t_{\mathrm{ramp}}$. In fact, as can be seen in Figures 8c, 8d, 9c, and 9d, isotropic remodeling reduces the capacity of the fibers of reorienting for the considered benchmark,

thereby making them less susceptible to follow the mechanical stimuli.

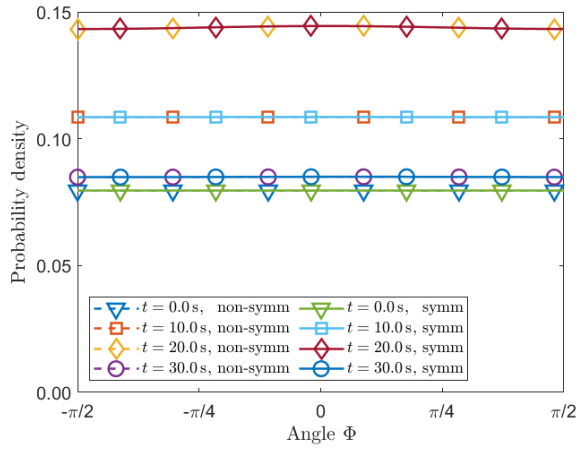
In our opinion, our results indicate that the anisotropic stresses and permeabilities predicted by our model should be viewed as phenomena related to two levels of descriptions. Indeed, the remodeling contributions associated with the reorientation of the fibers (resolved at the mesoscale through the Fokker–Planck equation) and those related to the anelastic distortions of the extracellular matrix (resolved at the scale of the tissue as a whole) affect significantly, but in different ways, the stress and the permeability distribution in the tissue.



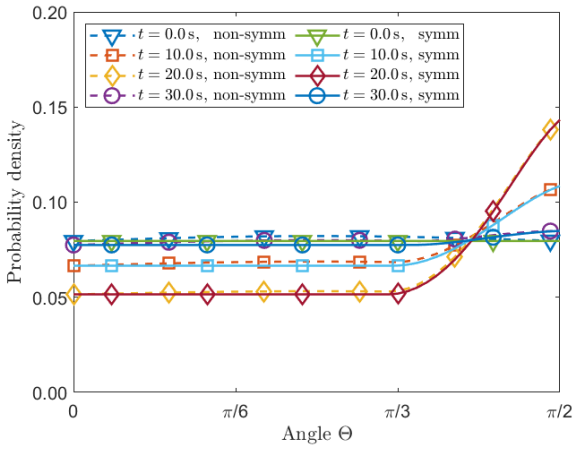
(a) Probability density distribution along Φ for $\Theta = \pi/2$, no remodeling, point X_{I}.



(b) Probability density distribution along Θ for $\Phi = \pi/2$, no remodeling, point X_{I}.



(c) Probability density distribution along Φ for $\Theta = \pi/2$, remodeling, point X_{I}.

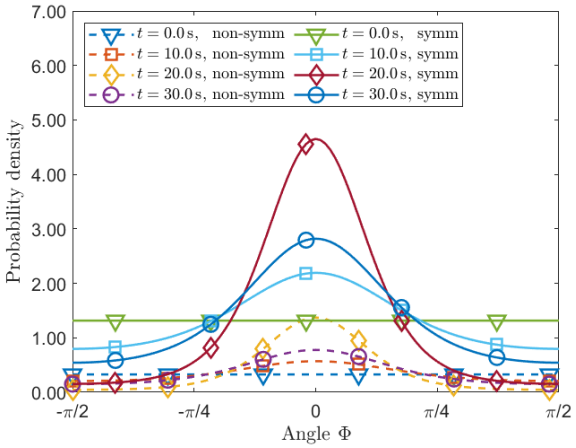


(d) Probability density distribution along Θ for $\Phi = \pi/2$, remodeling, point X_{I}.

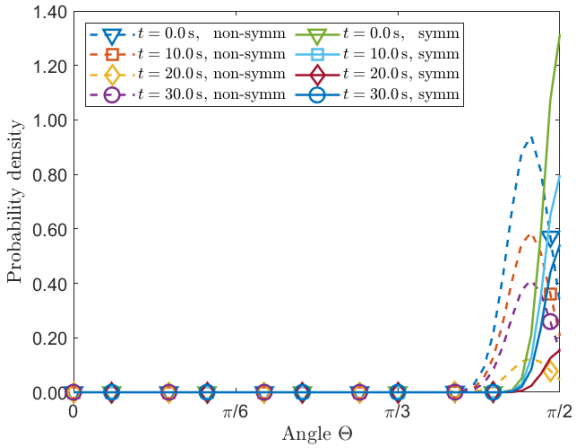
Figure 8: Comparison among fibers probability density distributions at the point X_{I} (see Figure 2b for reference) obtained by solving the Fokker–Planck equation with the drift term $\beta[\Pi + \Phi_{1\mathrm{s}}\mathcal{W}_{1\mathrm{a}}]$. The curves associated with the label "non-symm" refer to the simulations obtained with the initial probability density distribution given in Equation (71d), while the curves associated with the label "symm" adopt the symmetric probability density distribution discussed in the conclusions (cf. Equation (80)) as initial condition.

7 Concluding remarks and future developments

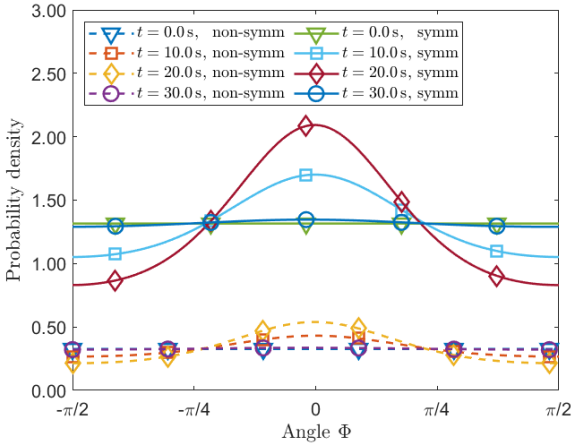
In this work, we presented a model of a fiber-reinforced, soft, hydrated, biphasic porous medium under the explicit constraints of saturation, incompressibility of its constituents, and of shared kinematics



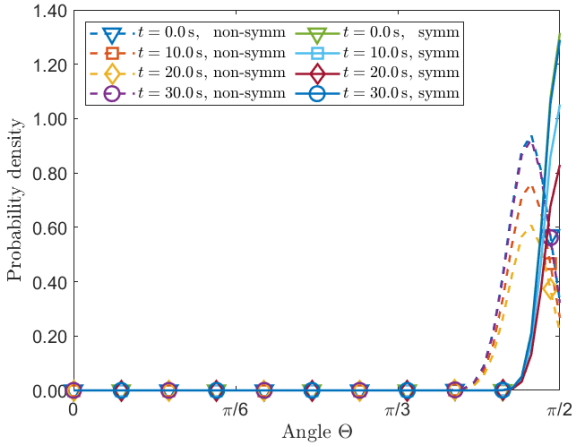
(a) Probability density distribution along Φ for $\Theta = \pi/2$, no remodeling, point X_{U}.



(b) Probability density distribution along Θ for $\Phi = \pi/2$, no remodeling, point X_{U}.



(c) Probability density distribution along Φ for $\Theta = \pi/2$, remodeling, point X_{U}.



(d) Probability density distribution along Θ for $\Phi = \pi/2$, remodeling, point X_{U}.

Figure 9: Comparison among fibers probability density distributions at the point X_{U} (see Figure 2b for reference) obtained by solving the Fokker–Planck equation with the drift term $\beta[\Pi + \Phi_{1\mathrm{s}}\mathcal{W}_{1\mathrm{a}}]$. The curves associated with the label "non-symm" refer to the simulations obtained with the initial probability density distribution given in Equation (71d), while the curves associated with the label "symm" adopt the symmetric probability density distribution discussed in the conclusions (cf. Equation (80)) as initial condition.

between extracellular matrix and fibers, whereas we considered the constraints of isochoric remodeling and of incompressibility of the overall mixture through the Lagrange multiplier technique. In this regard, we framed the model by recurring to the Principle of Virtual Power as used in [51, 52]. In addition, the solid phase, which comprises both the isotropic extracellular matrix and the fibers, is subjected to two processes of structural changes that, however, are modeled at different levels. In fact, we dealt with two remodeling processes, both of configurational nature, one described at the scale of the tissue and consisting of the production of anelastic distortions, while the other concerns the reorientation of the fibers and is affected by interactions of statistical type that take place at the mesoscopic scale. While both have been previously studied, e.g., in [32, 31, 61], the latter constitutes an enrichment of the framework of fiber-reinforced, statistically oriented materials for two reasons. First, the remodeling of the fibers, i.e., their reorientation, occurs through the evolution of their probability density distribution. This constitutes a step forward with respect to the works by Grillo et al. [31] and Crevacore et al. [32],

in which the functional form of the probability density distribution was given once and for all, although it was parameterized by the evolution of the direction of the most probable orientation of the fibers. The second reason is that, the probability density distribution determined in the present work is shaped by the deformation occurring in the medium, thereby establishing a two-way-coupling between the deformation and the evolution of the fibers. Indeed, the deformation determines the anisotropic strain energy density $\hat{\mathcal{W}}_{1a}$, which, in turn, updates the probability density distribution $\hat{f}_R$ (or $\hat{f}_{SR}$), which enters the directional averages of the macroscopic strain energy density itself and of the permeability.

We achieved the following results:

i) We derived a Fokker–Planck equation for the evolution of the probability density f_R associated with the Langevin-like process of the reorientation of the fibers, and we obtained the von Mises distribution as a particular case of stationary solution. We expanded the framework of Crevacore et al. [32] by introducing a target probability density distribution associated with a potential Π and, when specializing our model to articular cartilage, we formulated Π in order to identify the target probability density distribution in the absence of deformation with the one capable of recovering the histological pattern of the fibers.

ii) We characterized the mesoscopic properties of articular cartilage by fitting experimental curves, and we analyzed the uni-axial compression test of a hypothetical tissue undergoing remodeling with properties borrowed from articular cartilage. Our model predicts correctly the experimental curves showing the angular distribution of the collagen fibers under mechanical deformation in a slice of articular cartilage [109]. Moreover, the simulations of the uni-axial compression test showed that the two remodeling processes have a different influence on the evolution of the system under study: the anelastic distortions affect considerably the evolution of the overall stress fields, but the fiber reorientation alters significantly the anisotropic part of the permeability and stress tensors. These results are coherent with the ones of Tomic et al. [29] In particular, the magnitude of the remodeling contributions are comparable for the radial anisotropic stresses, even though the two processes are concerned with two different levels of description.

The results commented above emphasize how the introduction of Langevin-like processes to describe fiber reorientation could open many possibilities in a scientific scenario that has been widely investigated by researchers in the last decades. Since the aim of this work is to introduce a framework that combines configurational and statistical mechanics, based on the idea put forward in [6], we did not carry out a comparison between our results and the ones obtained with the models already present in the literature. However, a comprehensive review of the literature is well within our sight, and we believe that it would be of great benefit to the researchers that are active in the fields of fiber-reinforced media.

Moreover, there are three directions that we plan to explore in future works:

i) Modifying the constitutive framework adopted in this work to take into account more complex forms of self interactions or the formation of cross-links among the fibers;

ii) Studying the evolution of the material properties if the tissue due to the anelastic distortions is no more deemed to be isotropic, but follows an anisotropic evolutionary law.

iii) Modifying the probability density distribution by prescribing the potential $\hat{\Pi}$ to be

$$\begin{aligned}\hat{\Pi}(\Theta;\Theta_{hi},\omega) &:= \frac{\Pi_c}{\omega^2}\left\{\left[\cos\left(\Theta-\Theta_{hi}\right)\right]^2+\left[\cos\left(\Theta-(\pi-\Theta_{hi})\right)\right]^2\right\}\\ &= \frac{\Pi_c}{\omega^2}\left\{\left[\cos\left(\Theta-\Theta_{hi}\right)\right]^2+\left[\cos\left(\Theta+\Theta_{hi}\right)\right]^2\right\}\\ &= \frac{2\Pi_c[\sin\Theta_{hi}]^2}{\omega^2}+\frac{2\Pi_c\cos(2\Theta_{hi})}{\omega^2}[\cos\Theta]^2,\end{aligned} \tag{76}$$

with $\Theta_{hi} \in [0,\pi/2]$, and, thus, $\cos(2\Theta_{hi}) \in [-1,1]$. This, indeed, introduces the symmetry $\hat{f}_R(\Theta,\Phi) = \hat{f}_R(\pi-\Theta,\Phi)$, for all $\Phi \in [0,2\pi]$. However, since the first summand on the right-hand

side of Equation (76) is independent of Θ and Φ, it does not contribute to the calculation of the normalizing factor associated with the probability density distribution generated by $\hat{\Pi}$. Thus, we can focus on the *effective potential*

$$\hat{\Pi}_{\text{eff}}(\Theta;\Theta_{\text{hi}},\omega) := \frac{2\Pi_{\text{c}}\cos(2\Theta_{\text{hi}})}{\omega^2}[\cos\Theta]^2. \tag{77}$$

In this case, by recalling the presence of the factor $\beta = (D\gamma)^{-1} > 0$ stemming from the Fokker–Planck Equation (40), we introduce the parameter

$$b_{\text{hi}} := \frac{\beta\Pi_{\text{c}}\cos(2\Theta_{\text{hi}})}{\omega^2}, \tag{78}$$

which can be positive, null, or negative, depending on the values taken by $\cos(2\Theta_{\text{hi}})$. To account for this variability in view of the calculation of the von Mises probability density distribution generated by $\hat{\Pi}_{\text{eff}}$, which requires the determination of the square root of b_{hi} (to be understood in complex sense, when $b_{\text{hi}} < 0$), we formally rewrite b_{hi} as the complex number

$$\mathfrak{b}_{\text{hi}} = |b_{\text{hi}}|\exp\left(i\pi\frac{1-\text{sign}(b_{\text{hi}})}{2}\right), \qquad \text{with } |b_{\text{hi}}| = \frac{\beta\Pi_{\text{c}}|\cos(2\Theta_{\text{hi}})|}{\omega^2}, \tag{79}$$

where $\text{sign}(\,\cdot\,)$ is the sign function ($\text{sign}(\kappa) = \pm 1$ for $\kappa \gtrless 0$, and $\text{sign}(0) = 0$). Thus, we write the probability density distribution as

$$\hat{f}_{\text{SVM}}(\Theta;\Theta_{\text{hi}},\omega) = \begin{cases} \dfrac{1}{\mathcal{Z}_0}\exp\left(2b_{\text{hi}}[\cos\Theta]^2\right), & \text{for } b_{\text{hi}} \neq 0, \\ \dfrac{1}{4\pi}, & \text{for } b_{\text{hi}} = 0 \ (\Rightarrow\ \Theta_{\text{hi}} = \pi/4), \end{cases} \tag{80}$$

and the normalization factor $\mathcal{Z}_0$ can be computed by direct integration and is equal to

$$\mathcal{Z}_0 = \frac{2\pi\sqrt{\pi}}{\sqrt{2\mathfrak{b}_{\text{hi}}}}\text{erfi}\left(\sqrt{2\mathfrak{b}_{\text{hi}}}\right) = \begin{cases} \dfrac{2\pi\sqrt{\pi}}{\sqrt{2b_{\text{hi}}}}\text{erfi}\left(\sqrt{2b_{\text{hi}}}\right), & b_{\text{hi}} > 0 \ (\Rightarrow\ \Theta_{\text{hi}} \in [0,\pi/4[\,), \\ \dfrac{2\pi\sqrt{\pi}}{\sqrt{2|b_{\text{hi}}|}}\text{erf}\left(\sqrt{2|b_{\text{hi}}|}\right), & b_{\text{hi}} < 0 \ (\Rightarrow\ \Theta_{\text{hi}} \in \,]\pi/4,\pi/2]). \end{cases} \tag{81}$$

with $\lim_{b_{\text{hi}}\to 0}\mathcal{Z}_0 = \lim_{\Theta_{\text{hi}}\to\pi/4}\mathcal{Z}_0 = 4\pi$.

With the aid of Equations (80) and (81), the models referred to as "Model A" and "Model B" by Federico and Gasser [27] are condensed in one model, parameterized by Θ_{hi}.

Conflict of Interests

The Authors declare that they have no conflict of interests.

Authors' contributions

All authors have equally contributed to this work.

Acknowledgment

We thank Dr. Marco Coco and Dr. Salvatore Di Stefano for various fruitful discussions in the preliminary stages of this work. A. Grillo is partially supported by MIUR (Italian Ministry of Education,

University and Research) through the PRIN project n. 2017KL4EF3 on *"Mathematics of active materials: From mechanobiology to smart devices"*, the PRIN project n. 2020F3NCPX on *"Mathematics for industry 4.0 (Math4I4)"*. A. Grillo's research group is funded by the European Union - Next Generation EU. A. Grillo, A. Giammarini and A. Pastore have been supported by the Research Project Prin2022 PNRR of National Relevance P2022KHFNB on *"Innovative multiscale approaches, possibly based on Fractional Calculus, for the effective constitutive modeling of cell mechanics, engineered tissues, and metamaterials in Biomedicine and related fields"* granted by the Italian MUR. This study was carried out within the MICS (Made in Italy – Circular and Sustainable) Extended Partnership and A. Giammarini received funding from the European Union Next-GenerationEU (PIANO NAZIONALE DI RIPRESA E RESILIENZA (PNRR) – MISSIONE 4 COMPONENTE 2, INVESTIMENTO 1.3 – D.D. 1551.11-10-2022, PE00000004). This manuscript reflects only the authors' views and opinions, neither the European Union nor the European Commission can be considered responsible for them.

References

[1] Gunda S, Natarajan S and Barrera O. On the fractional transversely isotropic functionally graded nature of soft biological tissues: Application to the meniscal tissue. *Journal of the Mechanical Behavior of Biomedical Materials* 2023; 143: 105855.

[2] Ateshian G. On the theory of reactive mixtures for modeling biological growth. *Biomechanics and Modeling in Mechanobiology* 2007; 6(6): 423–445. DOI:10.1007/s10237-006-0070-x.

[3] Holmes M and Mow V. The nonlinear characteristics of soft gels and hydrated connective tissues in ultrafiltration. *Journal of biomechanics* 1990; 23: 1145–1156. DOI:10.1016/0021-9290(90)90007-P.

[4] Loret B and Simões F. A framework for deformation, generalized diffusion, mass transfer and growth in multi-species multi-phase biological tissues. *Eur J Mech A* 2005; 24: 757–781. DOI:10.1016/j.euromechsol.2005.05.005.

[5] Ambrosi D, Preziosi L and Vitale G. The insight of mixtures theory for growth and remodeling. *Z Angew Math Phys* 2010; 61: 177–191. DOI:10.1007/s00033-009-0037-8.

[6] Grillo A, Federico S and Wittum G. Growth, mass transfer, and remodeling in fiber-reinforced, multi-constituent materials. *Int J Nonlinear Mech* 2012; 47: 388–401. DOI:10.1016/j.ijnonlinmec.2011.09.026.

[7] Ateshian G and Weiss J. Anisotropic hydraulic permeability under finite deformation. *J Biomech Engng* 2010; 132: 111004–1–111004–7. DOI:10.1115/1.4002588.

[8] Holzapfel G, Gasser T and Ogden R. A new constitutive framework for arterial wall mechanics and a comparative study of material models. *J Elast* 2000; 61(1-3): 1–48.

[9] Pandolfi A and Manganiello F. A model for the human cornea: constitutive formulation and numerical analysis. *Biomechanics and Modeling in Mechanobiology* 2006; 5(4): 237–246. DOI:10.1007/s10237-005-0014-x.

[10] Pandolfi A and Holzapfel GA. Three-dimensional modeling and computational analysis of the human cornea considering distributed collagen fibril orientations. *Journal of Biomechanical Engineering* 2008; 130(6). DOI:10.1115/1.2982251.

[11] Gentleman E, Lay AN, Dickerson DA et al. Mechanical characterization of collagen fibers and scaffolds for tissue engineering. *Biomaterials* 2003; 24(21): 3805–3813. DOI:10.1016/s0142-9612(03)00206-0.

[12] Merodio J and Ogden R. Mechanical response of fiber-reinforced incompressible non-linearly elastic solids. *Int J Nonlinear Mech* 2005; 40(2-3): 213–227. DOI:10.1016/j.ijnonlinmec.2004.05.003.

[13] Gasser T, Ogden R and Holzapfel G. Hyperelastic modelling of arterial layers with distributed collagen fibre orientations. *J R Soc Interface* 2006; 3: 15–35. DOI:10.1098/rsif.2005.0073.

[14] Federico S, Grillo A, La Rosa G et al. A transversely isotropic, transversely homogeneous microstructural-statistical model of articular cartilage. *J Biomech* 2005; 38: 2008–2018. DOI:10.1016/j.jbiomech.2004.09.020.

[15] deBotton G, Hariton I and Socolsky E. Neo-hookean fiber-reinforced composites in finite elasticity. *Journal of the Mechanics and Physics of Solids* 2006; 54(3): 533–559. DOI:10.1016/j.jmps.2005.10.001.

[16] Spencer A and Soldatos K. Finite deformations of fibre-reinforced elastic solids with fibre bending stiffness. *International Journal of Non-Linear Mechanics* 2007; 42(2): 355–368. DOI:10.1016/j.ijnonlinmec.2007.02.015.

[17] Hariton I, deBotton G, Gasser T et al. Stress-driven collagen fiber remodeling in arterial walls. *Biomech Model Mechanobiol* 2007; 6(3): 163–175. DOI:10.1007/s10237-006-0049-7.

[18] Holzapfel GA and Ogden RW. Constitutive modelling of arteries. *Proceedings of the Royal Society A: Mathematical, Physical and Engineering Sciences* 2010; 466(2118): 1551–1597. DOI:10.1098/rspa.2010.0058.

[19] Holzapfel GA, Niestrawska JA, Ogden RW et al. Modelling non-symmetric collagen fibre dispersion in arterial walls. *Journal of The Royal Society Interface* 2015; 12(106): 20150188. DOI:10.1098/rsif.2015.0188.

[20] Holzapfel G and Ogden R. On fiber dispersion models: Exclusion of compressed fibers and spurious model comparisons. *J Elast* 2017; 129(1-2): 49–68. DOI:10.1007/s10659-016-9605-2.

[21] Melnik A, HB Da Rocha and Goriely A. On the modeling of fiber dispersion in fiber-reinforced elastic materials. *Int J Nonlinear Mech* 2015; 75: 92–106. DOI:http://dx.doi.org/10.1016/j.ijnonlinmec.2014.10.006.

[22] Itskov M and Aksel N. A class of orthotropic and transversely isotropic hyperelastic constitutive models based on a polyconvex strain energy function. *International Journal of Solids and Structures* 2004; 41(14): 3833–3848. DOI:10.1016/j.ijsolstr.2004.02.027.

[23] Nolan D, Gower A, Destrade M et al. A robust anisotropic hyperelastic formulation for the modelling of soft tissue. *Journal of the Mechanical Behavior of Biomedical Materials* 2014; 39: 48–60. DOI:10.1016/j.jmbbm.2014.06.016.

[24] Lanir Y. Constitutive equations for fibrous connective tissues. *J Biomech* 1983; 16: 1–12.

[25] Federico S and Herzog W. On the anisotropy and inhomogeneity of permeability in articular cartilage. *Biomech Model Mechanobiol* 2008; 7: 367–378. DOI:10.1007/s10237-007-0091-0.

[26] Federico S and Herzog W. Towards an analytical model of soft biological tissues. *J Biomech* 2008; 41: 3309–3313. DOI:https://doi.org/10.1016/j.jbiomech.2008.05.039.

[27] Federico S and Gasser T. Non-linear elasticity of biological tissues with statistical fibre orientation. *J R Soc Interface* 2010; 7: 955–966. DOI:10.1098/rsif.2009.0502.

[28] Federico S and Grillo A. Elasticity and permeability of porous fibre-reinforced materials under large deformations. *Mech Mater* 2012; 44: 58–71. DOI:10.1016/j.mechmat.2011.07.010.

[29] Tomic A, Grillo A and Federico S. Poroelastic materials reinforced by statistically oriented fibres — numerical implementation and application to articular cartilage. *IMA J Appl Math* 2014; 79: 1027–1059. DOI:10.1093/imamat/hxu039.

[30] Gizzi A, Pandolfi A and Vasta M. A generalized statistical approach for modeling fiber-reinforced materials. *Journal of Engineering Mathematics* 2017; 109(1): 211–226. DOI: 10.1007/s10665-017-9943-5.

[31] Grillo A, Carfagna M and Federico S. An Allen-Cahn approach to the remodelling of fibre-reinforced anisotropic materials. *J Eng Math* 2018; 109(1): 139–172. DOI:10.1007/s10665-017-9940-8.

[32] Crevacore E, Di Stefano S and Grillo A. Coupling among deformation, fluid flow, structural reorganisation and fibre reorientation in fibre-reinforced, transversely isotropic biological tissues. *International Journal of Nonlinear Mechanics* 2019; 111: 1–13. DOI:https://doi.org/10.1016/j.ijnonlinmec.2018.08.022.

[33] Maleki M, Hashlamoun K, Herzog W et al. Effect of structural distortions on articular cartilage permeability under large deformations. *Biomechanics and Modeling in Mechanobiology* 2019; 19(1): 317–334. DOI:10.1007/s10237-019-01213-6.

[34] Vasta M, Gizzi A and Pandolfi A. On three- and two-dimensional fiber distributed models of biological tissues. *Probabilist Eng Mech* 2014; 37: 170–179. DOI:http://dx.doi.org/10.1016/j.probengmech.2014.05.003.

[35] Holzapfel G, Ogden R and Sherifova S. On fibre dispersion modelling of soft biological tissues: a review. *Proc R Soc A* 2019; 475(2224): 1–22. DOI:https://doi.org/10.1098/rspa.2018.0736.

[36] Quinn T, Dierickx P and Grodzinsky A. Glycosaminoglycan network geometry may contribute to anisotropic hydraulic permeability in cartilage under compression. *Journal of Biomechanics* 2001; 34(11): 1483–1490. DOI:10.1016/s0021-9290(01)00103-8.

[37] Pierce DM, Ricken T and Holzapfel GA. A hyperelastic biphasic fibre-reinforced model of articular cartilage considering distributed collagen fibre orientations: continuum basis, computational aspects and applications. *Computer Methods in Biomechanics and Biomedical Engineering* 2013; 16(12): 1344–1361. DOI:10.1080/10255842.2012.670854.

[38] Hashlamoun K, Grillo A and Federico S. Efficient evaluation of the material response of tissues reinforced by statistically oriented fibres. *Z Angew Math Phys* 2016; 67: 113–145. DOI:10.1007/s10237-006-0049-7.

[39] MAROUDAS A and BULLOUGH P. Permeability of articular cartilage. *Nature* 1968; 219(5160): 1260–1261. DOI:10.1038/2191260a0.

[40] Epstein M and Maugin G. Thermomechanics of volumetric growth in uniform bodies. *International Journal of Plasticity* 2000; 16(7-8): 951–978. DOI:10.1016/s0749-6419(99)00081-9.

[41] Garikipati K, Arruda E, Grosh K et al. A continuum treatment of growth in biological tissue: the coupling of mass transport and mechanics. *J Mech Phys Solids* 2004; 52: 1595–1625. DOI:10.1016/j.jmps.2004.01.004.

[42] Wilson W, Driessen N, CC van Donkelaar et al. Prediction of collagen orientation in articular cartilage by a collagen remodeling algorithm. *Osteoarthr Cartil* 2006; 14: 1196–1202. DOI: 10.1016/j.joca.2006.05.006.

[43] Ambrosi D, Ateshian G, Arruda E et al. Perspectives on biological growth and remodeling. *Journal of the Mechanics and Physics of Solids* 2011; 59(4): 863–883. DOI:10.1016/j.jmps.2010.12.011.

[44] Lin WJ, Iafrati MD, Peattie RA et al. Growth and remodeling with application to abdominal aortic aneurysms. *Journal of Engineering Mathematics* 2017; 109(1): 113–137. DOI:10.1007/s10665-017-9915-9.

[45] Soldatos KP. Foundation of polar linear elasticity for fibre-reinforced materials. *Journal of Elasticity* 2013; 114(2): 155–178. DOI:10.1007/s10659-013-9433-6.

[46] Soldatos KP, Shariff MHBM and Merodio J. On the constitution of polar fiber-reinforced materials. *Mechanics of Advanced Materials and Structures* 2020; 28(21): 2255–2266. DOI:10.1080/15376494.2020.1729449.

[47] Driessen N, Wilson W, Bouten C et al. A computational model for collagen fibre remodelling in the arterial wall. *J Theor Biol* 2004; 226: 53–64. DOI:10.1016/j.jtbi.2003.08.004.

[48] Menzel A. Modelling of anisotropic growth in biological tissues — a new approach and computational aspects. *Biomechan Model Mechanobiol* 2005; 3: 147–171. DOI:10.1007/s10237-004-0047-6.

[49] Menzel A. A fibre reorientation model for orthotropic multiplicative growth. configurational driving stresses, kinematics-based reorientation and algorithmic aspects. *Biomechan Model Mechanobiol* 2007; 6(5): 303–320. DOI:10.1007/s10237-006-0061-y.

[50] Gizzi A, Cyron CJ, Falcinelli C et al. Evolution of fiber distributions in homogenized constrained mixture models of soft tissue growth and remodeling: Uniaxial loading. *Journal of the Mechanics and Physics of Solids* 2024; 183: 105491. DOI:10.1016/j.jmps.2023.105491.

[51] Grillo A and Di Stefano S. A formulation of volumetric growth as a mechanical problem subjected to non-holonomic and rheonomic constraint. *Mathematics and Mechanics of Solids* 2023; : 1–10DOI:10.1177/10812865231152228.

[52] Grillo A and Di Stefano S. Addendum to "a formulation of volumetric growth as a mechanical problem subjected to non-holonomic and rheonomic constraint". *Mathematics and Mechanics of Solids* 2023; 29(1): 62–70. DOI:10.1177/10812865231178291.

[53] Martins J, Pires E, Salvado R et al. A numerical model of passive and active behavior of skeletal muscles. *Computer Methods in Applied Mechanics and Engineering* 1998; 151(3–4): 419–433. DOI:10.1016/s0045-7825(97)00162-x.

[54] Blemker SS, Pinsky PM and Delp SL. A 3d model of muscle reveals the causes of nonuniform strains in the biceps brachii. *Journal of Biomechanics* 2005; 38(4): 657–665. DOI:10.1016/j.jbiomech.2004.04.009.

[55] Giantesio G, Musesti A and Riccobelli D. A comparison between active strain and active stress in transversely isotropic hyperelastic materials. *Journal of Elasticity* 2018; 137(1): 63–82. DOI:10.1007/s10659-018-9708-z.

[56] Olsson T and Klarbring A. Residual stresses in soft tissue as a consequence of growth and remodeling: application to an arterial geometry. *Eur J Mech A* 2008; 27(6): 959–974. DOI:10.1016/j.euromechsol.2007.12.006.

[57] Wilson W, Huyghe J and CC van Donkelaar. A composition-based cartilage model for the assessment of compositional changes during cartilage damage and adaptation. *Osteoarthr Cartil* 2006; 14: 554–560. DOI:10.1016/j.joca.2005.12.006.

[58] Pierce DM, Ricken T and Holzapfel GA. A hyperelastic biphasic fibre-reinforced model of articular cartilage considering distributed collagen fibre orientations: continuum basis, computational aspects and applications. *Computer Methods in Biomechanics and Biomedical Engineering* 2013; 16(12): 1344–1361. DOI:10.1080/10255842.2012.670854.

[59] Li K, Ogden R and Holzapfel G. Computational method for excluding fibers under compression in modeling soft fibrous solids. *Eur J Mech A/Solids* 2016; 57: 178–193. DOI:10.1016/j.euromechsol.2015.11.003.

[60] Garcia D, Zysset P, Charlebois M et al. A three-dimensional elastic plastic damage constitutive law for bone tissue. *Biomech Model Mechanobiol* 2009; 8(2): 149–165. DOI:10.1007/s10237-008-0125-2.

[61] Di Stefano S, Carfagna M, Knodel MM et al. Anelastic reorganisation of fibre-reinforced biological tissues. *Computing and Visualization in Science* 2019; 20(3-6): 95–109. DOI:10.1007/s00791-019-00313-1.

[62] Mićunović M. *Thermomechanics of Viscoplasticity*. Springer New York, 2009. DOI:10.1007/978-0-387-89490-4.

[63] DiCarlo A and Quiligotti S. Growth and balance. *Mechanics Research Communications* 2002; 29(6): 449–456. DOI:10.1016/s0093-6413(02)00297-5.

[64] Di Stefano S, Ramírez-Torres A, Penta R et al. Self-influenced growth through evolving material inhomogeneities. *International Journal of Non-Linear Mechanics* 2018; 106: 174–187. DOI:10.1016/j.ijnonlinmec.2018.08.003.

[65] Ciancio V, Dolfin M, Francaviglia M et al. Uniform materials and the multiplicative decomposition of the deformation gradient in finite elasto-plasticity. *J Non-Equilib Thermodyn* 2008; 33(3): 199–234. DOI:10.1515/JNETDY.2008.009.

[66] Marsden J and Hughes T. *Mathematical Foundations of Elasticity*. Dover Publications, Inc., Mineola, New York, 1983.

[67] Quiligotti S, Maugin G and F dell'Isola. An eshelbian approach to the nonlinear mechanics of constrained solid-fluid mixtures. *Acta Mech* 2003; 160: 45–60. DOI:10.1007/s00707-002-0968-z.

[68] Cermelli P, Fried E and Sellers S. Configurational stress, yield and flow in rate-independent plasticity. *Proc R Soc Lond A* 2001; 457: 1447–1467. DOI:10.1098/rspa.2001.0786.

[69] Giorgio I, dell'Isola F, Andreaus U et al. An orthotropic continuum model with substructure evolution for describing bone remodeling: an interpretation of the primary mechanism behind wolff's law. *Biomechanics and Modeling in Mechanobiology* 2023; 22(6): 2135–2152. DOI:10.1007/s10237-023-01755-w.

[70] Gantmacher F. *Lectures in Analytical Mechanics*. MIR Publishers, 1975.

[71] Llibre J, Ramírez R and Sadovskaia N. Nonlinear dynamics. *A new approach to the vakonomic mechanics* 2014; 78: 2219–2247. DOI:10.1007/s11071-014-1554-3.

[72] Pars L. *A treatise on Analytical Dynamics*. Heinemann, London, 1965.

[73] Hassanizadeh SM. Derivation of basic equations of mass transport in porous media, part 1. macroscopic balance laws. *Advances in Water Resources* 1986; 9(4): 196–206. DOI:10.1016/0309-1708(86)90024-2.

[74] Hassanizadeh S. Derivation of basic equations of mass transp. porous med., part 2. generalized Darcy's and Fick's laws. *Adv Water Resour* 1986; 9: 207–222.

[75] Bear J and Bachmat Y. *Introduction to Modeling of Transport Phenomena in Porous Media*. Kluwer, Dordrecht, 1990.

[76] Bennethum L, Murad M and Cushman J. Macroscale thermodynamics and the chemical potential for swelling porous media. *Transport in Porous Media* 2000; 39(2): 187–225. DOI:10.1023/a:1006661330427.

[77] Ateshian G and Humphrey J. Continuum mixture models of biological growth and remodeling: Past successes and future opportunities. *Annual Review of Biomedical Engineering* 2012; 14(1): 97–111. DOI:10.1146/annurev-bioeng-071910-124726.

[78] Holzapfel GA and Ogden RW. An arterial constitutive model accounting for collagen content and cross-linking. *Journal of the Mechanics and Physics of Solids* 2020; 136: 103682. DOI:10.1016/j.jmps.2019.103682.

[79] Moo EK, Tanska P, Federico S et al. Collagen fibres determine the crack morphology in articular cartilage. *Acta Biomaterialia* 2021; 126: 301–314. DOI:10.1016/j.actbio.2021.03.031.

[80] Maugin GA and Metrikine AV. *Mechanics of Generalized Continua: One Hundred Years After the Cosserats*. Springer New York, 2010. ISBN 9781441956958. DOI:10.1007/978-1-4419-5695-8.

[81] Baaijens F, Bouten C and Driessen N. Modeling cartilage remodeling. *J Biomech* 2010; 43: 166–175. DOI:10.1016/j.jbiomech.2009.09.022.

[82] Grillo A, Wittum G, Tomic A et al. Remodelling in statistically oriented fibre-reinforced materials and biological tissues. *Math Mech Solids* 2015; 20(9): 1107–1129. DOI:10.1177/1081286513515265.

[83] Loy N and Preziosi L. A statistical mechanics approach to describe cell reorientation under stretch. *Bulletin of Mathematical Biology* 2023; 85(7). DOI:10.1007/s11538-023-01161-4.

[84] Federico S and Herzog W. On the permeability of fibre-reinforced porous materials. *Int J Solids Struct* 2008; 45: 2160–2172. DOI:https://doi.org/10.1016/j.ijsolstr.2007.11.014.

[85] Federico S and Grillo A. *Linear Elastic Composites with Statistically Oriented Spheroidal Inclusions*. Springer International Publishing. ISBN 9783319527949, 2017. pp. 307–346. DOI:10.1007/978-3-319-52794-9_11.

[86] Grillo A, Carfagna M and Federico S. Non-Darcian flow in fibre-reinforced biological tissues. *Meccanica* 2017; 52: 3299–3320. DOI:10.1007/s11012-017-0679-0.

[87] Carfagna M and Grillo A. The spherical design algorithm in the numerical simulation of biological tissues with statistical fibre-reinforcement. *Comput Vis Sci* 2017; 18: 157–184. DOI:10.1007/s00791-017-0278-6.

[88] Grillo A, Di Stefano S, Ramírez-Torres A et al. A study of growth and remodeling in isotropic tissues, based on the anand-aslan-chester theory of strain-gradient plasticity. *GAMM-Mitteilungen* 2019; 42(4). DOI:10.1002/gamm.201900015.

[89] Destrade M, Donald BM, Murphy JG et al. At least three invariants are necessary to model the mechanical response of incompressible, transversely isotropic materials. *Computational Mechanics* 2013; 52(4): 959–969. DOI:10.1007/s00466-013-0857-4.

[90] Hamdaoui ME, Merodio J, Ogden RW et al. Finite elastic deformations of transversely isotropic circular cylindrical tubes. *International Journal of Solids and Structures* 2014; 51(5): 1188–1196. DOI:10.1016/j.ijsolstr.2013.12.019.

[91] Simo J. A framework for finite strain elastoplasticity based on maximum plastic dissipation and the multiplicative decomposition: Part i. continuum formulation. *Computer Methods in Applied Mechanics and Engineering* 1988; 66(2): 199–219. DOI:10.1016/0045-7825(88)90076-x.

[92] Green AE and Naghdi PM. A general theory of an elastic-plastic continuum. *Archive for Rational Mechanics and Analysis* 1965; 18(4): 251–281. DOI:10.1007/bf00251666.

[93] Wu JZ and Herzog W. Finite element simulation of location- and time-dependent mechanical behavior of chondrocytes in unconfined compression tests. *Annals of Biomedical Engineering* 2000; 28(3): 318–330. DOI:10.1114/1.271.

[94] Athanasiou KA, Darling EM and Hu JC. *Articular Cartilage Tissue Engineering*. Springer International Publishing, 2010. DOI:10.1007/978-3-031-02578-5.

[95] Grillo A and Di Stefano S. An a posteriori approach to the mechanics of volumetric growth. *Mathematics and Mechanics of Complex Systems* 2023; 11(1): 57–86. DOI:10.2140/memocs.2023.11.57.

[96] Pericak-Spector KA and Spector SJ. On the representationtheorem for linear, isotropic tensor functions. *Journal of Elasticity* 1995; 39(2): 181–185.

[97] Holzapfel GA and Ogden RW. Constitutive modelling of passive myocardium: a structurally based framework for material characterization. *Philosophical Transactions of the Royal Society A: Mathematical, Physical and Engineering Sciences* 2009; 367(1902): 3445–3475. DOI:10.1098/rsta.2009.0091.

[98] Risken H. *The Fokker-Planck Equation: Methods of Solution and Applications*. Springer Berlin Heidelberg, 1996. ISBN 9783642615443. DOI:10.1007/978-3-642-61544-3.

[99] Jordan R, Kinderlehrer D and Otto F. The variational formulation of the fokker–planck equation. *SIAM Journal on Mathematical Analysis* 1998; 29(1): 1–17. DOI:10.1137/s0036141096303359.

[100] Aspden RM and Hukins DW. Collagen organization in articular cartilage, determined by x-ray diffraction, and its relationship to tissue function. *Proceedings of the Royal Society of London Series B Biological Sciences* 1981; 212(1188): 299–304. DOI:10.1098/rspb.1981.0040.

[101] Clark A, Barclay L, Matyas J et al. In situ chondrocyte deformation with physiological compression of the feline patellofemoral joint. *Journal of Biomechanics* 2003; 36(4): 553–568. DOI:10.1016/s0021-9290(02)00424-4.

[102] Mollenhauer J, Aurich M, Muehleman C et al. X-ray diffraction of the molecular substructure of human articular cartilage. *Connective Tissue Research* 2003; 44(5): 201–207. DOI:10.1080/03008200390244005.

[103] Mansour J. *Biomechanics of cartilage*, chapter 5. 2013. pp. 69–83.

[104] Hedlund H, Mengarelli-Widholm S, Reinholt FP et al. Stereologic studies on collagen in bovine articular cartilage. *APMIS* 1993; 101(1–6): 133–140. DOI:10.1111/j.1699-0463.1993.tb00092.x.

[105] Chen S, Falcovitz Y, Schneiderman R et al. Depth-dependent compressive properties of normal aged human femoral head articular cartilage: relationship to fixed charge density. *Osteoarthritis and Cartilage* 2001; 9(6): 561–569. DOI:10.1053/joca.2001.0424.

[106] Rodriguez E, Hoger A and McCulloch A. Stress-dependent finite growth in soft elastic tissues. *J Biomech* 1994; 27: 455–467. DOI:10.1016/0021-9290(94)90021-3.

[107] Hardin R and Sloane N. McLaren's improved snub cube and other new spherical designs in three dimensions. *Discrete Comput Geom* 1996; 15: 429–441.

[108] Markowich P and Villani C. On the trend to equilibrium for the Fokker-Planck equation: an interplay between physics and functional analysis. *Mat Contemp* 2000; .

[109] Mansfield JC, Mandalia V, Toms A et al. Collagen reorganization in cartilage under strain probed by polarization sensitive second harmonic generation microscopy. *Journal of The Royal Society Interface* 2019; 16(150): 20180611. DOI:10.1098/rsif.2018.0611.

[110] Giverso C, Stefano SD, Grillo A et al. A three dimensional model of multicellular aggregate compression. *Soft Matter* 2019; 15(48): 10005–10019. DOI:10.1039/c9sm01628g.

[111] Grillo A, Carfagna M and Federico S. The Darcy-Forchheimer law for modelling fluid flow in biological tissues. *Theoretical and Applied Mechanics (TEOPM7)* 2014; 41(4): 283–322.

[112] Pins GD, Huang EK, Christiansen DL et al. Effects of static axial strain on the tensile properties and failure mechanisms of self-assembled collagen fibers. *J Appl Polym Sci* 1997; 63(11): 1429–1440.

[113] Holmes MH. Finite deformation of soft tissue: Analysis of a mixture model in uni-axial compression. *Journal of Biomechanical Engineering* 1986; 108(4): 372–381. DOI:10.1115/1.3138633.

[114] Rohatgi A. Webplotdigitizer. URL https://automeris.io.

[115] Holzapfel GA and Ogden RW. A damage model for collagen fibres with an application to collagenous soft tissues. *Proceedings of the Royal Society A: Mathematical, Physical and Engineering Sciences* 2020; 476(2236). DOI:10.1098/rspa.2019.0821.